NTNU

Norwegian University of
Science and Technology

Synthesis and applications of carbon nanomaterials: from quanta dots to microspheres

Daniel Skodvin

Chemical Engineering and Biotechnology
Submission date: June 2017
Supervisor: De Chen, IKP

Norwegian University of Science and Technology
Department of Chemical Engineering

Preface

This Masters thesis is the result of the work performed during the spring semester of 2017 at the Catalysis Group, Department of Chemical Engineering, NTNU.

I would like to express sincere gratitude to my supervisor at NTNU, Professor De Chen for his valuable help and guidance throughout the semester. I am thankful that I have learned so much from Professor De Chen. Also, I would like to express sincere gratitude to my co-supervisor Dr. Qinjun Chen for his help during my work. In addition, I want to thank Yahao Li for his help in the laboratory, as well as Xuehang Wang for the assistance and guidance during the start-up of my work.

I also want to thank Karin Wiggen Dragsten and Ken Roger Ervik for giving me necessary training in the laboratories.

Abstract

In this work, activated carbon fibers and activated carbon spheres were prepared through physical activation with CO_2 and steam. The precursors used were polyaniline (PANI) and resorcinol-formaldehyde polymer spheres (RF polymer spheres). Various activation conditions, such as activation time, activation temperature and partial pressure of CO_2 were investigated in the CO_2 activation process, as well as the effect of carbonization temperature. It was found that a carbonization temperature of 650°C resulted in the largest BET surface area and pore volume after the activation process. Moreover, the results suggests that the BET surface area, total pore volume and mesopore volume increases with increasing activation time, while the micropore volume goes through a maximum at an activation time of three hours. Also, the BET surface area, total pore volume and mesopore volume increases with increasing activation temperature, whereas the micropore volume goes through a maximum at 950°C. The results shows that the fiber structure is mostly retained during the CO_2 activation process, however a decrease in macroporosty and destruction of fibers occurs with an activation time of 4 hours at an activation temperature 950°C. Also, an activation temperature of 1000°C results in a decrease in macroporosity.

In the combined CO_2 and steam activation process, the BET surface area goes through a maximum at a water temperature of 40°C. The results show that at each activation time, the obtained BET surface area is higher for the combined CO_2 and steam activation process compared to that obtained using pure CO_2 activation. Also, at each activation temperature, the obtained BET surface area is higher for the combined CO_2 and steam activation process compared to that obtained using pure CO_2 activation. In the optimization part, a high BET surface area of 2552.6 m^2g^{-1} is obtained with a burn-off equal to 83.6 wt.%.

Supercapacitors constructed by electrode materials prepared from the activated carbon fibers and activated carbon spheres provided a specific capacitance at low current densites, in which the highest specific capacitance obtained was 416.5 F/g at a current density of 0.1 A/g. However, the supercapacitors showed a poor rate capability, where activated carbon spheres provided the best rate capability of only 53.3 % at a current density of 3.45 A/g. Also, the cycling stability was very low for the supercapacitors prepared in this work, where activated carbon spheres showed to best cycling stability of only 48 % retention of the initial capacitance after 1200 cycles. CV curves indicated that pseudocapacitance was present in all of the supercapacitors. This was reasonable due to the presence of nitrogen and oxygen in the activated carbons.

Contents

1 Introduction

Activated carbons are attractive materials for many industrial applications, including water treatment, gas storage, purification and separation, catalyst support, waste water reclamation and energy storage [32]. Activated carbons possess good physical and chemical properties, such as high specific surface area, electric and thermal conductivity, low density, chemical and thermal stability and well developed porosity, which makes them applicable in a wide range of industrial processes [20]. In addition, activated carbons have a wide availability, with many organic precursors, including wood, polymers, coal and fruit shell [43]. The choice of precursor and activation method enables activated carbons to be produced with special characteristics suitable for a given application.

Activated carbons are usually prepared by physical or chemical activation [12]. Physical activation is normally carried out in two steps, where the first step involves carbonization of carbonaceous material and the second step is a controlled gasification process in the presence of activation agents, such as carbon dioxide, steam or air [3]. Chemical activation is usually carried out as a one step process, where pyrolysis and activation take place simultaneously in the presence of a dehydrating agent such as potassium chloride, sulfuric acid or zinc chloride [32]. The physical activation process is considered to be cheaper and more environmentally friendly compared to the chemical activation process, which is mainly due to the disposal issues of toxic chemicals related to the chemical activation process [10]. Also, extensive washing of the carbon is required after the chemical activation method, in order to remove residual reactants as well as inorganic residue [21].

The rapidly growing mobile energy storage and renewable energy market, results in a increasing demand for electrical energy storage devices [26]. Until now, batteries have been the most widely used energy storage device. However, batteries are not advantageous for high-power applications, since they store energy through Faradaic reactions [26]. Supercapacitors have a higher specific power compare to most batteries, however their specific energy is a bit lower [21]. In addition, the long cycling life and good safety performance of supercapacitors, makes them possible replacements for batteries in applications requiring high power. However, in order to achieve this, the specific energy of supercapacitors needs to be imroved [26]. Electrical double-layer capacitors (EDLCs) are well suited to rapidly store and release energy [21]. Carbon materials are desirable electrode materials for EDLCs because they are available with high surface areas.

Considering that the physical activation process is regarded as cheaper and and more environmentally friendly compared to the chemical activation process, the objective of this work is to produce activated carbon fibers and activated carbon spheres with the use of CO_2 and steam as activation agents. CO_2 was selected as the activation agent because it is clean and easy to handle, while it provides good controllability of the activation process due to the slow reaction rate of the endothermic reaction between CO_2 and carbon [10]. Steam was also introduced in the activation processes, because steam generates wider pore size distribution compared to CO_2, which makes it possible to tune the pore structure of activated carbons [4]. Two precursors were used, namely polyaniline (PANI) and resorcinol-formaldehyde polymer spheres (RF polymer spheres). As the main focus in the specialization project was the synthesis and application of carbon spheres, the focus is now towards physical activation of carbon fibers derived from PANI. Several activation conditions, such as activation time, activation temperature and partial pressure of CO_2 were investigated. In addition, various amount of steam was introduced to the activation process and the effect on the BET surface area and pore structure was examined.

The objective of this work does also include application of the obtained activated carbons in energy storage. Activated carbon fibers and activated carbon spheres were used as electrode material for the preparation of supercapacitor cells. The performance of the supercapacitor cells were examined by cyclic voltammetry, frequency response analysis, galvanostatic charge-discharge tests and cycling stability tests.

Several characterization techniques were applied in order to investigate the properties of activated carbon fibers and activated carbon spheres. The morphology was examined by scanning electron microscopy and the BET surface area and pore structure were determined with nitrogen and CO_2 adsorption/desorption at 77 K and 0°C, respectively. The oxygen and nitrogen content of activated carbons were investigated by energy-dispersive X-ray spectroscopy. Thermal gravimetric analysis was applied in order to investigate the reactivity of carbon fibers during the activation process. Also, mass spectrometry combined with TGA was used to examine both the gaseous species formed during the activation process and the removal of oxygen containing groups on the surface of activated carbon.

2 Literature review

2.1 Synthesis of carbon spheres

In 1968 it was reported a method called the Stober method that described a process to synthesize monodispersed inorganic silica particles through the hydrolysis and condensation of tetraethyl orthosilicate applying an aqueous ammonia catalyst in an alcohol-water solvent [7]. Later it became interesting to extend the Stober method to carbonaceous spheres and it was demonstrated that this method could be used to synthesize spherical polymeric resins derived from the reaction between resorcinol and formaldehyde using sodium carbonate as catalyst in an aqueous medium at 85°C in 24 hours [7].

It was also demonstrated that this method could be applied to prepare monodispersed resorcinol-formaldehyde resin polymers with the use of ammonia as catalyst in an ethanol-water solvent at 100°C in 24 hours [7]. Later, it has been reported that a rapid synthesis of nitrogen-doped nonspherical porous carbon has been achieved in 5 minutes by copolymerization of resorcinol and formaldehyde using lysine under ultrasonic irradiation [7]. Finally, monodispersed spherical resorcinol-formaldehyde resin polymers was prepared in a rapid synthesis using ammonia as catalyst in an ethanol-water solvent under ultrasonic irradiation for a duration of 5 minutes [7].

2.1.1 Ultrasonic irradiation

Resorcinol-Formaldehyde polymer spheres (RF polymer spheres or RF-resins) can, using ultrasonic irradiation, be prepared in 5 minutes. Ultrasonic irradiation makes this rapid synthesis feasible because it generates extreme temperatures and pressures, which drive chemical reactions [7]. These extreme conditions are caused by continuous nuceation, bubble growth and impulsive collapse of cavitating bubbles in the applied solvent [7]. During the bubble collapse, hot spots are formed that excite water molecules into vibrational, rotational and various electronic states [7]. The resulting energy causes water molecules to dissociate into H• and OH• radicals [7]. These radicals initiate the polymerization reaction between resorcinol and formaldehyde and leads to an increased reaction rate, which lets the synthesis to be carried out in milder conditions [8]. In addition to an increased reaction rate, ultrasound chemical reactions can alter the reaction path, which also allows the reaction to take place in milder conditions [7]. Hence, ultrasonic irradiation can be applied to initiate polymerization reactions as well as shorten the gelation or cross-linking time [7].

In addition to an increased reaction temperature, a reaction time of 24 hours is required when synthesizing RF-resins without the use of ultrasonic irradiation. In addition, without ultrasonic irradiation the prepared RF-resins are highly agglomerated and the spherical morphology is reduced [8]. Therefore it can be concluded that ultrasonic irradiation is important for the spherical morphology of the RF-resins.

RF-resins are generated by copolymerization and polycondensation of resorcinol and formaldehyde in the presence of aqueous ammmonia as catalyst in an ethanol-water solvent [7]. The fact that RF sonogels obtained by ultrasonic irradiation using sodium carbonate as catalyst is not spherical in shape, can be explained by the important role of ammonia as catalyst in the copolymerization of resorcinol [7]. This process is initiated by aminomethylates that contain two active hydrogens and an iminium ion, which is created from an amine in the presence of formaldehyde [7]. Also, free radicals generate hydroxymethyl substituted species on the surfaces, which interact electrostatically with ammonia molecules [7]. This leads to cross-linking and cluster formation which results in colloidal spheres [7][34].

The spherical size of RF-resins can be tuned from 200 to 1000 nm by varying the catalyst concentration, the concentration of RF precursors, the ratio between alcohol and water or the alkyl chain of alcohol [34]. As shown in previous work at NTNU, the particle size of the RF-resins decreases with increasing ammonia concentration [16] [7]. In addition, previous work at NTNU has shown that monodispersed nitrogen-doped RF polymers can be synthesized with the method presented by Vilas et al [7], but excluding the use of ethanol in the solvent [41].

2.1.2 Reaction mechanism

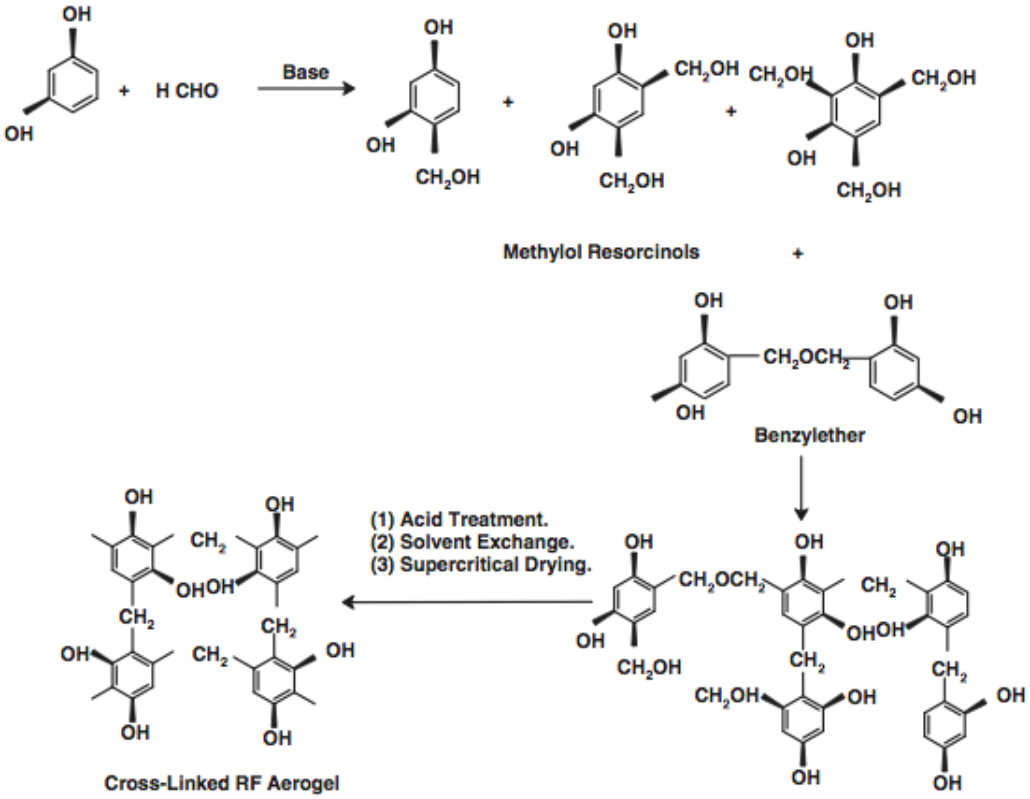

Figure 2.1: A proposed mechanism for the base-catalyzed gelation of resorcinol and formaldehyde [19].

Figure (2.1) shows a proposed mechanism for the polymerization reaction between resorcinol and formaldehyde. First, a base catalyzed addition reaction between resorcinol and formaldehyde takes place. This reaction forms methylol compounds, such as monomethylol resorcinol and dimethylol resorcinol [19]. Next, these methylol compounds go through a condensation reaction with each other. This reaction creates nanometer sized clusters, which subsequently crosslink to produce a gel network [19]. The creation of clusters is influenced by reaction temperature, concentration of reactants and pH [19]. The particle size is controlled by the concentration of the catalyst, whereas the density of the gel network is determined by the degree of dilution [19].

2.2 Synthesis of polyaniline

Polyaniline (PANI) is a conducting polymer that has attracted attention due to its unique architectural diversity and flexibility, exceptional doping and dedoping mechanism and low cost of the monomer precursor [17]. In addition, the conductivity is easily controlled by changing the oxidation and protonation states [17]. PANI exists in three states, namely leucoemeraldine, emeraldine and pernigraniline, which correspond to the fully reduced state, the half oxidized state and the fully oxidized state, respectively [17]. PANI has several potential applications, including electronic and optical devices such as sensors, electronic circuit boards and fuel cells. However, PANI is normally applied as a hydrophilic polymeric material for blending with different polymers in order to increase membrane hydrophilicity and increase performance [17].

PANI is synthesized by free-radical polymerization. Hence, it has a wide molecular weight distribution and is composed of thousands of polymer chains with various molecular weight [17]. PANI that is composed by short chains or a high level of branched chains, will have shorter conjugation lengths, which may increase the conductivity and solubility of the material [17]. Also, it has been reported that the use of soluble neutral salts has increased the conductivity and the molecular weight of protonated PANI, by keeping the reaction mixture mobile at lower temperatures [17]. Low temperature synthesis results in PANI with high molecular weight, but it typically has irregularities in the structure of the polymer chain. These structural irregularities can be explained by the formation of pernigraniline, as an intermediate step in the polymerization [17].

The usual chemical oxidative polymerization of aniline is conducted in an aqueous solution. Aniline is dissolved in a strong acidic solution, typically using HCl and a reaction temperaure of 0°C. Next, the polymerization is initiated by the addition of an oxidant, typically ammonium peroxydisulfate [18]. Various types of nanostructures, including fibers, wires, rods and tubes can be obtained by using a structural director. Structural directors can be soft templates, which include surfactants and organic dopants that assist in the self-assembly of PANI nanostructures, or hard templates, which include porous membranes and zeolites [18].

The key in order to synthesize PANI nanofibers is to prevent secondary growth [18]. By adding the oxidant dopant solution slowly to the aniline, PANI nanofibers form initially as the polymerization begins, however since nanofibers are exposed to aniline and oxidant, they are put through secondary growth. This secondary growth creates irregularly shaped agglomerates containing nanofibers and particulates [18]. Secondary growth can be avoided using interfacial polymerization

at an aqueous-organic interface [18]. In this method, polymerization occurs only at the interface, since the aniline and the oxidant are separated by the aqueous and organic phase. The PANI nanofibers formed at the interface are hydrophilic, since they are in the doped emeraldine salt form, and can rapidly diffuse into the aqueous phase, where they are excluded from the reaction front [18].

Another way to suppress secondary growth is to add the initiator solution (ammonium peroxydisulfate in 1M HCl) into the monomer solution (aniline in 1M HCl) all at once [18]. The initiator and monomer molecules are evenly distributed before polymerization by mixing with a magnetic stirrer. Hence, the initiator molecules induce the generation of PANI nanofibers by polymerizing monomers in their local area. All the initiator molecules are consumed to create nanofibers, hence reducing secondary growth [18]. This fast-mixing method, schematically illustrated in Figure (2.2), can be performed in a wide range of temperatures (0 to 100°C) without effecting the high-quality nanofibers obtained[18].

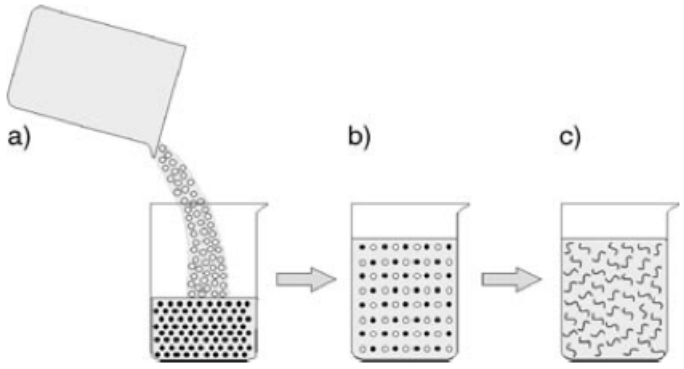

Figure 2.2: The synthesis of PANI nanofibers by the fast-mixing method [18]. a) The oxidant (open circle) dopant solution is added, all at once, into the aniline (solid circles) dopant solution and mixed. b) A homogeneous solution, where fast polymerization occurs across the entire solution. c) Secondary growth is inhibited, since all the reactants are consumed.

Thus, essentially pure PANI nanofibers can be produced without the use of templates or seeds, by inhibiting secondary growth of PANI nanofibers, either by the interfacial polymerization method or the fast-mixing method [18].

2.3 Carbonization

During a carbonization process, chemical bonds thermally break in the presence of an inert argon or nitrogen atmosphere [7]. During carbonization of RF-resins in a

nitrogen atmosphere, loss of hydrogen and oxygen atoms occur as a result of thermal breakage of chemical bonds [7]. This improves the structural carbon network by the evolution of dimentional nanolayers [7]. Also, the spherical morphology and the surface smoothness of the RF-resins are maintained during the slow-heating carbonization process [7]. The thermally unstable RF-resins, containing C, H and O, are gradually converted into a stable carbonaceous material. During this process, the remaining water is released by condensation of OH-groups at 200°C, followed by the release of hydrogen, oxygen and hydrocarbons such as CO_2 and CH_4 at 380°C. Finally, aromatization occurs at 600°C [7]. The carbonization process fabricates mainly microporous carbons, which have some macropores within the structure [7]. Also, the carbonization process converts electrically insulating polymeric RF resins into a conducting carbon matrix, making the material suitable in applications such as catalyst support and electrode material in supercapacitors [7].

2.4 Activated carbons

Activated carbons, also referred to as porous carbons, are currently used worldwide in many different industrial applications, such as water treatment, waste water reclamation, gas storage, purification and separation, catalyst support and energy storage [32] [42]. The importance of activated carbons is reflected in the worldwide increasing consumption [3]. The extremely wide application range of activated carbons is due to their good physical and chemical properties, which include high specific surface area, electric and thermal conductivity, chemical and thermal stability and low density [43]. Also, activated carbons has a wide availability, with many organic precursors, such as wood, coal, fruit shell and polymers [43].

Porous carbons are usually classified by their pore diameters as microporous (pore width $\leq$ 2 nm), mesoporous (2 nm $\leq$ pore width $\leq$ 50 nm) and macroporous (pore width $\geq$ 50 nm) [43]. Activated carbons have a complex network of pores and the choice of precursor and activation method enables activated carbons to be produced with special characteristics suitable for a given application. Activated carbons are normally produced by physical or chemical activation [12]. Physical activation is usually carried out in two steps, in which the first step involves carbonization of carbonaceous material in an inert atmosphere at high temperatures (500-1000°C). This is done in order to remove volatile matter, oxygen and hydrogen, which results in rudimentary structures in the carbon material [4] [32]. The second step is a controlled gasification process at high temperatures (800-1100°C) in the presence of activation agents, such as carbon dioxide, steam or air [3]. In this step, the chars produced from the carbonization step react with the activation

agent, which leads to the formation of carbon oxides from the carbon surface [10]. This is a complex heterogeneous process, which includes several steps. First, the transportation of activating agent to the carbon surface, followed by diffusion of the activation agent into the pores. Next, the sorption of activation agent on the pore surface and the reaction with the carbon matrix. Then, the desorption of the reaction products from the pore surface and finally, the diffusion of the reaction products to the atmosphere [10]. It is important to stress that the physical activation method can also be referred to as a chemical activation process, due to the oxidation reaction taking place between the activation agent and the carbon surface.

The cost of precursors and the energy requirement related to the physical activation process has made air an interesting activation agent, in addition to low cost precursors or waste materials. In an economical perspective, air activation has several advantages, such as being free, low heat requirements and short processing time [12]. However, air activation is not widely applied due to the high reactivity of oxygen. This makes it difficult to control excessive carbon burn-off [12]. Therefore, the use of less reactive precursors, such as demineralised kraft lignin, is required in activation with air [12].

The chemical activation method is normally carried out as a one step process, where pyrolysis and activation take place simultaneously in the presence of a dehydrating agent such as potassium chloride, sulfuric acid or zinc chloride [32]. Compared to physical activation, chemical activation is normally carried out at lower temperatures (400-700°C) [21]. In this method, the carbon precursor is mixed with the dehydrating agent, introducing the chemical into the interior of the carbon precursor particles [10]. This restricts the formation of tars, while the chemical reacts with the thermal decomposition products from the precursor. This minimizes both the creation of volatile matter and the particle shrinkage in the carbon material [10]. Next, the chemical gets removed after the heat treatment, resulting in a large internal porosity within the carbon network [10]. Activation with potassium hydroxide is one of the most common activation agents in the chemical activation method. KOH is a stronger activation agent compared to CO_2 and hence, creates larger micropores (up to 2.1 nm) [38]. In fact, KOH is such a strong activation agent that it has the potential to destroy the original morphology of the carbon material [38].

By comparing the two activation methods, it is clear that the physical activation process is considered to be cheaper and more environmentally friendly compared to the chemical activation process. This is mainly due to the disposal issues of

toxic chemicals related to the chemical activation process [10]. After the chemical activation method, washing of the carbon is required in order to remove residual reactants as well as inorganic residue [21].

2.5 Chemical activation with CO_2

CO_2 activation is a process often used to increase the specific surface area and pore volume of carbon materials. The obtained activated carbon materials usually have high specific surface areas and pore volumes, with a very high fraction of micropores and ultramicropores. Micropores and ultramicropores are classified to have pore diameters smaller than 2 and 0.7-1.0 nm respectively [38]. Normally, CO_2 activation is carried out at high temperatures after carbonization in inert atmosphere.

During CO_2 activation, pores are generated by evaporation of volatile carbon and oxidation, in which CO_2 acts as an oxidizing agent. The endothermic reaction involved during the physical activation process is expressed in equation (2.1) [2].

$$C + CO_2 \rightarrow 2CO \qquad \Delta H = 173 \text{ kJ mol}^{-1} \tag{2.1}$$

In CO_2 activation, the yield decreases with increasing activation temperature because the increase in activation temperature promotes both the endothermic oxidation reaction and the release of volatile carbon [2].

One of the the main advantages of CO_2 activation is that the morphology of the carbon fibers are preserved, while significantly development of pore structures within the carbon matrix have occurred [38]. Compared to activation with KOH, which is a stronger activation agent than CO_2 and hence creates a larger specific surface area, has the potential to destroy the original morphology of the carbon material [38].

In the CO_2 activation process, the development of pore structure is mainly dependent on temperature and activation time. On average, the micropore volume can account for up to about 93% of the total pore volume of activated carbon fibers [38]. Thus, CO_2 activation carried out at high temperatures, normally between 750 to 900°C, can produce porous carbon structures with a high percentage of micropores, which are suitable as adsorbents in purification and separation processes [10].

2.6 Chemical activation with H_2O

Steam activation has proven to be one of the most effective methods in producing activated carbons with high surface area and controllable pore structure [4]. Steam activation is normally performed at elevated temperatures after carbonization of a carbonaceous material. This method provides good controllability of pore structure by adjusting the activation conditions such as activation temperature or activation time. The pore structure gets enhanced by partial oxidation of the carbonized material. [4]. In general, the average pore diameter and pore volume increase remarkably with increasing activation temperature [4].

As seen from equation (2.2), steam acts as an oxidizing agent and is able to remove carbon atoms from the carbon network [3].

$$C + H_2O \rightarrow CO + H_2 \qquad \Delta H = 117 \text{ kJ mol}^{-1} \tag{2.2}$$

The reaction is endothermic and is thermodynamically favored at high temperatures. In general, steam activation produces a wider pore size distribution compared to CO_2 activation. As previously described, CO_2 activation produces mainly microporosity, whereas steam activation provide larger developement of wide micropores and mesopores [4]. The reason why CO_2 creates mainly microporous structures is attributed to the better control of the activation process, where the carbon atoms are removed from the particle inside [27]. Therefore, both the creation of new pores and the enlargement of micropores are enhanced [27].

In the activation process CO_2 is less reactive than steam. This is due to CO_2 having a larger molecular size compared to H_2O [27]. Also, as seen from equation (2.1) and (2.2), the reaction between CO_2 and carbon is more endothermic than the reaction between steam and carbon. Hence, in order to achieve the same reactivity, higher reaction temperatures are required for the reaction between CO_2 and carbon [27].

In both CO_2 activation and steam activation, the porosity, pore size distribution and the nature of the internal surfaces can be controlled mainly by activation temperaure and activation time, but also by the gaseous environment as the partial pressure of the activating agent [21]. The surface area and pore volume are increased by a controlled carbon burn-off as the activating agent reacts with the carbon, in addition to elimination of volatile pyrolysis products [21]. The most important factor related to the quality of the activated carbon is possibly the degree of burn-off [21]. The level of burn-off is mainly controlled by activation temperature and activation time [21]. There is a trade-off between the degree of activation and the burn-off, in which a high level of activation is achieved by increased burn-

off [21]. Also, a high degree of activation is accompanied by a reduction in carbon strength, a lower density, a decrease in yield and pore widening [21].

2.7 Energy storage

Along with batteries and fuel cells, electrochemical supercapacitors are considered to be one of the most effective and practical appliance for electrochemical energy conversion and storage [22]. Attractive properties like high power density and long lifecycle have resultet in a great focus towards supercapacitors. Compared to regular capacitors, supercapacitors have higher energy density and are able to deliver a high amount of energy per unit time [22]. The specific energy of supercapacitors is, in fact, several orders of magnitude higher compared to conventional capacitors [21]. Hence, supercapacitors are very suitable and important in a wide range of applications which require a large energy pulse [22].

Compared to most batteries, supercapacitors have a higher specific power, however their specific energy is a bit lower [21]. The wide range in both specific energy and specific power, makes supercapacitors very versatile as a stand-alone energy supply. As seen from Figure (2.3), the unique combination of good specific energy and high specific power, permits supercapacitors to occupy a functional position between regular capacitors and batteries.

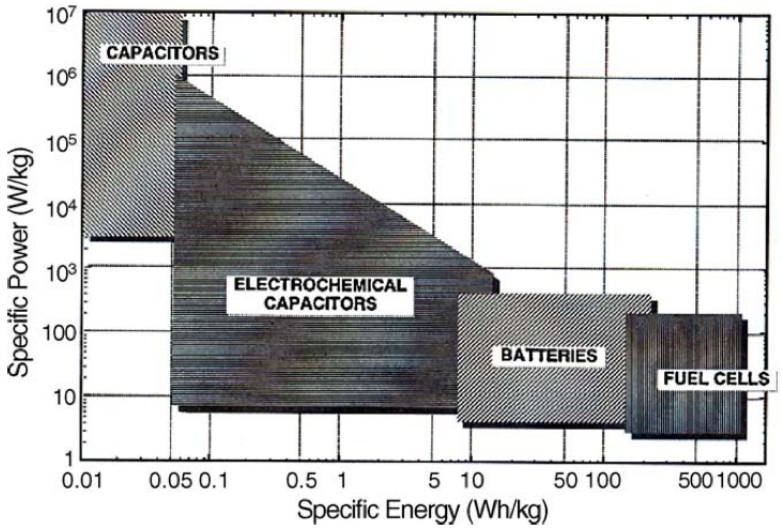

Figure 2.3: Specific energy and specific power of capacitors, supercapacitors (electrochemical capacitors), batteries and fuel cells. The indicated areas are only approximate guidelines [21].

The characteristics of supercapacitors complement the deficiencies of other

power sources, including batteries and fuel cells [21]. This makes supercapacitors especially useful, as they can be combined with batteries in a hybrid system [21]. Compared to batteries, supercapacitors have longer cycle-lifes and can be quickly charged and discharged, due to the mechanism of energy storage [21]. For electrical double-layer capacitors, the mechanism of energy storage is very fast, because it purely involves movement of ions to and from electrode surfaces. Batteries, on the other hand, have additional slow steps in the energy storage and delivery process, such as heterogeneous charge transfer and chemical phase changes. [21]. This difference in energy storage mechanism is the most important difference between a battery and a supercapacitor [22]. In batteries, storage of charge is accomplished by electron transfer that generates a redox reaction in the electroactive material according to Faraday´s law. In electrical double-layer capacitors, the charge storage process is nonfaradaic [22].

2.8 Supercapacitors

Supercapacitors are energy-storage devices that are well suited to rapidly store and release energy [21]. In general, there are three types of supercapacitors specifically electrical double-layer capacitors, pseudocapacitors and hybrid capacitors [31]. As the name suggests, electrical double-layer capacitors (EDLCs) store energy in the electrical double-layer located at the interface between the electrodes and the electrolyte [22]. As seen from Figure (2.4) the design and manufacture of EDLCs are similar to batteries, in which the EDLC is composed by two electrodes electrically isolated by a separator [22].

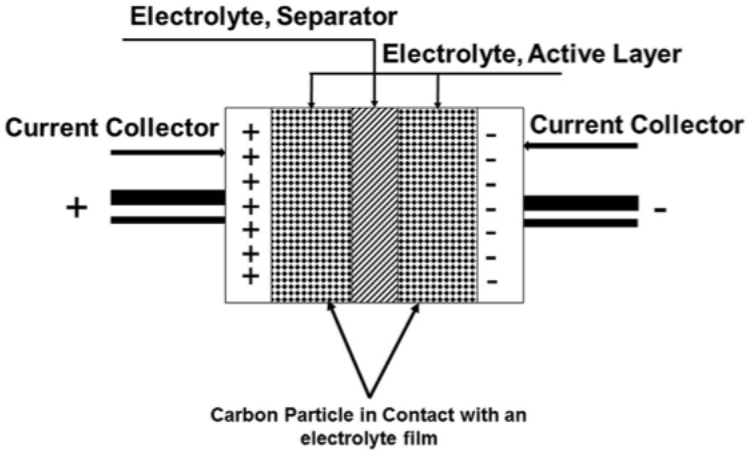

Figure 2.4: Characteristics of a single cell electrical double-layer capacitor [22].

Also, it can be seen from Figure (2.4) that the interface between the conduct-

ing solid particles, known as the active material, and the electrolyte is able to separate and store electrical charges. During Charging and discharge, electrical charges of opposite charge are stored at the interface at the two electrodes by accumulation [SC-1]. This process is known as a non-Faradaic process, in which the active material on the electrodes is not electrochemically active [SC-1]. In other words, there is no chemical reactions taking place on the electrode material, since this process does not include the charge transfer between the electrodes and the electrolyte [phd]. The capacitance of the EDLC is given by equation (2.3)

$$C = \frac{\epsilon \cdot A}{4\pi \cdot d} \tag{2.3}$$

where ϵ is the relative permittivity of the electrolyte, A is the surface area of the active electrode material and d is the thickness of the electrical double-layer [22]. As seen from equation 2.3, for a given electrolyte the surface area of the active material on the electrodes should be maximized. Thus, with a large surface area comes a large interface which is able to store a lot of electrical charges. Due to the charge storage mechanism of EDLCs, the cycling stability is usually very high with a potential of maintaining stability up to 10^6 cycles of charge and discharge. The main disadvantage of EDLCs is that the energy stored is relatively small [phd]. Charging and discharging of a positive electrode in an EDLC are represented in equation (2.4) and (2.5) respectively. Whereas charging and discharging of a negative electrode are represented in equation (2.6) and (2.7) respectively. Finally, the total charge/discharge cycle is represented in equation (2.8) and (2.9). Here, E_{s1} and E_{s2} represent the electrodes and // represents the interface between the electrodes and the electrolyte. [22]

$$E_{s1} + A^- \rightarrow E_{s1}^+ // A^- + e^- \tag{2.4}$$

$$E_{s1}^+ // A^- + e^- \rightarrow E_{s1} + A^- \tag{2.5}$$

$$E_{s2} + C^+ + e^- \rightarrow E_{s2}^- // A^- \tag{2.6}$$

$$E_{s2}^- // A^- \rightarrow E_{s2} + C^+ + e^- \tag{2.7}$$

$$E_{s1} + E_{s2} + A^- + C^+ \rightarrow E_{s1}^+ // A^- + E_{s2}^- // C^+ \tag{2.8}$$

$$E_{s1}^+ // A^- + E_{s2}^- // C^+ \rightarrow E_{s1} + E_{s2} + A^- + C^+ \tag{2.9}$$

Normally, as can also by seen from equation (2.4), (2.5), (2.6) and (2.7), the electrode where the electrical double-layer is formed by cation adsorption and the electrode where the electrical double-layer is formed by anion adsorption is referred to as the negative and positive electrode respectively [25]. Another class of supercapacitors is referred to as pseudocapacitors or faradaic supercapacitors. Here, the active material on the electrodes is electrochemically active and can directly store charge during charging [22]. Hence, the energy gets stored by charge transfer between the electrolyte and the electrodes, which includes oxidation-reduction reactions taking place on the electrode material [22]. This allows for charges to pass through the electrical double-layer, resulting in faradaic current passing through the supercapacitor [22]. In addition to oxidation-reduction reactions, two other faradaic processes take place at the electrodes. These are reversible adsorption processes and reversible electrochemical doping-dedoping, the latter occur in conductive polymer electrodes [22]. The electrochemical processes take place both at the surface of the electrode material and in the bulk of the electrolyte [22]. The chemical reactions taking place on the electrodes, result in greater capacitance and energy density compared to electrostatic supercapacitors. However, the cyclic stability of faradaic supercapacitors is not as good, due to the oxidation-reduction reactions at the electrodes [31]. Also, faradaic supercapacitors normally have lower power density than EDLCs, because faradaic processes are slow compared to non-faradaic processes [22]. Conductive polymers and metal oxides such as RuO_2 and MnO_2, are used as electrode material in faradaic supercapacitors [31].

Another class of supercapacitors is the hybrid capacitors. These supercapacitors use both faradaic and non-faradaic processes to store charges, which results in good cyclic stability [31]. There are usually three types of hybrid capacitors namely asymmetrical, composite and battery-type [31]. In the asymmetric electrode configuration, one electrode is composed by electrostatic carbon (EDLC electrode) and one electrode is composed by faradaic capacitance material (pseudocapacitor electrode) [22]. The main constituents of the composite electrode are conducting polymers with materials based on carbon and metal oxides [phd]. The battery-type electrode configuration includes a supercapacitor electrode and a battery electrode, which usually consists of metal oxides containing lithium [31].

2.8.1 Electrode materials

As previously described, the surface area of the active electrode material should be as large as possible in order to achieve a high specific capacitance. A large surface area can be obtained by using porous electrode materials.

Carbon materials are desirable electrode materials for EDLCs because they are available with high surface areas. Hence, activated carbons with high porosity are normally used for EDLCs [30]. However, in addition to surface area, the pore structure and pore size distribution are also important for the performance of EDLCs [30]. This is due to the fact that micropores, which have a great effect on specific surface area, do not provide enough space for the solvated ions in the electrolyte. Hence, micropores does not contribute much to the size of the electrical double-layer [30]. Therefore, the presence of mesopores which provide less resistance for transfering ions is considered important [30]. The energy density and power density of EDLCs are dependent on the pore size distribution of the electrode material. Hence, control of pore structure of carbon materials is important to obtain desirable performance. Moreover, the effect of pore structure on the performance of EDLCc is complex and currently under discussion [30].

Activated carbons often have many functional groups containing oxygen, which includes ketone, carbonyl and phenolic groups, as well as nitrogen-containing groups [22] [23]. Hence, oxidation-reduction reactions between the electrolyte and the oxygen and nitrogen functional groups can give an increase in capacitance by providing pseudocapacitance [23]. This additional pseudocapacitance can make up about 5 - 10% of the total capacitance [22]. However, the drawback of these functional group is that the oxidation-reduction reactions increase the internal resistance [22].

Carbon materials also exhibit other chemical and physical properties that are desirable for electrode materials, specifically high conductivity, high corrosion resistance, high thermal stability, compatibility in composite materials and controllable pore structure [21]. In addition to a higher surface area, activated carbons have a relatively low cost compared to metal oxides and conducting polymers. However, conductive polymers and metal oxides have normally higher conductivity than activated carbons [22]. Also, carbon materials do not contain heavy metals, which is environmentally friendly [23].

2.8.2 Electrolytes

The performance of the supercapacitor is, in addition to the electrode material, also dependent on the electrolyte. Mostly, three different types of electrolytes are used in supercapacitors specifically aqueous electrolyte, organic electrolyte and ionic liquids. Desirable properties of electrolytes include wide operating voltage window, electrochemical stability, high concentration of ions, small ionic radius, low viscosity and volatility, low resistivity, low toxicity, low cost and last but not least high purity [22].

Advantages of aqueous electrolytes, which include KOH, Na_2SO_4, H_2SO_4 and NH_4Cl, is high conductivity, high ionic concentration, low resistance and low cost [22] [31]. The major drawback of aqueous electrolytes is the small operating voltage window which limits the energy and power density of the supercapacitor [22]. The narrow operating voltage window of aqueous electrolytes, about 1 V, is a result of the thermodynamic decomposition voltage of H_2O at 1.23 V [31].

Organic electrolytes possess a wider operating voltage window up to 2-3 V, which results in higher specific energy [22] [31]. However, main limitation of organic electrolytes is that the water content can not exceed 3-5 ppm. Also, the specific power could be lower because of the higher electrical resistivity of organic electrolytes compared to aqueous electrolytes [31]. Examples of widely used solvents are propylene carbonate and acetonitrile [22].

Ionic liquids have an even higher operating voltage window of 4-4.5 V [22]. Other advantageous properties include high thermal and chemical stability, good electrical conductivity and low vapor pressure [31] [22]. The main disadvantages of both organic electrolytes and ionic liquids are high cost, flammability and toxicity [31].

Other electrolytes that have recieved increased attention are polymer electrolytes based on polyethylene oxide, polyacrylonitrile and poly(methyl methacrylate) and gelled electrolytes [31]. Supercapacitors assembled with polymer electrolytes are very invulnerable against deformation, but these electrolytes usually have low ionic conductivity [31]. Gelled electrolytes fabricated by polyvinyl alcohol and H_2SO_4 have a very high ionic conductivity as well as they are environmentally friendly [31]. However, stability and mechanical strength are issues that need to be handled [31].

2.8.3 Configuration of supercapacitors

There are two types of configurations of supercapacitor cells, namely the symmetric and asymmetric type. The configuration depends on the materials of the positive and negative electrodes, in which the symmetric type is composed of the same electrode material on both electrodes and the asymmetric type is composed of different materials on each electrode [31]. For the symmetric configuration of supercapacitors, the specific energy is relatively low. This is due to the limited operating voltage window, especially if aqueous electrolyte is used. The disadvantage of relatively low specific energy is overcome for the asymmetric supercapacitor, because the different electrode materials can increase the operating voltage

window. For an asymmetric supercapacitor with a transition metal oxide as the positive electrode and activated carbon as the negative electrode, the increase of operating voltage window is accomplished by the reversible electrochemical hydrogen storage in the pores of activated carbon [31]. Hence, the configuration of supercapacitors is an important part of the supercapacitor design in regards to electrochemical performance, particularly if aqueous electrolyte is used.

2.8.4 Performance tests

Several techniques can be used to determine the specific capacitance of a supercapacitor cell. A unit cell test can be used to determine the specific capacitance for a two-electrode system and a half-cell test can be used for a three-electrode system [22]. The electrodes are usually constructed by mixing the active material with a conductive agent, such as acetylene black, and a binder, such as polytetrafluoroethylene (PTFE) or polyvinylidene fluoride (PVDF) [25]. Next, a compression molding press is used to form a tablet, which is pressed on a collector mesh or foil [25]. The mass of the active material is required to be known and ideally the electrode volume should be determined. A two-electrode system is recommended when examining the performance, because this system is key to estimate the power density, the energy density and the cyclic stability of the cell. Usually, the potential difference between two equal electrodes which is separated by a separator, is monitored and controlled. Theoretically, for a symmetric two-electrode system, the total cell capacitance in Fg^{-1} is 1/4 of the capacitance of a single electrode measured in a three-electrode system [25]. The capacitance must always be based on the total mass of active material on both electrodes [25]. In the literature, a significant amount of capacitance values are indistinctive whether they are total cell capacitances or capacitances of a single electrode. Also, the specific capacitance values found from literature are not always consistent, mostly due to the experimental methods used to obtain them [22]. The capacitance of a single electrode determined from a two-electrode system does not match the capacitance determined from a three-electrode system. This is due to the difference in sizes between the solvated cation and anion, and the different potential changes of positive and negative electrodes during the charge and discharge measurements [25].

For a three-electrode system, the electrode performance is usually investigated by cyclic voltammetry (CV), galvanostatic chronopotentiometry (GCP) and electrochemical impedance spectroscopy (EIS) [25]. In the case where only the electrical double-layer constitutes the capacitance, the CV curves have a rectangular shape. Here, the capacitance (C) can be estimated from the current density at the middle point of the measured potential range (I) and the potential scan rate (r), as C = I/r [25]. The potential range (ΔV) applied depends on the type of electrolyte. In

the case where also the pseudo-capacitance contributes to the capacitance, the CV curves are not always rectangular in shape. Therefore, when estimating the capacitance in this case, the point of potential should be selected case-by-case [25]. Also, when the supercapacitor exhibits pseudo-capacitance, the CV curves become distorted and more asymmetric when the scan rate is increased. The total electric charge (Q) is obtained by integrating the CV curve and is often used to estimate the capacitance as C = Q/(2ΔV) [25]. In general, a high performance is obtained at low scan rates, since the capacitance decreases with increasing scan rates [25].

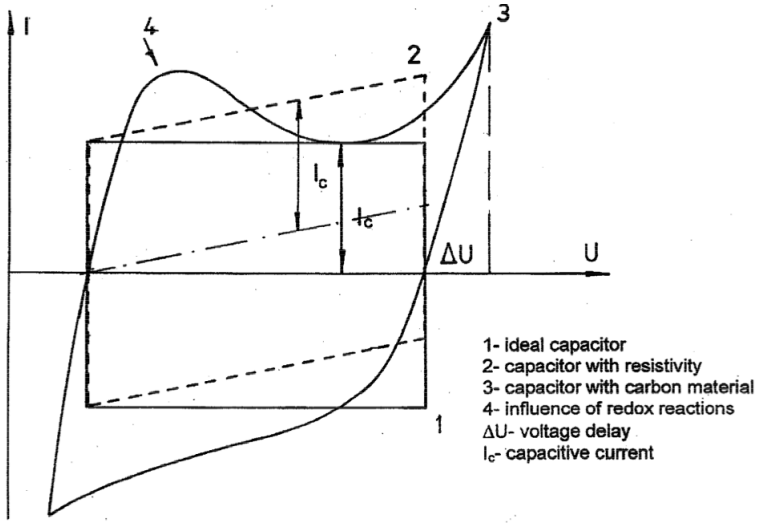

Figure 2.5: Typical charge/discharge CV characteristics of a supercapacitor [24].

As seen from Figure (2.5), an ideal electrical double-layer behavior of an electrode material is expressed as a rectangular shape of the CV curve. Here, the capacitance is purely electrostatic and the current is independent of potential. Also, upon a reversal of the potential sweep, the sign of the current is immediately reversed [24]. Figure (2.5) also shows the characteristic shape of the CV curve for electrode materials with pseudo-capacitance properties, in which reversible redox peaks connected with pseudo-faradaic reactions are significant [24]. Here, the accumulated charge in the supercapacitor is heavily dependent on the electrode potential. The characteristic delay of potential during the reversing the potential sweep is directly related to a kinetically slow process involved during charging the pseudo-capacitance [24].

In the GCP method, the potential of chronopotentiograms (V) changes linearly with time at constant current density, when the capacitance originates from the electrical double-layer only. Here, the capacitance is given by the slope of dV/dt, as C = I/(dV/dt) [25]. When pseudo-capacitance contributes to the capacitance, the

chronopotentiograms deviate from the linear trend and the capacitance is often estimated as C = I $\cdot t_T/\Delta$V. Here, t_T is the total time for either positive or negative process and ΔV is the potential difference after correcting an IR drop. The IR drop is estimated from the initial jump of the chronopotentiograms [25].

EIS measurements are usually performed at the open-circuit potential by introducing a small amplitude of alternative potential over a broad range of frequencies (f) [SC-4]. The impedance (|Z|) is plotted against the frequency and the capacitance can be estimated by using a linear part of log |Z| against log f, also known as a Bode plot, as C = $1/(2\pi f|Z|)$ [25]. A plot where the imaginary part of impedance is plottet as a function of the real part of impedance is referred to as a Nyquist diagram. This diagram can be used to estimate the resistance, in which a charge transfer resistance is given by the diameter of a semicircle. This method can not give precise values of resistance, since perfect semicircles are not normally obtained [25].

For a two-electrode system, the electrode performance is usually examined by galvanostatic charge/discharge (GCD) measurements. The capacitance is given by the current density, the discharge time (t) and the voltage range (U), as C = I·t/U [31]. The most widely used indexes of performance are capacitance per mass and capacitance per volume, although the volume is not easy to estimate accurately for laboratory scale electrodes [25]. The capacitance values per mass should be evaluated carefully, since the bulk density affects the power and energy densities of practical capacitators [25]. Also, it is recommended that both three-electrode and two-electrode cell measurements are conducted for the same active material [25].

2.9 Thermal Gravimetric Analysis

Thermogravimetric analysis (TGA) is a method carried out in order to investigate the change in weight with respect to change in temperature [15]. This method is dependent on critical measurements, such as weight, time and temperature [15]. The sample is exposed to a controlled atmosphere and the sample mass is measured as a function of temperature or time [33]. The mass of the sample can be recorded at constant, increasing or decreasing temperature, and the temperature ranges usually from room temperature to 1000°C. The atmosphere can be inert, oxidizing or reducing, and is generated by a purge gas flowing through a balance that holds the sample [33]. TGA is typically combined with evolved gas analysis measurements such as gas chromatography or mass spectroscopy, since TGA alone does not provide information about the material lost during the heat treatment.

The enthalpi changes during the measurement is expressed by the DSC curve. This curve can discover reactions and transitions that do not result in changes in weight [33]. This method can provide information about thermal stability, composition and adsorption capacity [33]. Information about adsorption capacity can be obtained by gravimetric adsorption, where an additional gas, such as CO_2, is added to the atmosphere. In this method, the amount of adsorbed gas is measured by continuously weighing the sample [9].

Currently, TGA is a preferred method in thermal and kinetic studies because of its simplicity and the dependency of few observations to determine the kinetics for the whole temperature range [15]. Also, the relation between weight and temperature is convenient when creating procedures for catalysts regeneration and other processes relevant in the reactor [9]. On the other hand, some of the disadvantages regarding the TGA method, include the ability to measure only small amounts of sample (10-20 mg), low heating rate and being time consuming [15].

2.10 Mass spectrometry

Mass spectrometry is often combined with TGA. TGA is an important method for investigating pyrolysis kinetics and can provide accurate for global mass loss kinetics. However, it can not analyze pyrolysis products qualitatively [14]. TGA coupled with mass spectrometry enables identification of gaseous species formed during various heat treatments, such as pyrolysis and activation processes [13].

In mass spectroscopy, volatile species are identified by their mass-to-charge ratio [33]. Thus, molecules are distinguished based on the mass and the charge of the ions they generate in an ion source [5]. Also, it is possible to detect compounds at very low concentrations in complex mixtures [6]. In general, MS involves four instrumental stages, namely introduction of sample, ionization, analysis of generated ions and detection.

The first stage involves the introduction of vaporized sample to the ionization chamber. This is easily realized for organic materials, due to the developed vapor pressure during heating [6]. In the next process, gas molecules are ionized in a vacuum chamber when colliding with an electron beam. The analysis of generated ions can be carried out with several techniques, including time of flight, electrostatic and Fourier-transform [6]. In the time of flight method, the sudden use of a voltage drives the charged molecules to travel through a vacuum chamber. With the assumption that the electrostatic charge is equal for all ions, the kinetic energy which is transferred after the voltage pulse is equal in each

particle [6]. Thus, the difference in ion mass results in different speed, which results in different travelling times. This method has a mass accuracy of 10^{-5} [6]. In the electrostatic method, a quadrupole retains all ions, except for ions with a particular mass range [6]. In the Fourier-transform method, the electrostatically accelerated ion jet is exposed to a magnetic field, which results in ions rotating in circular paths corresponding to their mass-to-charge ratio [6]. These ion movements produce radiofrequency signals, which are analyzed by Fourier transform and a mass spectrum can be obtained. This method provides an accuracy of 10^{-6} [6].

2.11 The BET Method

The BET method is frequently used in order to obtain information about physical properties of materials, such as specific surface area, total pore volume, mesopore volume, micropore volume and pore size distribution [9]. This method is based on physisorption of nitrogen at 77 K and the specific surface area is obtained by measuring the number of N_2 molecules adsorbed at monolayer coverage. Information about the specific surface area can be obtained by the Brunauer Emmett and Teller (BET) isotherm because it provides the correlation between the volume of N_2 adsorbed at a given partial pressure and the volume adsorbed at monolayer coverage [9]. The specific surface area can be calculated based on the fact that each N_2 molecule occupies 0.162 nm^2 of the surface at a temperature of 77 K [28].

The BET isotherm is obtained by separating the surface into regions covered by various adsorbate layers [28]. The BET equation can be seen from equation (2.10),

$$\frac{P}{V_a(P_0 - P)} = \frac{1}{\chi V_0} + \frac{(\chi - 1)}{\chi V_0}\frac{P}{P_0} \tag{2.10}$$

where P_0 is the equilibrium pressure of the condensed gas, P is the adsorption pressure, V_0 is the volume of gas adsorbed in the first monolayer, V_a is the total volume of adsorbed gas and χ is the ratio of adsorption heats of first and next molecular layer [9]. A straight line with a slope equal to $(\chi - 1)/\chi V_0$ that intercepts the y-axis at $1/\chi V_0$ can be obtained by plotting $P/[V_a(P_0 - P)]$ against P/P_0. Next, V_0 can be converted to the number of molecules adsorbed in the first monolayer by the relationship $N_0 = PV_0/k_BT$. Then, the total surface area can be determined using $A = N_0A_0$, where A_0 is the area of each nitrogen molecule [28]. Finally, by dividing the total surface area by the mass of the sample, yields the specific surface area.

The BET surface area should be determined at relative pressures between 0.05 and 0.3 P/P_0, as this pressure range provides the most accurate result [9]. There

are several assumptions that need to be taken under considuration in order to obtain a valid BET isotherm. These include that the rate of both adsorption and desorption in any adsorption layer is equal and that molecules in the first layer adsorb on equivalent adsorption sites. Also, that the heat of adsorption is equal for the second and consecutive layers and that the heat of adsorption for the first layer is independent of the other layers. In addition, the surface must be constant during the adsorption process [9].

The Kelvin equation can be used to determine the different type of pores and the pore size distribution inside a material. The Kelvin equation can be seen from equation (2.11),

$$ln\frac{P}{P_0} = \frac{2\sigma V cos\theta}{rRT} \tag{2.11}$$

where P is the measured pressure, P_0 is the saturation pressure, T is the absolute temperature, R is the gas constant, V is the molar volume of liquid nitrogen, θ is the contact angle, σ is the surface tension of liquid nitrogen and r is the pore radius [9]. During the desorption process, capillary condensation occurs in small pores. This phenomenon can be described by the Kelvin equation [28]. The desorption process requires lower pressure compared to the adsorbtion process, because of capillary condensation taking place in mesoporous materials [9]. The Barrett-Joyner-Halenda (BJH) method uses the Kelvin equation and can be applied to determine the pore size distribution of a material. This method relates the pore size to the amount of nitrogen removed, as the relative pressure decreases [44].

One of the limitations regarding the BET method is that multilayer adsorption can not occur in microporous materials. This is because of space limitations inside micropores [9]. !!!t-plot method!!!

2.12 Scanning Electron Microscopy

Properties such as morphology, particle size, crystallography and chemical composition can be, when combined with an X-ray detector, examined by scanning electron microscopy (SEM) [28]. In this method, a thin electron beam scans the surface of the sample and detects the yield of secondary or backscattered electrons as a function of the location of the primary beam [28]. Backscattering is a result of electrons getting scattered back when colliding with atoms in the sample. As the mass of the atom increases, backscattering gets more effective. These electrons give information about the chemical composition of the sample. This is because heavy elements scatter electrons more efficiently, making them appear brighter in the image [28].

Secondary electrons mainly have low energies and get emitted by atoms located on the surface of the sample [28]. The contrast is partly generated by the surface orientation, due to the fact that the parts of the surface facing the detector appear brighter compared to the parts oriented away from the detector. Hence, the contrast is generated by both the topology and the chemical composition of the surface [28].

2.13 Energy-dispersive X-ray spectroscopy

Energy-dispersive X-ray analysis (EDX) is a technique frequently applied in order to investigate the chemical composition of a sample[28]. This method is local, meaning that specific parts of a sample can be examined. EDX is normally combined with transmission electron microscopy (TEM) or SEM. In this method, emitted X-rays are detected while the sample is exposed to the electron beam. The chemical composition of a selected part of the sample can be examined due to the fact that each element emits X-rays with a characteristic wavelength [28]. However, light elements such as hydrogen, lithium and beryllium are not possible to detect, due to their poor scattering of electrons.

3 Experimental

3.1 Synthesis of carbon spheres

Resorcinol-Formaldehyde polymer spheres (RF polymer spheres) were synthesized by ultrasonic irradiation (SONOPULS HD 3200, 200W, Bandelin, Germany) for 5 minutes. Initially, resorcinol (1 g, 99%, Sigma-Aldrich) was mixed with deionized water (140 ml) in a beaker (250 ml). Prior to adding aqueous ammonia (0.75 ml, minimum 25% solution, VWR), the resorcinol was dispersed by ultrasonic irradiation for 1 minute at 30% power. Next, formaldehyde (1 ml, 37 wt.% in H_2O, Sigma-Aldrich) was added and the mixture was treated with ultrasonic irradiaton in room temperature for 5 minutes at 30% power.

3.1.1 Washing and separation

The solution of RF polymer spheres were centrifuged at 1100 rpm for 20 minutes. Next, the solid RF polymer spheres were separated and mixed with deionized water. In order to enhance the washing effect, the mixture was exposed to ultrasonic irradiation for 10 minutes. Next, the mixture was centrifuged and the same procedure described above was carried out twice. After the third separation, the solid RF polymer spheres was dried in room temperature for 12 hours.

3.1.2 Carbonization

The desired amount of RF polymer spheres was loaded into a calcination reactor and heated inside a furnace in a flowing nitrogen atmosphere. In order to maintain the morphology of the RF polymer spheres, the heating rate was set at 1.5°C min^{-1}. The cooling rate was set at 10°C min^{-1}. The maximum temperature was held for a 2 hours dwell.

3.2 Synthesis of polyaniline

Polyaniline (PANI) fiber was prepared by an oxidation reaction between aniline monomer and ammonia peroxidisulfate in an acidic environment. Aniline (7.5 g, Sigma-Aldrich) was dissolved in HCl (1 M, 250 ml, Sigma-Aldrich) in a beaker (500 ml) and ammonia peroxidesulfate (4.6 g, Sigma-Aldrich) was dissolved in HCl (1 M, 250 ml) in a beaker (250 ml). Next, the ammonia peroxidesulfate solution was added to the aniline solution under rapid stirring (500 rad min^{-1}) and stirred for 20 minutes. The resulting PANI fibers were separated by filtration, using a total of three filters where every filter was washed with distilled water until the filtrate was equal to pH 7. Finally, the PANI fibers were dried at 80°C for 12 hours.

3.3 Carbonization of polyaniline

The desired amount of PANI fibers was loaded into a calcination reactor and heated inside a furnace under flowing nitrogen. The heating rate was set at 20°C min^{-1} and the carbonization temperature (600, 650 or 700°C) was maintained for 2 hours dwell. The cooling rate was set at 10°C min^{-1}.

3.4 Physical activation with CO_2

The desired amount of carbonized PANI or carbon spheres was loaded into a calcination reactor and heated inside a furnace to a maximum activation temperature ranging from 750 to 1000°C. The heating and cooling rate were set at 5 and 10°C min^{-1}, respectively. The duration of activation at the maximum temperature was held at a dwell varying from 1 to 5 hours. CO_2 and/or argon was introduced to the reactor at 25°C as the temperature program was turned on. The CO_2 flow was turned of at the point the activation was finished and the furnace began cooling. Also, different partial pressures of CO_2, varying from 0.2 to 1.0 $P_{CO_2}P_{total}^{-1}$, was applied in the activation, with a constant total flow rate of 100 ml min^{-1}.

3.5 Physical activation with CO_2 and H_2O

The desired amount of carbonized PANI or carbon spheres was loaded into a calcination reactor and heated inside a furnace to a maximum activation temperature ranging from 850 to 950°C. As for the CO_2 activation, the heating and cooling rate were set at 5 and 10°C min^{-1}, respectively. In this activation process, the activation time was varied from 1 to 3 hours and the partial pressure of CO_2 was varied from 0.6 to 1.0 $P_{CO_2}P_{total}^{-1}$. CO_2, steam and/or argon were introduced to the reactor at 25°C as the temperature program was turned on. Steam was introduced to the reactor by having CO_2 and/or argon pass through a water saturator [H2O-1] [H2O-3]. The amount of steam was controlled by heating the water in an oil bath at different temperatures, ranging from 25 to 90°C. At the end of the activation process, the CO_2 flow was stopped and the product was cooled under a flowing argon atmosphere. The steam was removed by using a by-pass, which was activated at the end of the activation process.

3.6 Characterization

The BET surface area, total pore volume, mesopore volume, micropore volume and pore size distribution (pore width ≥ 1.5 nm) were examined by nitrogen adsorption and desorption isotherms at 77 K. This was done with a Tristar 3000 surface area and porosity analyser instrument from Micrometrics. Prior to analysis, the samples (50-100 mg) were degassed at 200°C for 12 hours, or until the pressure reached 100 mTorr, using a VACPREP 061 degas instrument. The adsorption/desorption isotherms were measured at relative pressure ranging from 0 to 1 P/P_0 and the BET surface areas were determined by the Brunauer-Emmet-Teller (BET) equation using relative pressure between 0.05 and 0.3 P/P_0 [H2O-2]. The total pore volumes were determined by the amount of nitrogen adsorbed at a relative pressure of 0.99 P/P_0 and the t-plot method was used in order to calculate the micropore volumes [H2O-2] [CO2-1]. The mesopore volumes were calculated as the difference between the total pore volumes and the micropore volumes. [CO2-4]. The pore size distribution (pore width ≥ 1.5 nm) was determined by non-local density functional theory (NLDFT) [H2O-1].

The pore size distribution of narrow micropores (0.5 nm ≤ pore width ≤ 1.5 nm) was determined with density functional theory (DFT) by performing CO_2 adsorption and desorption at 0°C [CO2-2].

Scanning electron microscopy (SEM) was used to investigate the morphology of the carbon materials, both after the carbonization and activation procedure. A Hitachi S-5500 microscope (S(T)EM) with a secondary electron (SE) detector was

used to obtain the SEM images at different magnification. Prior to the measurement, a small amount of sample was loaded on a conductive tape and mounted on a sample holder. The acceleration voltage was set to be 10 kV and the beam current was set to be 10 μA.

Energy-dispersive X-ray analysis (EDX) was used to examine the elemental composition of activated carbon fibers. The elemental composition was obtained by using energy dispersive spectroscopy (EDS) coupled with SEM. In this method, the acceleration voltage and beam current were set to be 10 kV and 20 μA, respectively. Next, the measuring mode was switched to analysis and the conductive lens was reduced in order to increase the electron count.

Thermal gravimetric analysis (TGA) was carried out in order to investigate the reactivity of carbon fibers derived from PANI during the CO_2 activation process. In this method, a small amount of carbon fibers (10-20 mg) was put in a crucible and placed on a balance. The reactivity was indicated by the weight loss during the activation process. The activation time was 3 hours at different activation temperatures and the heating rate and cooling rate was set to be 5 and 10°C min^{-1}, respectively. The atmosphere was a mixture of CO_2 and argon at a partial pressure of 0.8 and 0.2, respectively. The total flow rate was 100 ml min^{-1}. The CO_2 was removed after three hours of activation and the activated carbon fibers were cooled in an argon atmosphere.

Mass spectrometry (MS) combined with TGA was used in order to examine the gaseous species formed during the CO_2 activation process. The formation of CO and the consumption of CO_2 were investigated at different activation temperatures. In addition, the release of nitrogen atoms through the formation of nitrogen containing gases, such as NO, NO_2, N_2O_3 and NH_3 was examined during activation at various temperatures. Activated carbon fibers prepared with the combined CO_2 and steam activation process was subjected to a one hour heat treatment at 950°C in an argon atmosphere. In this process, the release of oxygen atoms through the formation of CO and CO_2 was investigated. The flow rate of argon was set to be 50 ml min^{-1} during the whole heat treatment. The heating and cooling rate were set to be 5 and 10°C min^{-1}, respectively.

3.7 Electrochemical measurements

The active materials on the electrodes were manufactured by milling the activated carbons with 8 wt.% polytetrafluoroethylene (PTFE solution, Sigma-Aldrich), which acted as a binder and 20 μL ethanol. The electrodes were prepared by loading approximately 6 mg of the electrode active material on two nickel foam disks (Alfa

Acsar), which resulted in an equal mass loading of approximately 1.7 mg cm^{-2} on each electrode. Next, the activated carbon-PTFE mixture on top of the nickel foam disks was pressed into the nickel foam at 6 MPa for 2 minutes. Then the resulting electrodes were dried in a vacuum oven at 120°C for 12 hours before assembling the supercapacitor cell.

After the drying, the electrodes were weighted in order to ensure equal mass loading on the electrodes. The electrolyte was neat ionic liquid, 1-ethyl-3-methylimidazolium tetrafluoroborate ($EMIMBF_4$) and a 25 μm thin microporous monolayer membrane (Celgard, 3501) was used as a separator. The supercapacitor cell was assembled in a glove box with an argon atmosphere, where the concentration of oxygen and water was below 0.1 ppm. A Split Test Cell (MTI, 20 mm) was used to fabricate a symmetric supercapacitor where two electrodes with same mass loading where separated by a separator and 20 μL of electrolyte was added to both side of the separator. Prior to the electrochemical performance tests, the finished supercapacitor cells were stabilized at room temperature for a duration of 12 hours.

The electrochemical performance of the supercapacitor cells were investigated by cyclic voltammetry (CV), frequency response analysis, galvanostatic charge-discharge tests (GCD) and cycling stability tests. CV and frequency response analysis were performed on a Princeton VersaSTAT potentiostat analyser. CV measurements were carried out with a voltage window from 0 to 4 V with various scan rates of 0.05, 0.1, 0.2 and 0.3 Vs^{-1}. Frequency response analysis was performed with an amplitude of 5 mV RMS and a start and end frequency of 10^5 Hz and 0.01 Hz respectively. GCD tests and cycling stability tests were performed on a MTI 8-channel battery analyser. GCD tests were carried out with a wide voltage window of 4 V and different current densities ranging from 0.1 to 4 Ag^{-1}. Cycling stability tests were performed with a current density of 1 Ag^{-1}. All of the electrochemical performance tests were done at 25°C.

The GCD curves were used to obtain the specific capacitance of a single electrode. The specific capacitance of a single electrode was calculated using equation (3.1)

$$C_{sp} = \frac{4 \cdot I \cdot \Delta t}{m \cdot V} \tag{3.1}$$

where C_{sp} is the specific capacitance of one electrode (F g^{-1}), I is the discharge current (A), Δt is the discharge time (s), m is the total mass of the active material on both electrodes (g) and V is the voltage change during the discharge process (V) excluding the voltage drop at the starting point of the discharge process. In additon, the specific energy and the average specific power of the supercapacitor

were calculated by equation (3.2) and (3.3) respectively.

$$E_{sp} = \frac{C_{sp} \cdot V^2}{8} \tag{3.2}$$

$$P_{sp} = \frac{E_{sp}}{\Delta t} \tag{3.3}$$

4 Results and discussion

4.1 Carbonization yield

Sample	Carbonization temperature [°C]	Yield [%]
CS500	500	68.0
CS600	600	57.5
CS750	750	52.5

Table 4.1: Carbonization yield of carbon spheres.

Figure (4.1) shows the carbonization yield of carbon spheres carbonized at different temperatures. The carbonization yield of PANI was also reduced when increasing carbonization temperature was used. The carbonization yield of PANI at an carbonization temperature of 650°C, was 51.2 wt.%. As would be expected, the carbonization yield decreases with increasing carbonization temperature, as volatile components and heteroatoms are released at increasing temperatures [7].

4.2 Chemical activation with CO_2

4.2.1 Carbonization temperature

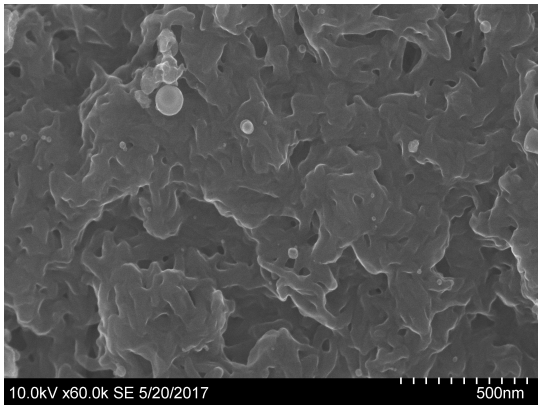

(a) P600

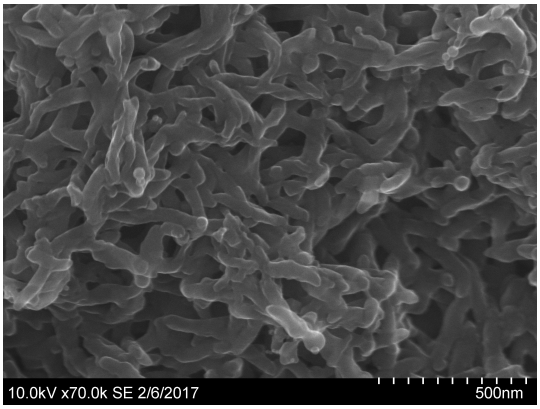

(b) P650

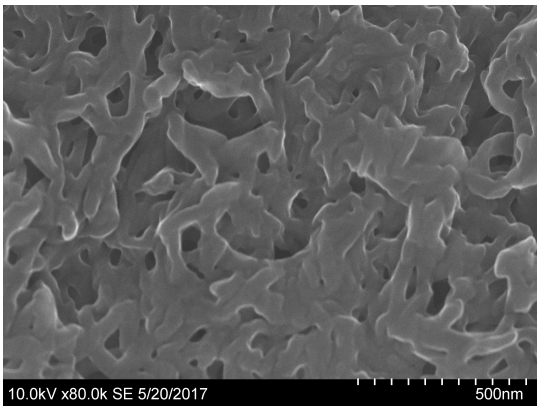

(c) P700

Figure 4.1: SEM images of carbon fibers derived from polyaniline prepared with carbonization temperatures ranging from 600 to 700°C.

Figure (4.1) shows the morphology of carbonized polyaniline obtained with carbonization temperatures of 600, 650 and 700°C. As can be seen, a carbonization temperature of 600°C results in a collapsed structure, while a carbonization temperature of 650°C results in a stable macroporous structure like the original polyaniline fiber structure. As the carbonization temperature is increased to 700°C, the amount of macropores is reduced compared to the structure obtained with a carbonization temperature of 650°C. A carbonization temperature of 650°C results in a fiber structure that possesses many hundred-nm-scaled three-dimensional oriented macropores, with an average fiber thickness of about 50 nm.

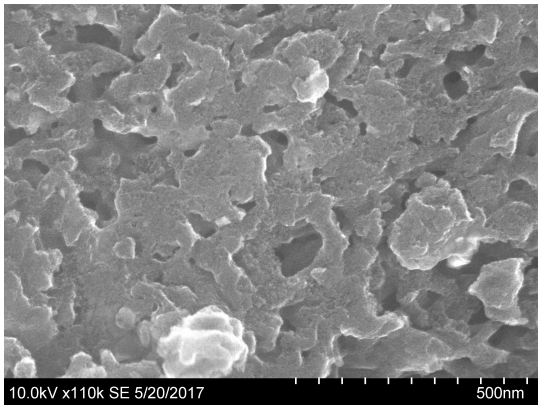

(a) P600a950

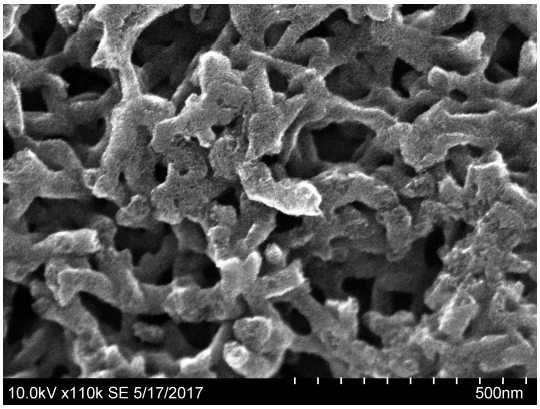

(b) P650a950

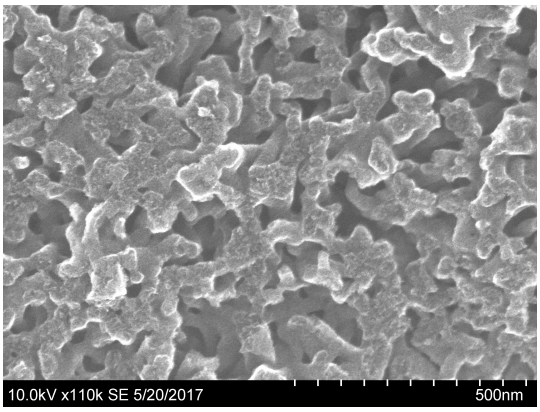

(c) P700a950

Figure 4.2: SEM images of activated carbon fibers derived from polyaniline prepared with different carbonization temperatures and an activation temperature of 950°C. The activation time was set to be 3 hours.

Figure (4.2) shows activated carbon fibers obtained with different carbonization temperatures and equal activation temperature. Clearly, it can be seen that the morphology obtained after the carbonization process has a large impact on the final fiber structure after the activation process. Also, it can be seen by comparing Figure (4.1b) and (4.2b) that the activation process has reduced the fiber thickness to about 40 nm, and more notably the fiber length has decreased. The fibers are bridged and linked together, forming a macroporous framework also after activation. Also, the macroporous structure obtained with a carbonization and activation temperature of 650 and 950°C has a thin average framework thickness, which can result in short ion diffusion distances when the macropores are filled with electrolyte [xue].

Properties	P600a950-3h	P650a950-3h	P700a950-3h
S_{BET} [m^2/g]	1508.9	1927.7	1295.8
V_T [cm^3/g]	0.985	1.151	0.861
V_{micro} [cm^3/g]	0.515	0.675	0.513
V_{meso} [cm^3/g]	0.470	0.476	0.348
V_{meso}/V_T [%]	47.7	41.4	40.4
V_{micro}/V_T [%]	52.3	58.6	59.6
Burn-off [wt.%]	65.6	67.5	57.1

Table 4.2: Physical properties of activated carbon fibers derived from polyaniline prepared with different carbonization temperatures and an activation temperature of 950°C. The activation time was set to be 3 hours.

As seen from Table (4.2), in addition to having the most homogeneous marcoporosity, a carbonization and activation temperature of 650 and 950°C also results in the highest BET surface area. In addition, these temperatures also produce the highest total pore volume, mesopore volume and micropore volume. This could be explained by the fact that lower carbonization temperatures gives more amorphous carbons which makes them more reactive in the activation process. The reason why a carbonization temperature of 600°C results in a lower BET surface area compared to a carbonization temperature of 650°C, could be that the structure had collapsed after the 600°C carbonization making the carbon less accessible for reaction during the activation process.

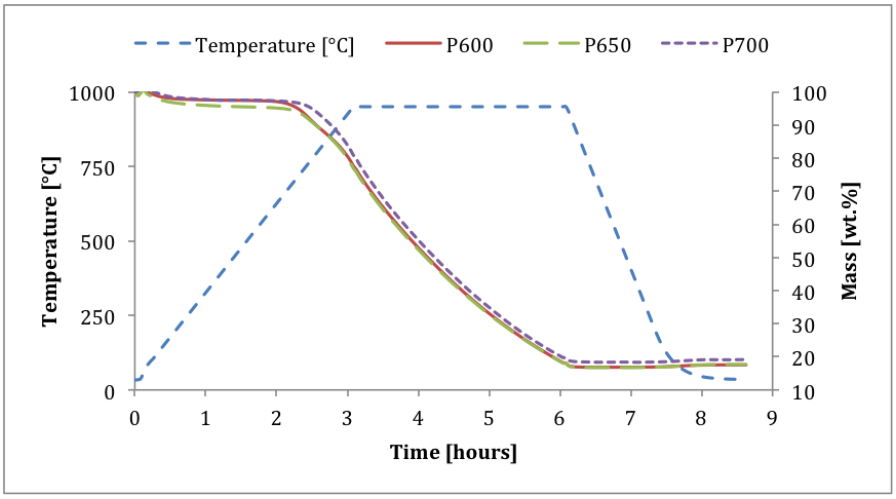

Figure 4.3: Thermal gravimetric analysis of CO_2 activation at 950°C of precarbonized polyaniline at different carbonization temperature.

The mass loss during the CO_2 activation process for the different carbonization temperatures is shown in Figure (4.3). The carbon obtained by a carbonization temperature of 700°C show the smallest amount of mass loss during the activation, which is reasonable due to the lower reactivity of carbons carbonized at higher temperatures. However, the difference in mass loss for carbonization temperatures of 600 and 650°C is indistinguishable.

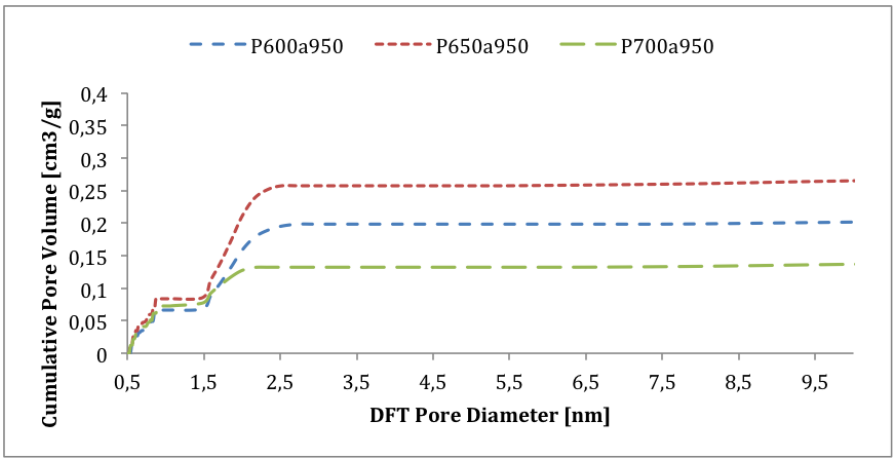

Figure 4.4: Cumulative pore volume of CO_2 activated carbon fibers derived from polyaniline produced by different carbonization temperatures and an activation temperature of 950°C. The activation time was 3 hours.

As seen from Figure (4.4), the cumulative pore volume of activated carbon becomes largest with a carbonization temperature of 650°C. Also, up until a pore diameter of about 1.5 nm, a carbonization temperature of 700°C provides a larger pore volume than a carbonization temperature of 600°C. However, as the pore size increases further, a carbonization temperature of 600°C gives a larger pore volume. This is reasonable because the interaction between the activation agent and the carbon obtained at lower carbonization temperature is more intensive, thus giving a larger pore volume [20]. From the sharp increase in pore volume at about 1.5 nm and very small increase in pore volume at pore diameter larger than about 2 nm, it seems that the CO_2 activation mainly created pores with diameters between about 1.5 and 2 nm. This is in the micropore region, which is consistent with the fact that CO_2 activation mainly produces micropores [38]

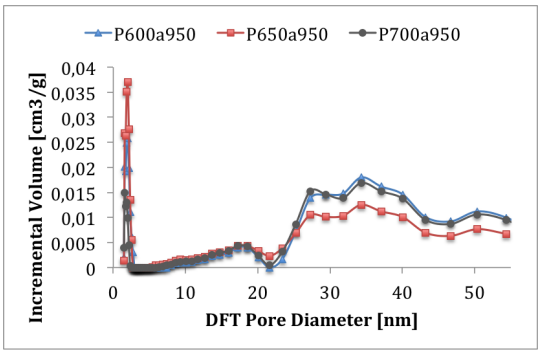

(a) PSD calculated by NLDFT.

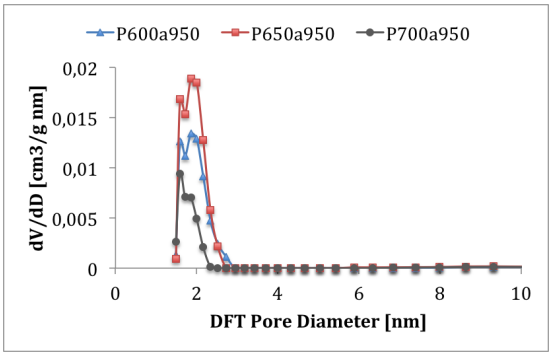

(b) PSD calculated by NLDFT.

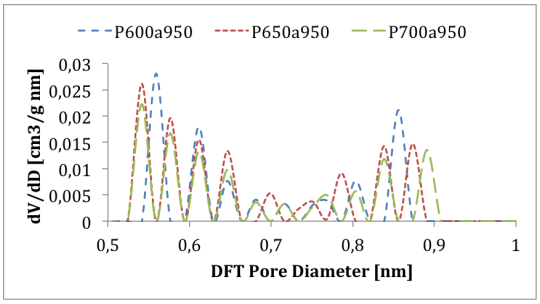

(c) PSD obtained with NLDFT from CO_2 adsorption/desorption at 0°C.

Figure 4.5: Pore structure of CO_2 activated carbons derived from PANI obtained with different carbonization temperature and an activation temperature of 950°C. The activation time was 3 hours.

4.2.2 Activation time

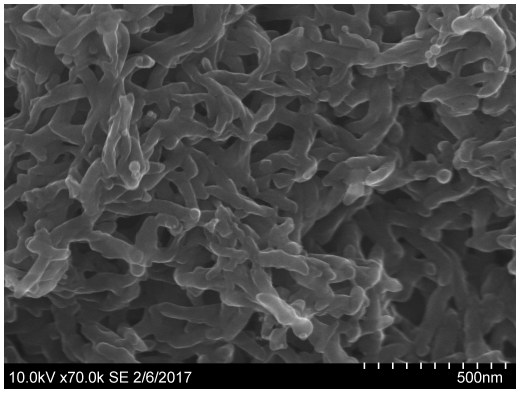

(a) P650

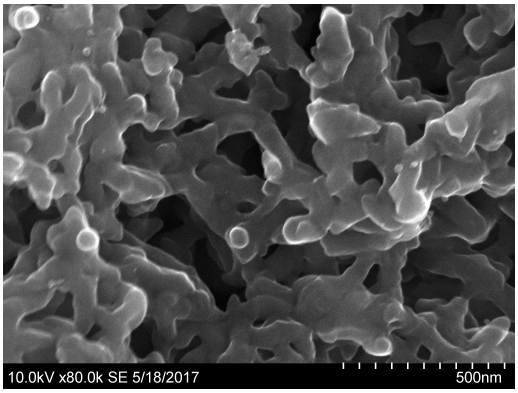

(b) P650a950-1h

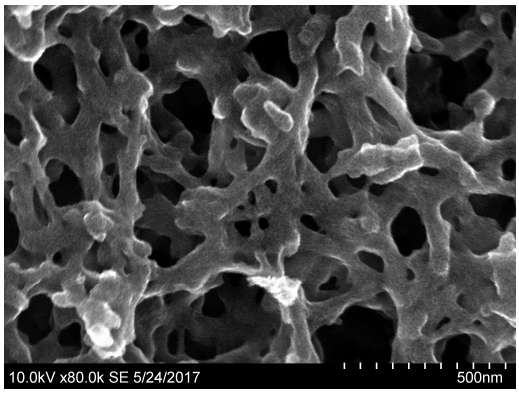

(c) P650a950-2h

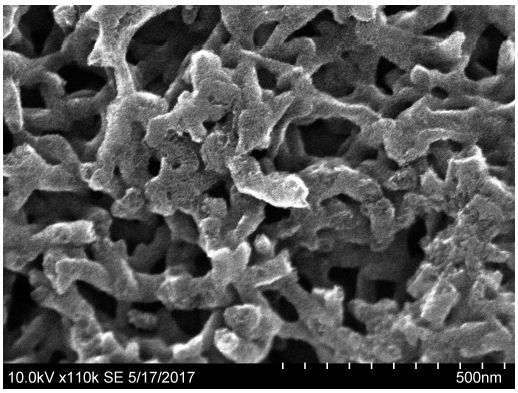

(d) P650a950-3h

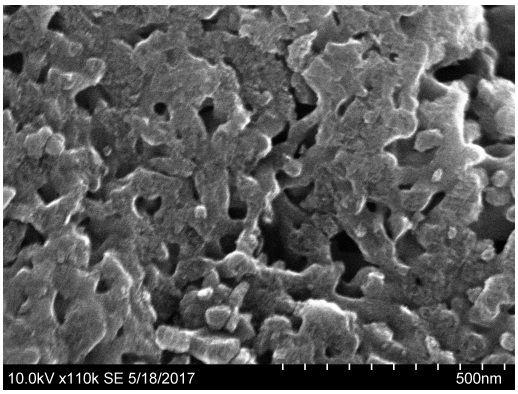

(e) P650a950-4h

Figure 4.6: SEM images of activated carbon fibers derived from polyaniline through a carbonization temperature and an activation temperature of 650 and 950°C, respectively. Duration of activation was varied from 1 to 4 hours.

Figure (4.6) shows the morphology of activated PANI nanofibers at various activation times ranging from 1 to 4 hours. It can be seen that the fiber structure is maintained up to an activation time of three hours. However, the fiber structure is almost completely broken with an activation time of four hours. This indicates that an activation time of four hours, at a temperature of 950°C, is to harsh in order to maintain the nanofiber structure. The results show that up until an activation time of three hours at 950°C, the CO_2 activation process is able to create pores without destroying the fiber structure, which is consistent with literature [38].

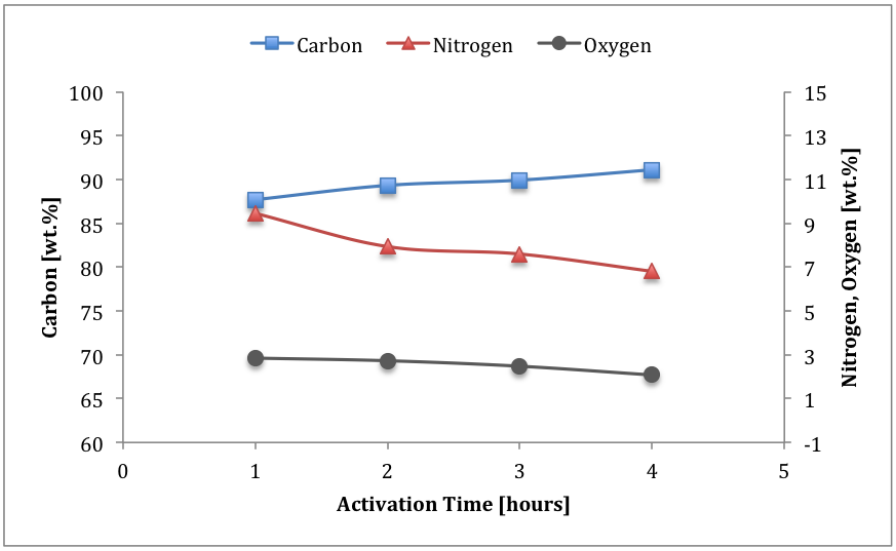

Figure 4.7: Elemental composition, estimated by EDX, as a function of activation time for activated carbon fibers derived from polyaniline. The carbonization temperature and the activation temperature were 650 and 950°C, respectively.

As seen from Figure (4.7), both the nitrogen and oxygen content decreases with increasing activation time. This is reasonable because more oxygen and nitrogen atoms are released as a result of thermal breakage of chemical bonds, as the activation time increases.

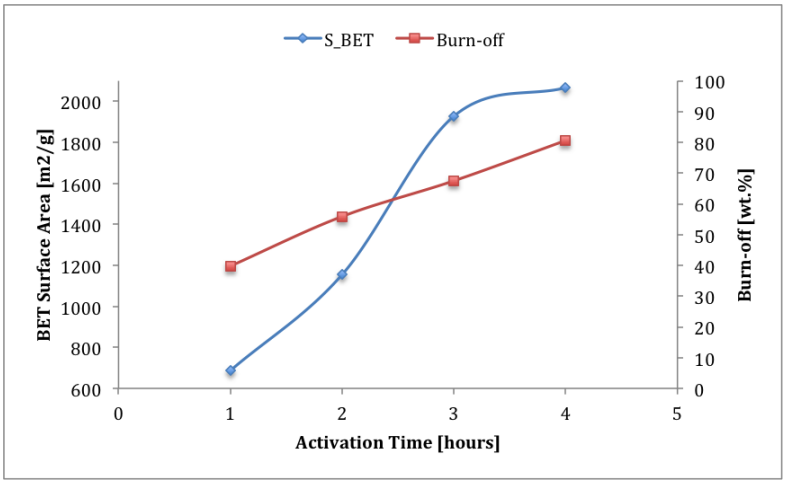

(a) BET surface area and burn-off as a function of activation time.

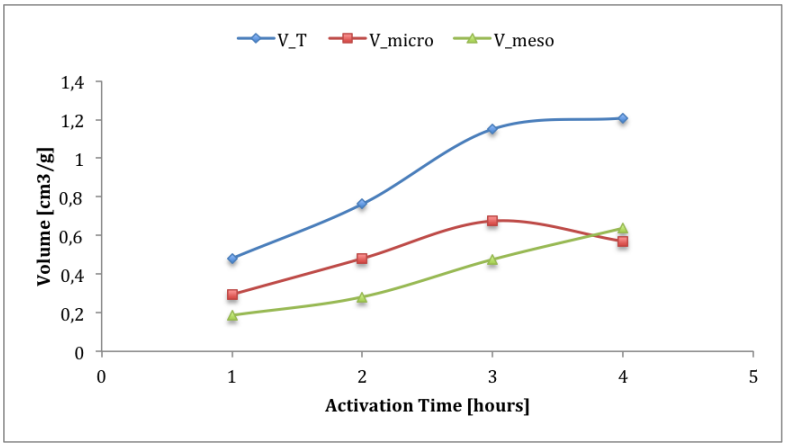

(b) Total pore volume, micropore volume and mesoporevolume as a function of activation time.

Figure 4.8: Physical properties of CO_2 activated carbon fibers derived from polyaniline through a carbonization temperature and an activation temperature of 650 and 950°C, respectively. Duration of activation was varied from 1 to 4 hours.

As seen from Figure (4.8a), the BET surface area increases with increasing activation time. Also, the burn-off increases approximately linearly with the activation time. The highest increase in the BET surface area is between two and three hours of activation, which indicates that a three hour activation time is necessary in order to obtain a high BET surface area. With an activation time of three hours, the BET surface area is 1927.7 m^2g^{-1}, while the burn-off is 67.5 wt.%. With an additional hour of activation, the BET surface area increases to 2066.7 m^2g^{-1}, whereas the burn-off increases to 80.6 wt.%. This increase in BET surface

area is small compared to the increase in burn-off. The degree of burn-off is an important parameter in terms of commercial feasibility of the process, moreover it is regarded as one of the most important factors related to the quality of the activated carbon [21]. Due to the trade-off between degree of activation and level of burn-off, it is reasonable to select an activation time of three hours to be the optimal activation time in this process. The increase in burn-off is with activation time is inevitable, because more volatile material is released as the duration of activation increases [2].

As seen from Figure (4.8b), both the total pore volume and mesopore volume increase with increasing activation time. The micropore volume increases with increasing activation time ranging from one to three hours. As seen from Table (A.1) in appendix A, after three hours of CO_2 activation, the total pore volume, micropore volume and mesopore volume are 1.151, 0.675 and 0.476 cm^3g^{-1} respectively. After an activation time of four hours, the micropore volume decreases to 0.570 cm^3g^{-1}, while the total pore volume and mesopore volume increases 1.208 and 0.638 cm^3g^{-1}, respectively. Therefore, an activation time of three hours is also ideal with respect to micropore volume. The decrease in micropore volume for activation times longer than three hours, effects the total pore volume, in which the total pore volume increases slightly after three hours. Hence, the only contribution to the increase in total pore volume after three hours of activation is the increase in mesopore volume. Considering that the CO_2 activation process mainly produces micropores from the oxidation reaction between CO_2 and carbon, this result suggests that three hours of activation is sufficient to obtain completely activated carbon [38]. Moreover, the results indicate that the oxidation reaction is less important after three hours of activation and that more mesopore volume is created at the expense of micropore volume. This mesopore volume is likely to be generated from release of volatile carbon, as the burn-off increases with approximately equal slope as in the first three hours of activation.

As seen from Figure (A.1) in appendix A, the increase in cumulative pore volume in the large mesopore region, from about 6 to 50 nm, is very similar for the activated carbons obtained with different activation temperature. This result suggests that large mesopores are not very effected by the activation process.

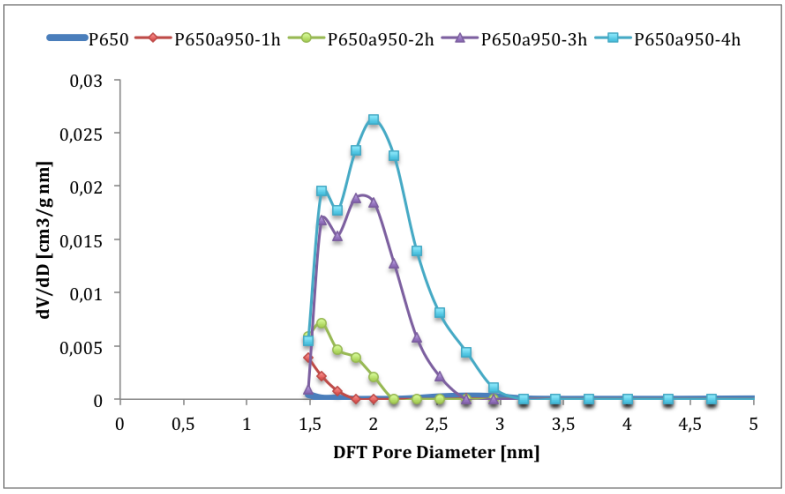

(a) Pore size distribution calculated by NLDFT.

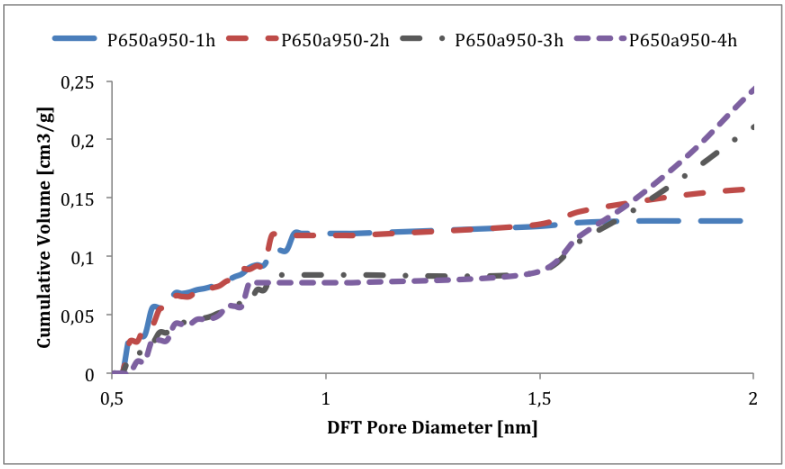

(b) Cumulative pore volume obtained from CO_2 and N_2 adsorption/desorption.

Figure 4.9: Pore structures of activated carbon fibers derived from polyaniline through a carbonization temperature and an activation temperature of 650 and 950°C, respectively. Duration of activation was varied from 1 to 4 hours.

Figure (4.9a) shows the pore size distribution of CO_2 activated carbon derived from PANI at different activation times. Compared to the PANI sample carbonized at 650°C (P650), it can be seen a gradual evolution of pores with increasing activation time. It is not only the pore volume at specific pore diameters that increases, but the range in pore width where the pores are generated also increases with activation time. One hour of CO_2 activation mainly generates pores with a pore diameter ranging from 1.5 to 1.8 nm, whereas two hours mainly produces pores having a pore diameter between 1.5 and 2.2 nm. By increasing the

activation time to three and 4 hours, the generated pore volumes have become significantly greater, compared to the pore volumes obtained with one and two hours of activation. As can be seen, activation times of three and four hours, mainly generate pores with a pore width ranging from about 1.5 to 2.75 and 1.5 to 3.1 nm, respectively. Considering that the CO_2 activation process mainly creates micropores (pore width ≤ 2 nm), it can be assumed that ...

Figure (4.9b) shows the cumulative pore volumes obtained with different activation times. This result indicates that the number of pores having a diameter ranging from 0.5 to 1.5 nm, is higher when using an activation time of one or two hours, compared to using an activation time of three or four hours. This also indicates that large micropores and small mesopores are generated mainly from smaller micropores.

Properties	P650a1000-1,5h	P650a1000-3h
S_{BET} [m^2/g]	1946.9	2439.2
V_T [cm^3/g]	1.229	1.852
V_{micro} [cm^3/g]	0.520	0
V_{meso} [cm^3/g]	0.709	1.852
V_{meso}/V_T [%]	57.7	100
V_{micro}/V_T [%]	42.3	0
Burn-off [wt.%]	71.6	98.0

Table 4.3: Physical properties of activated carbon fibers derived from polyaniline. The carbonization temperature and the activation temperature were 650 and 1000°C, respectively. The duration of activation was 1.5 and 3 hours.

The effect of activation time was also studied using an activation temperature of 1000°C. The activation time was set at 1.5 and 3 hours. Also at this activation temperature, Table (4.3) shows that the BET surface area and total pore volume increase with increasing activation time. However, under these conditions, the micropore volume is zero after an activation time of three hours. This indicates that an activation temperature of 1000°C is too harsh, in which all micropores have been converted into mesopores. This is also reflected by the massive burn-off of 98 wt.%.

4.2.3 Activation temperature

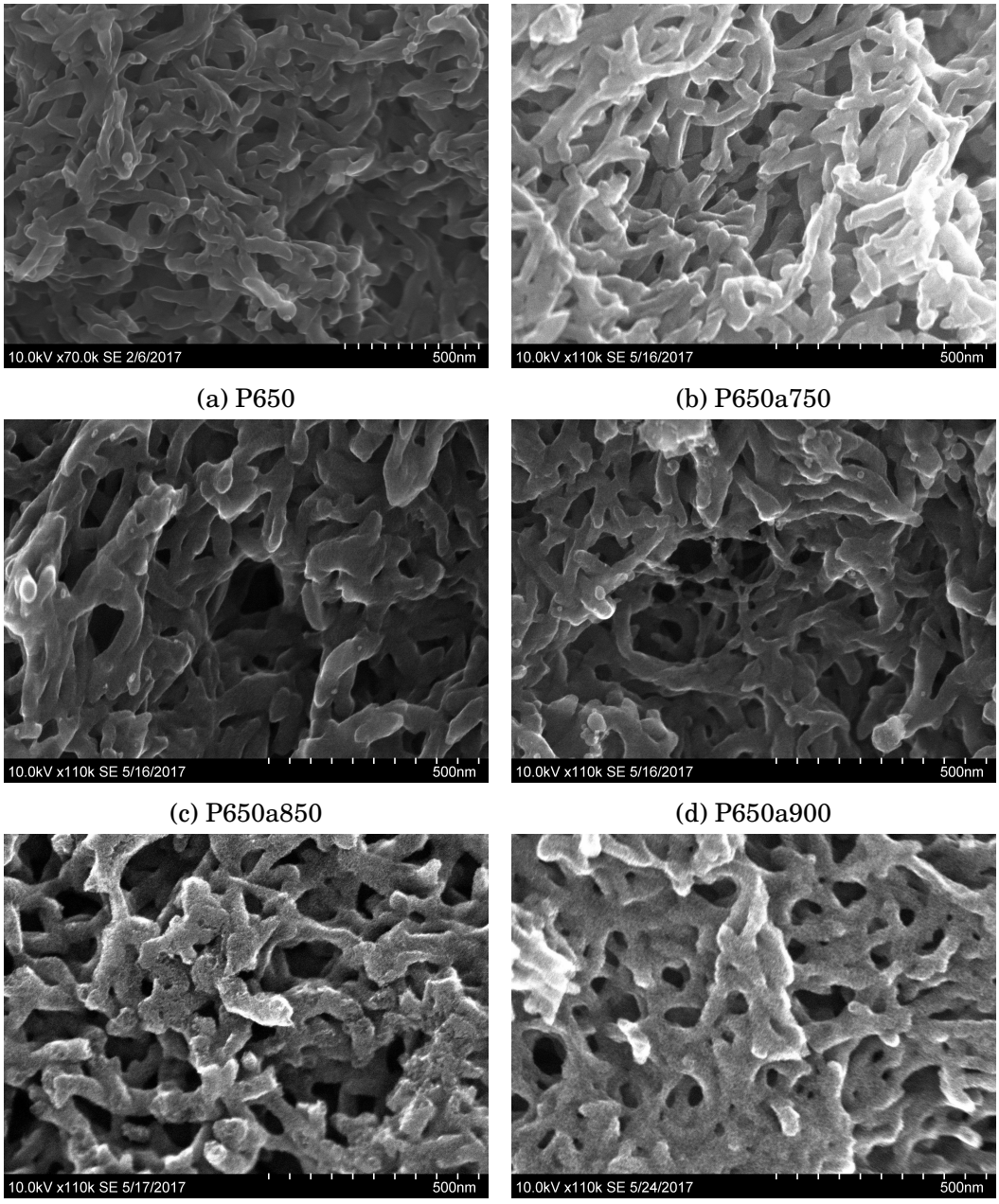

(a) P650 (b) P650a750

(c) P650a850 (d) P650a900

(e) P650a950 (f) P650a1000

Figure 4.10: SEM images of activated carbon fibers derived from polyaniline through a carbonization temperature of 650°C and an activation time of 3 hours. The activation temperature was varied from 750 to 1000°C.

Figure (4.10) shows that the nanofibrous structure of CO_2 activated carbon is retained after various activation temperatures ranging from 750 to 1000°C. This is consistent with literature, in which the CO_2 activation process is able to develop pore structures within the carbon matrix without destroying the carbon fibers [38]. This also shows the high thermal stability of the PANI nanofibers [21].

However, it can be seen that the fiber length decreases especially after high activation temperatures of 950 and 1000°C. This effects the macropore volume (pore diameter ≥ 50 nm), where it can be seen that the macropore volume is strongly reduced when using an activation temperature of 1000°C. A reduction in the macropore volume has shown to have a negative effect on the rate capability of supercapacitors, in which the macroporous structure is important to obtain a small diffusion resistance and short ion diffusion distances [26].

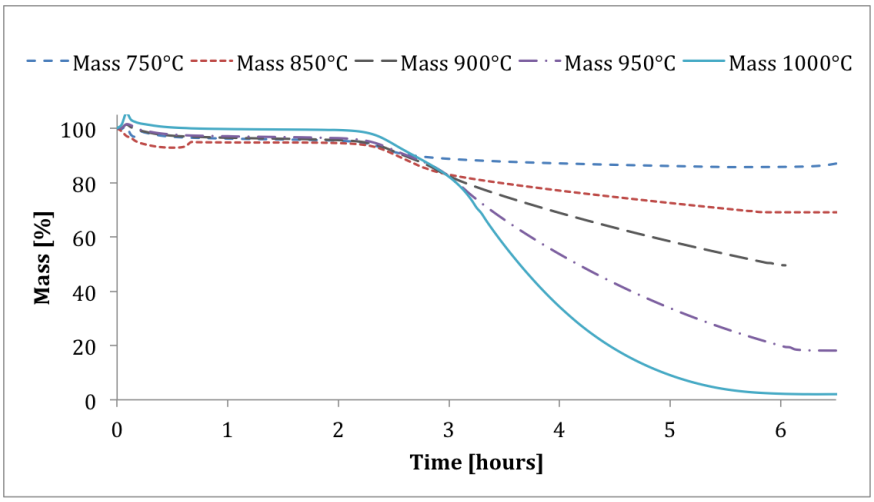

Figure 4.11: Thermal gravimetric analysis of CO_2 activation at various activation temperatures of pre-carbonized PANI. The activation time was 3 hours, while the flow rate of CO_2 and argon was 80 and 20 ml min^{-1}, respectively.

As seen from Figure (4.11), the mass loss during the CO_2 activation process increases with increasing activation temperature, at which almost all carbon is removed using an activation temperature of 1000°C. In the CO_2 activation process, the burn-off increases with increasing activation temperature because the increase in activation temperature promotes the endothermic oxidation reaction and the release of volatile carbon [2]. The release of volatile carbon is mainly due to gaseous pyrolysis products formed by the heat during the activation process, but carbon is also removed by the reaction with CO_2. The reaction rate of the oxidation reaction increases with increasing activation temperature, which leads

to more carbon being removed as CO. This can be seen from Figure (4.12a), where the formation of CO is shown for different activation temperatures. The amount of CO is directly related to the area beneath the peaks and it can be seen that as the activation temperature increases more CO is formed. Also, an activation temperature of 750°C is sufficient to initiate the endothermic oxidation reaction, in which a small peak of CO occurs. Figure (4.12b) shows the consumption of CO_2 for different activation temperatures. These results do not show the expected trend in the consumption of CO_2, where the consumption increases with activation temperature [2]. However, it can be seen that the consumption of CO_2 is highest with the use of activation temperatures of 950 and 1000°C.

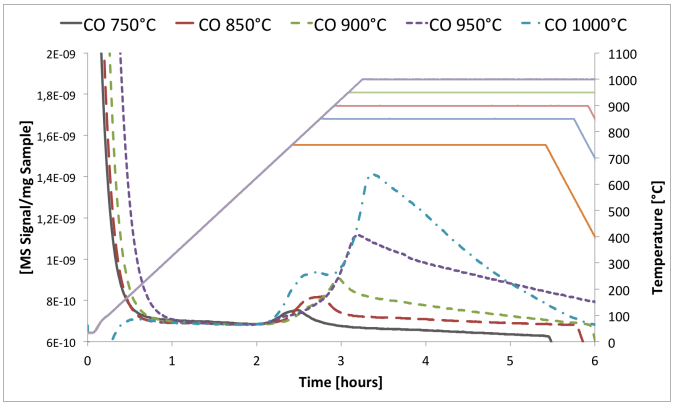

(a) The formation of CO at various activation temperatures.

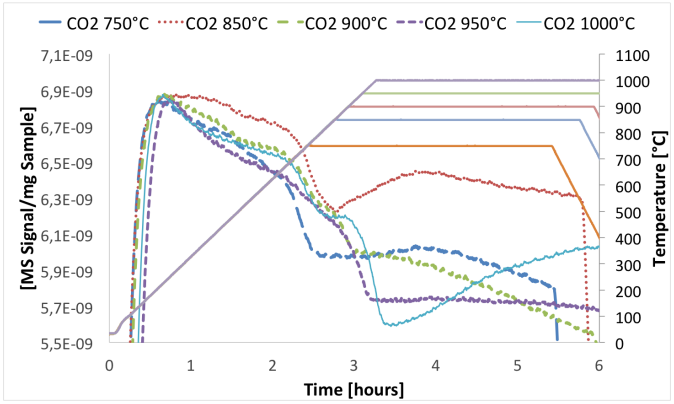

(b) The consumption of CO_2 at various activation temperatures.

Figure 4.12: MS results for CO_2 activation at different activation temperatures. The activation time was 3 hours, while the flow rate of CO_2 and argon was 80 and 20 ml min^{-1}, respectively.

Also, as seen from Figure (4.11), the mass loss during the first two hours is mainly the release of volatile species, such as water. Then, a sharp decrease in weight occurs for all samples after about 2.2 hours. This corresponds to the formation of CO, which is detected at approximately the same time (after about 2.2 hours) for all the samples, as seen from Figure (4.12a). In addition, the consumption of CO_2 is also detected after about 2.2 hours. Moreover, it can be seen from Figure (4.12a), that the width of the CO peaks increases with increasing activation temperature. This suggests that the oxidation reaction is active in a longer period of time when using higher activation temperatures. The formation of CO is consistent with the weight loss, because the weight loss curves at activation temperatures between 750 and 950°C flattens out after the sharp decrease at about 2.2 hours. This could be due to the fact that the formation of CO decreases after a short period of time at these activation temperatures.

It can also be seen from Figure (4.12a), that by using an activation temperature of 1000°C, two peaks appear in the detection of CO. The first peak is located at about 2.5 hours, while the second peak is located at about 3.5 hours. As seen from Figure (4.11), this is consistent with the mass loss because two sharp declines in weight occur after approximately 2.5 and 3.5 hours.

However, the weight loss during the CO_2 activation process is also due to the removal of nitrogen, which is released as various nitrogen-containing gases. Figure (4.13a) shows the formation of NO for different activation temperatures. These results confirm that nitrogen is removed as NO at activation temperatures ranging from 750 to 1000°C. However, a trend in which the amount of NO formed increases with increasing activation temperature is not evident in these results. The smallest amount of NO formed, is using an activation temperature of 900°C, while the largest amount is produced using an activation temperature of 950°C. The results represented in figure (4.13b) indicate that no nitrogen is removed as NO_2, in which no obvious peak for the detection of NO_2 is obtained.

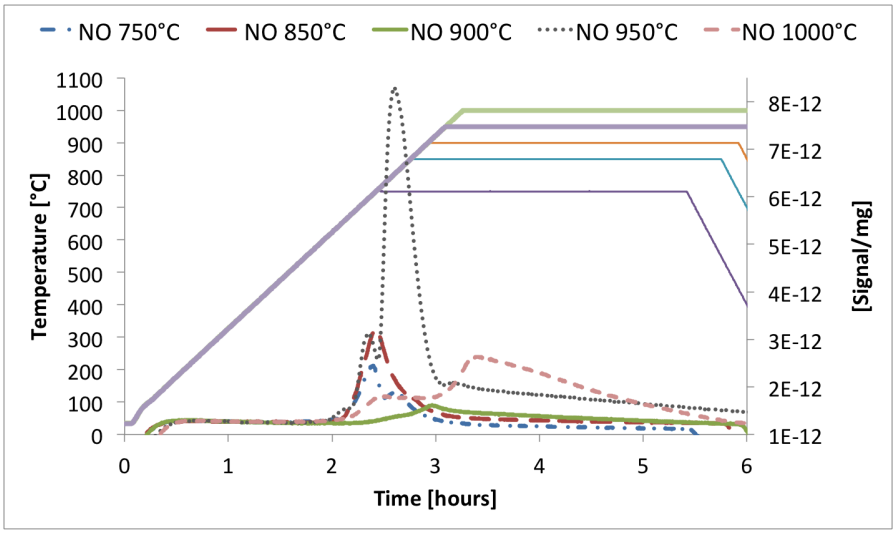

(a) The formation of NO at various activation temperatures.

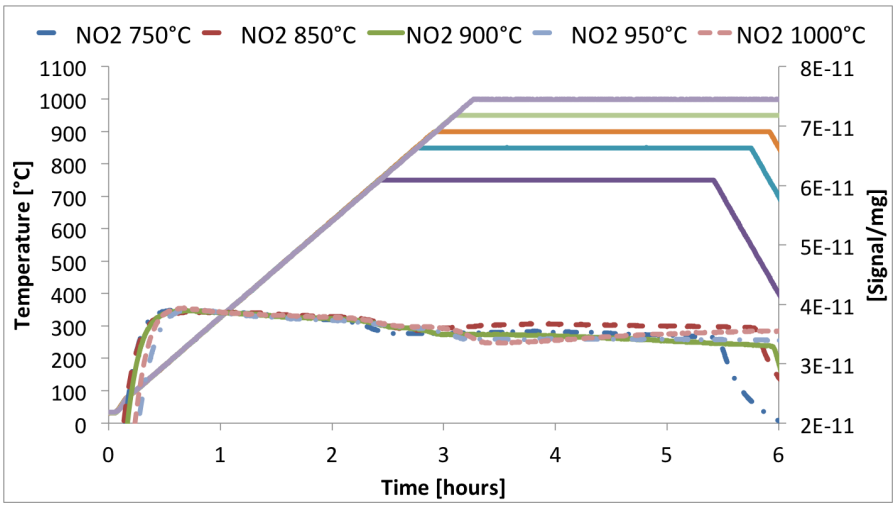

(b) The formation of NO_2 at various activation temperatures.

Figure 4.13: MS results for CO_2 activation at different activation temperatures. The activation time was 3 hours, while the flow rate of CO_2 and argon was 80 and 20 ml min^{-1}, respectively.

Figure (4.14a) shows the formation of N_2O_3 using various activation temperatures. These results indicate that nitrogen gets removed as N_2O_3 at a temperature of 1000°C. However, no significant peaks are detected at temperatures below 1000°C, suggesting that N_2O_3 is not formed at these temperatures. Figure (4.14b) shows the formation of NH_3 at various activation temperatures. These results suggest that nitrogen is removed as NH_3 at temperatures ranging from 750 to 1000°C. A clear trend between formation of NH_3 and activation temperature is not

obtained in these results. Nevertheless, it can be seen that the highest amount of nitrogen gets released as NH_3 using an activation temperature of 1000°C.

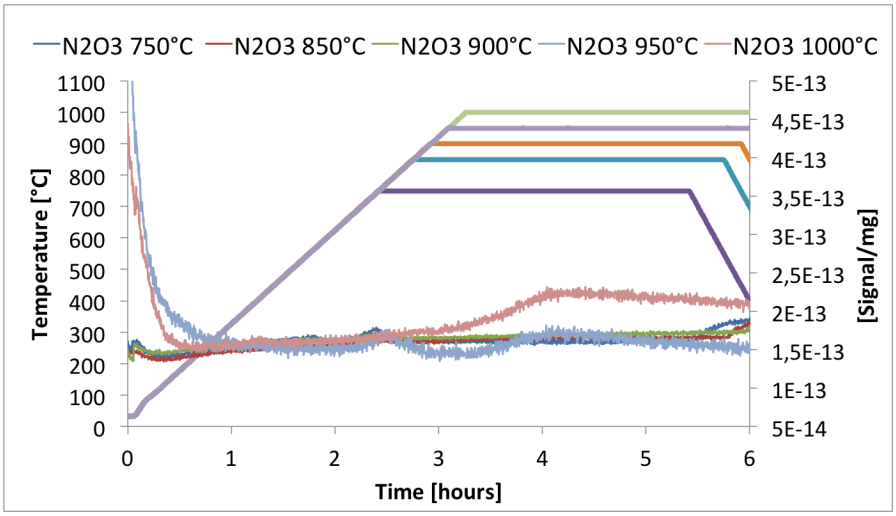

(a) The formation of N_2O_3 at various activation temperatures.

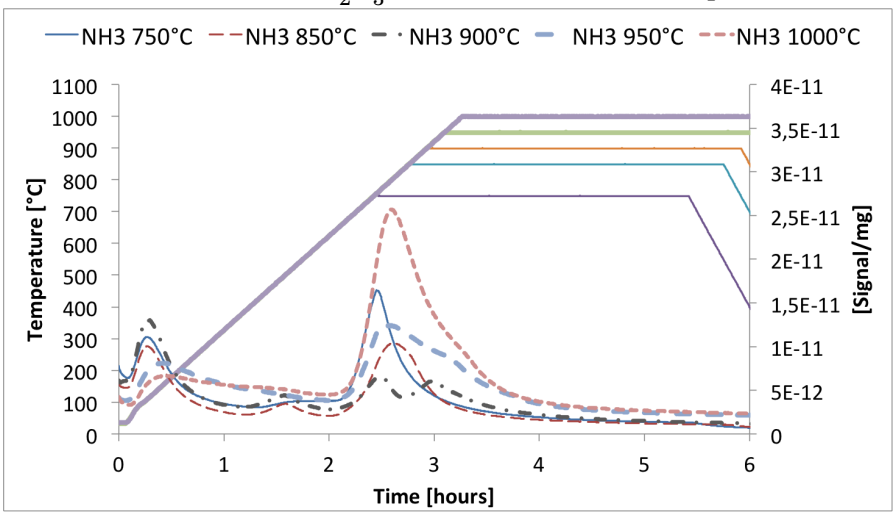

(b) The formation of NH_3 at various activation temperatures.

Figure 4.14: MS results for CO_2 activation at different activation temperatures. The activation time was 3 hours, while the flow rate of CO_2 and argon was 80 and 20 ml min^{-1}, respectively.

Figure (4.15) shows the carbon, nitrogen and oxygen content as a function of activation temperature. These results show that both the nitrogen and oxygen content decreases with increasing activation temperature. This is reasonable because loss of oxygen and nitrogen atoms occur as a result of thermal breakage of

chemical bonds, which is enhanced at higher temperatures [7].

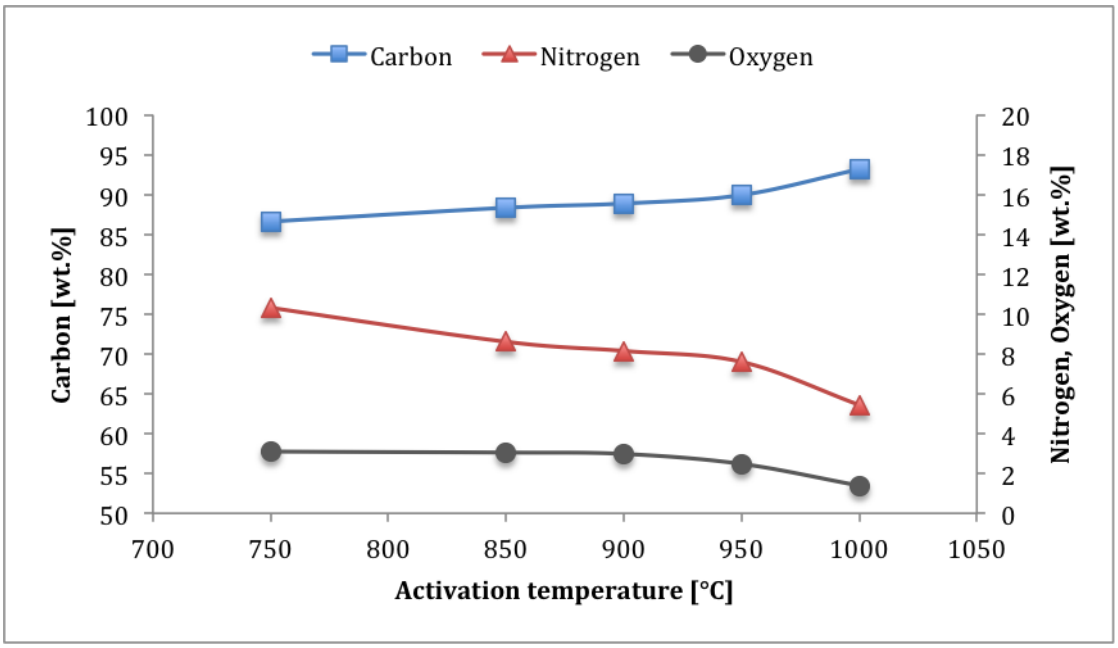

Figure 4.15: Elemental composition, estimated by EDX, as a function of activation temperature for activated carbon fibers derived from polyaniline. The carbonization temperature and the activation time were 650°C and 3 hours, respectively.

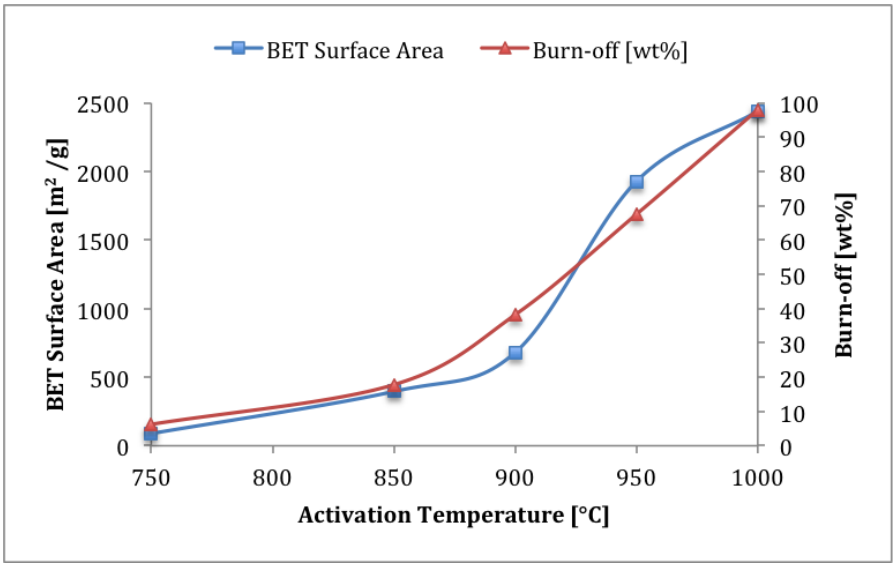

(a) BET surface area and burn-off as a function of activation temperature.

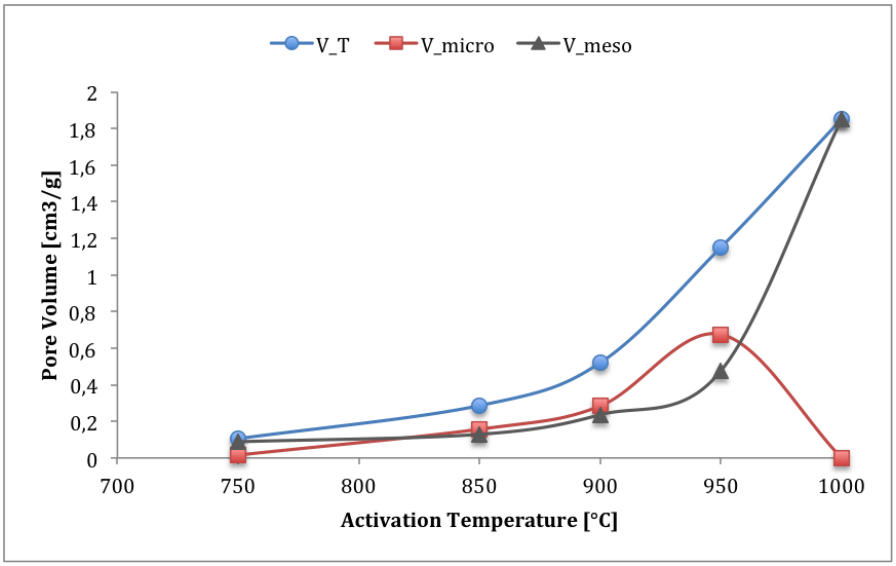

(b) Total pore volume, micropore volume and mesopore volume as a function of activation temperature.

Figure 4.16: Physical properties of activated carbon fibers derived from polyaniline through a carbonization temperature of 650°C and an activation time of 3 hours. The activation temperature was varied from 750 to 1000°C.

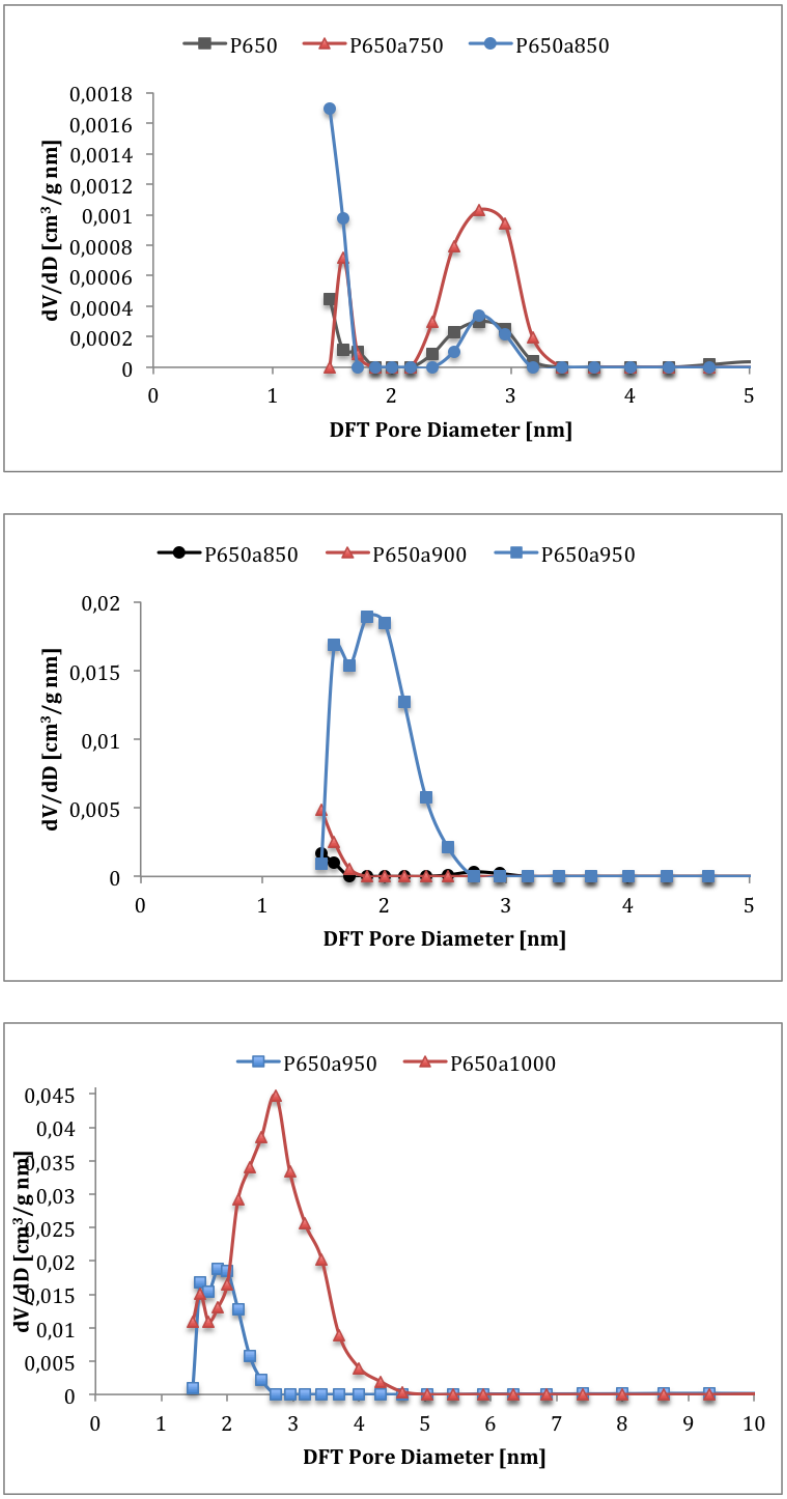

Figure 4.17: Pore size distribution, determined by NLDFT, of activated carbon fibers derived from PANI through a carbonization temperature of 650°C and an activation time of 3 hours. The activation temperature was varied from 750 to 1000°C.

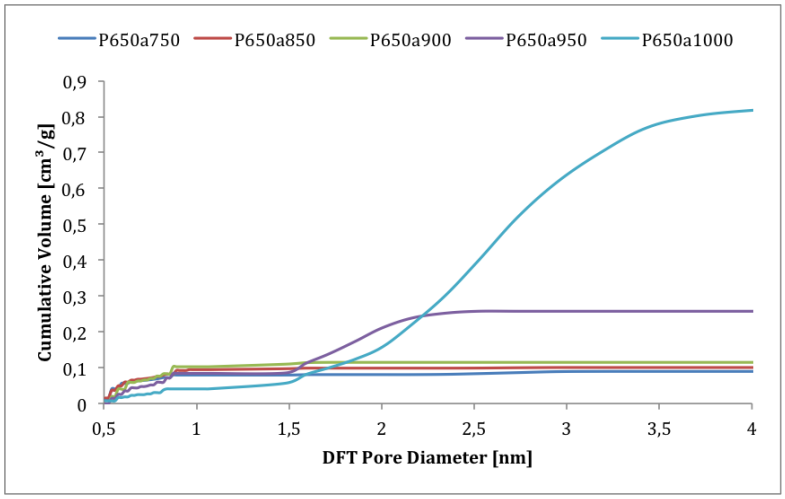

Figure 4.18: Cumulative pore volume, determined by CO_2 and N_2 adsorption/desorption, of activated carbon fibers derived from PANI through a carbonization temperature of 650°C and an activation time of 3 hours. The activation temperature was varied from 750 to 1000°C.

As seen from Figure (4.16a), the BET surface area increases with increasing activation temperature. The curve shows a small increase in BET surface area with activation temperatures ranging from 750 to 900°C, while a large increase in BET surface area occurs at an activation temperature of 950°C. This indicates that the reaction rate of the oxidation reaction between CO_2 and carbon, which is endothermic, increases significantly at an activation temperature of 950°C. This is also consistent with Figure (4.12a), where the formation of CO is much larger at a temperature of 950°C, compared to that of lower temperatures. From Table (A.2), it can be seen that an activation time of 750°C provides a BET surface area, total pore volume and micropore volume of 86.8 $m^2\ g^{-1}$, 0.104 and 0.016 $cm^3\ g^{-1}$, respectively. Table (A.1) shows that carbonized PANI with a carbonization temperature of 650°C has a BET surface area, total pore volume and micropore volume of 298.3 $m^2\ g^{-1}$, 0.202 and 0.109 $cm^3\ g^{-1}$, respectively. The decrease in BET surface area, total pore volume and micropore volume using an activation temperature of 750°C, could be due to the fact that, at this temperature, the thermal destruction of pores is more significant compared to the generation of pores through the oxidation reaction. This is reasonable due to the very small amount of CO generated at this temperature, as shown in Figure (4.12a). With an activation temperature of 850°C, the BET surface area, total pore volume and micropore volume incease to 395.7 $m^2\ g^{-1}$, 0.286 and 0.157 $cm^3\ g^{-1}$, respectively. This result suggests that an activation temperature of 850°C is sufficient to generate pores through the CO_2 oxidation reaction.

Figure (4.16a) shows that the burn-off increases with increasing activation temperature. This is consistent with the increase in mass loss with increasing activation temperature detected using TGA, as seen from Figure (4.11). In addition, the increase in burn-off is largest at activation temperatures above 900°C, which indicates the unavoidable trade of between burn-off and activation [21]. By changing the activation temperature from 950 to 1000°C, the BET surface area and total pore volume increase from 1927.7 to 2439.2 $m^2\ g^{-1}$ and 1.151 to 1.852 $cm^3\ g^{-1}$ respectively. However, the micropore volume decreases from 0.675 to 0 $cm^3\ g^{-1}$. As previously mentioned, this result indicates that an activation temperature of 1000°C is too severe for the aim of producing mainly microporous carbons. Considering the level of burn-off, it is reasonable to select an activation temperature of 950°C to be the most favorable activation temperature.

Figure (4.16b) shows the total pore volume, micropore volume and mesopore volume as function of activation temperature. The total pore volume and mesopore volume increases with activation temperature, while the micropore volume goes through a maximum at an activation temperature of 950°C. By changing the activation temperature from 900 to 950°C, a large increase in total pore volume occurs, which is also reflected in the BET surface area. This increase in total pore volume is mainly due to the large increase in micropore volume. The total pore volume continues to increase as the activation temperature becomes 1000°C. However, this increase in total pore volume is due to the large increase in mesopore volume, as the micropore volume decreases to zero.

The activation temperature determines if the oxidation reaction between CO_2 and carbon is chemically or diffusionally controlled. The reaction rate of the oxidation reaction increases with increasing temperature, hence at low temperatures the reaction is chemically controlled, where CO_2 molecules diffuse into the carbon particles through defects and superficial groups and then reacting with the carbon to produce porosity. At higher temperatures, the reaction shifts to being diffusionally controlled, in which the reaction between CO_2 and carbon occurs on the outside of the particles, which does not significantly enhance the porosity [11]. This could explain the development of pores at different temperatures, in which the micropore volume goes through a maximum at 950°C meaning that the oxidation reaction is still mainly chemically controlled allowing CO_2 molecules to diffuse into the particles, which mainly creates micropores. However, the micropore volume is zero at an activation temperature of 1000°C, which indicates that the oxidation reaction is partly diffusionally controlled. When the reaction is diffusionally controlled, the oxidation reaction is so fast that the transportation of

CO_2 towards the carbon surface is the limiting step in the reaction mechanism. The large increase in mesopore volume at an activation temperature of 1000°C suggests that the oxidation reaction is partly diffusionally controlled, where the speed of the activation is determined by a combination of the reaction rate and the diffusion of CO_2 into the pores [11]. This results most likely in pore widening, as the CO_2 molecules are not fully transported to the interior of the particles, which could explain the increase in mesopore volume. This is also reasonable considering that CO_2 mainly creates micropores when the activation reaction is chemically controlled [38].

Figure (4.17) shows the pore size distribution generated with various activation temperatures ranging from 750 to 1000°C. Compared to the carbonized PANI (P650), it can be seen that the amount of micropores with a pore diameter between about 1.5 and 1.75 nm increases with activation temperatures of 750 and 850°C. Also, an activation temperature of 750°C generates mesopores having a pore width ranging from about 2.2 to 3.4 nm. These mesopores is most likely not generated by the oxidation reaction, due to the small amount of CO formed at this temperature and the fact that CO_2 activation mainly produces micropores [38]. An activation temperature of 900°C gives a small increase in the amount of micropores, compared to that of an activation temperature of 850°C. A further increase in activation temperature up to 950°C gives a very large increase in pore volume at pore diameters ranging from about 1.5 to 2.8 nm, which is reflected in the large increase in BET surface area. Finally, with an activation temperature of 1000°C, a huge pore volume is generated in the mesoporous region. Hence, these results do not only indicate that the development of pores is enhanced by increasing activation temperature, but also that the pores generated shift from being mainly micropores to become mostly mesopores. This is reasonable because, by increasing the activation temperature, the degree of activation is enhanced, which is accompanied by reduction in carbon strength, a decrease in density and yield and pore widening [21].

Figure (4.18) shows the cumulative pore volume obtained using different activation temperatures. These results indicate that the generation of mesopores is at the expense of micropores when using high activation temperatures, especially a temperature of 1000°C.

4.2.4 Partial pressure of CO_2

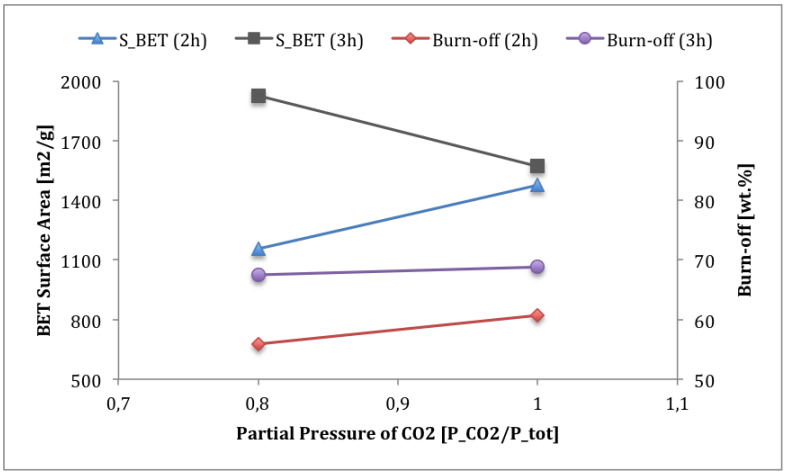

(a) BET surface area and burn-off as a function of the partial pressure of CO_2.

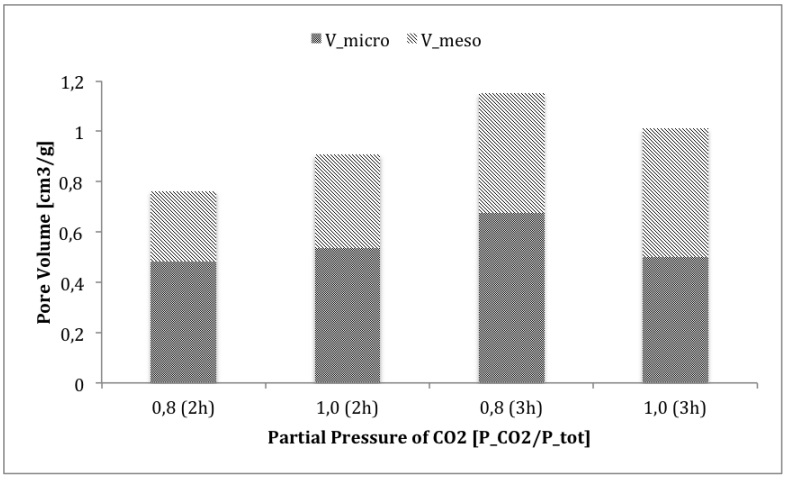

(b) Total pore volume, micropore volume and mesopore volume related to the partial pressure of CO_2 and activation time.

Figure 4.19: Physical properties of activated carbon derived from polyaniline through a carbonization temperature and an activation temperature of 650 and 950°C, respectively. The gaseous environment was a mixture of CO_2 and argon with a total flow rate of 100 ml/min, where the partial pressure of CO_2 was 0.8 or 1.0. The activation time was 2 and 3 hours.

Figure (4.19a) shows the BET surface area and the burn-off obtained at a partial pressure of CO_2 equal to 0.8 and 1.0 P_{CO_2}/P_{tot} in the CO_2 activation process

carried out with an activation time of two and three hours. In the two hours activation process, both the BET surface area and the burn-off increases with increasing partial pressure of CO_2. Also, it can be seen from Figure (4.19b) that the total pore volume, micropore volume and mesopore volume increases with increasing partial pressure of CO_2 in the two hour activation process. Table (A.3) in appendix A shows that the BET surface area increases from 1154.9 to 1476.1 m^2g^{-1} and the total pore volume, micropore volume and mesopore volume increases from 0.763 to 0.909, 0.481 to 0.537 and 0.282 to 0.372 cm^3g^{-1}, respectively. It can be seen from Figure (4.20) that in the two hour activation process, more pores having diameters ranging from about 1.6 to 2.7 nm are generated when increasing the partial pressure of CO_2 from 0.8 to 1.0 P_{CO_2}/P_{tot}. This increase in both micropore volume and mesopore volume is the reason why the BET surface area increases. This is reasonable, because as the partial pressure of CO_2 increases, more CO_2 molecules are introduced to the activation process, which are able to diffuse into the carbon structure and react with the carbonized material, thereby creating porosity [38].

In the three hour activation process, the BET surface area decreases with increasing partial pressure of CO_2, going from 1927.7 to 1570.4 m^2g^{-1} at partial pressures equal to 0.8 and 1.0 P_{CO_2}/P_{tot}, respectively. The burn-off is approximately constant, only changing from 67.5 to 68.8 wt.%. In addition, the total pore volume and micropore volume goes from 1.151 to 1.011 and 0.675 to 0.501 cm^3g^{-1}, respectively. However, the mesopore volume increases with increasing partial pressure of CO_2, going from 0.476 to 0.510 cm^3g^{-1}.

These results suggest that in the three hour activation process, more mesopores are formed at the expense of micropores when increasing the partial pressure of CO_2. This could be the reason why the BET surface area decreases, because micropores contributes more to the BET surface area than mesopores. Figure (4.20) shows that in the three hour activation process, the volume consisting of pores ranging from about 1.6 and 2.2 nm is larger when using a partial pressure of 0.8, compared to that using a partial pressure of 1.0. It can be seen that by using a partial pressure of 1.0, larger mesopores ranging from about 2.3 to 3 nm are formed at the expense of smaller mesopores and micropores. This is most likely due to the long reaction time of three hours, because at a reaction time of two hours, both the micropore volume and mesopore volume increased with increasing partial pressure of CO_2. Hence, by using an activation time of three hours, the increase in partial pressure results in more CO_2 molecules reacting with the carbon material, making the activation process too severe in order to create micropores. This indicates that the micropores created after two hours of activation are enlarged as the activation time increases further. These results suggest that a

partial pressure of CO_2 equal to 1.0 P_{CO_2}/P_{tot} is favorable in the two hour activation process, while a partial pressure of 0.8 P_{CO_2}/P_{tot} is favorable in the three hour activation process. This is also the case when considering the yield of activated carbon, as the burn-off is lower when using a partial pressure of 0.8 P_{CO_2}/P_{tot} in the three hour activation process. In the two hour activation process, the increase in burn-off is relatively low compared to the gain in BET surface area.

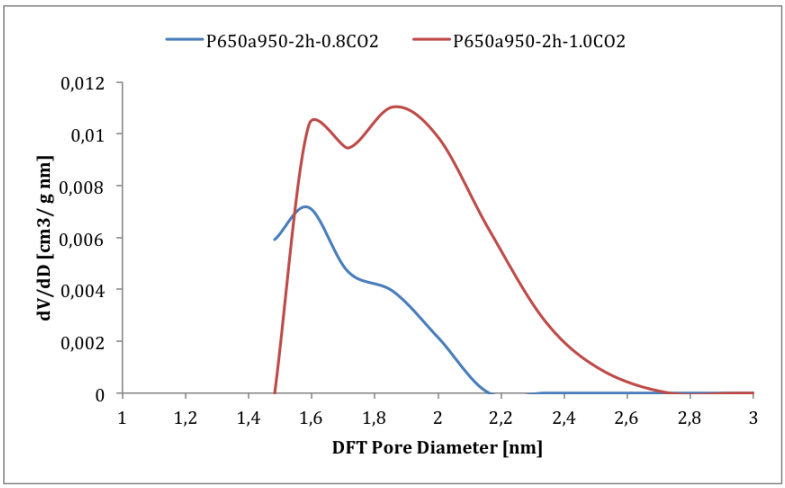

(a) Two hours of activation.

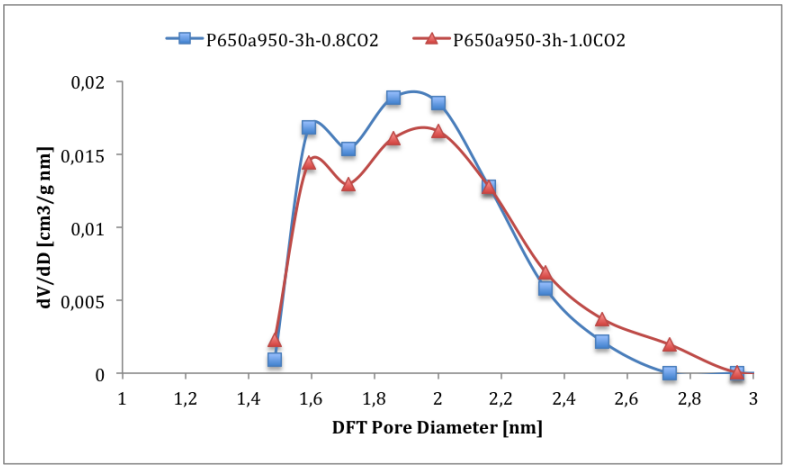

(b) Three hours of activation.

Figure 4.20: Pore size distribution, determined by NLDFT, of activated carbon derived from polyaniline through a carbonization temperature and an activation temperature of 650 and 950°C, respectively. The gaseous environment was a mixture of CO_2 and argon with a total flow rate of 100 ml/min, where the partial pressure of CO_2 was 0.8 or 1.0. The activation time was 2 and 3 hours

4.3 Chemical activation with CO_2 and H_2O

4.3.1 Water temperature

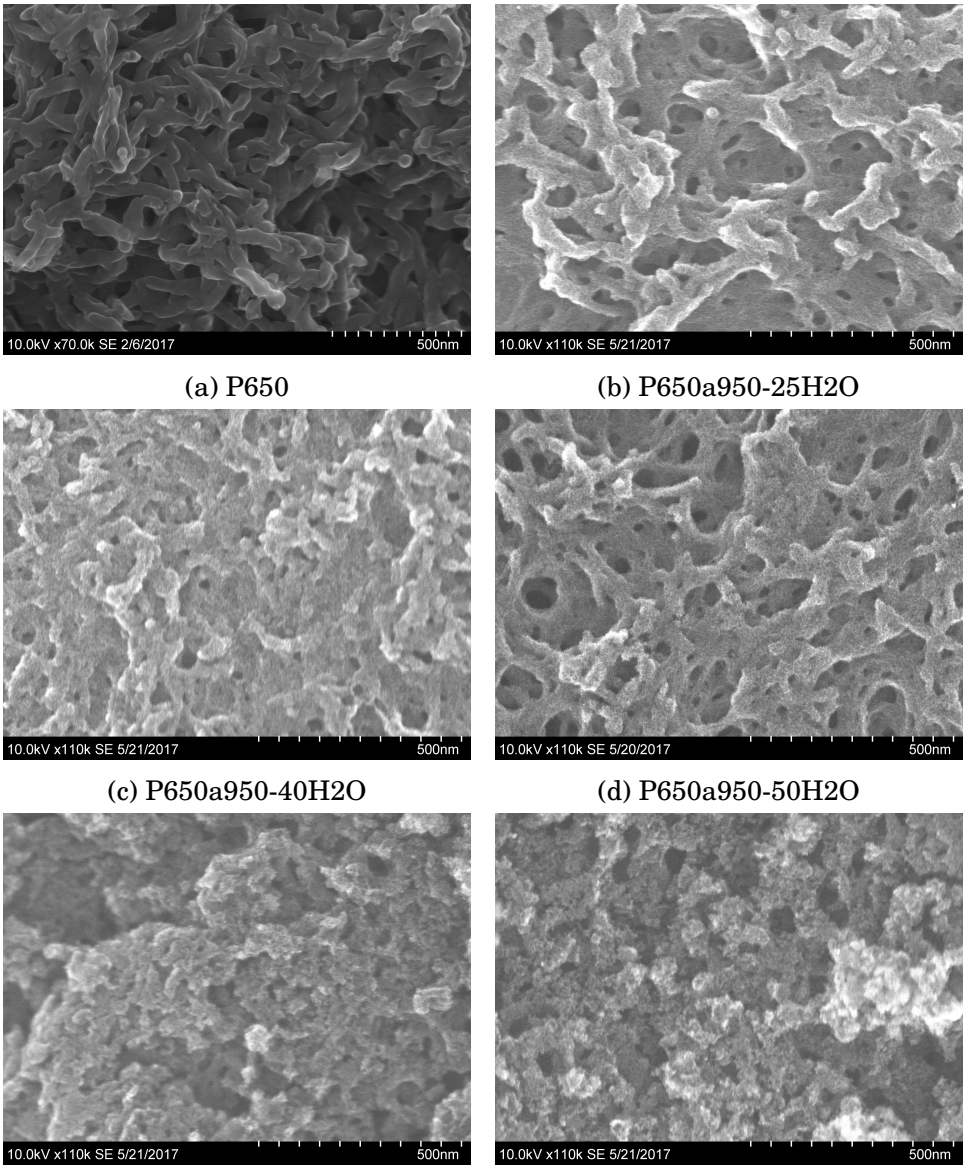

(a) P650 (b) P650a950-25H2O

(c) P650a950-40H2O (d) P650a950-50H2O

(e) P650a950-70H2O (f) P650a950-90H2O

Figure 4.21: SEM images of activated carbon fibers derived from PANI through a carbonization temperature and an activation temperature of 650 and 950°C, respectively. The water temperature was varied from 25 to 90°C and the activation time was 3 hours.

Figure (4.21) shows that, with an activation temperature and activation time of 950°C and three hours, the nanofibers gradually get destroyd with increasing water temperature. The amount of steam fed to the activation process increases with the water temperature and it can be seen that water temperatures of 70 and 90°C, completely destroy the nanofibers. The destruction of the fiber structure is most likely due to the introduction of steam to the process. As previously discussed, the fiber structure is retained after CO_2 activation carried out with an activation temperature and activation time of 950°C and three hours. Therefore, the fact that steam is more reactive than CO_2, could be the reason why the fiber structure collapsed during the activation process.

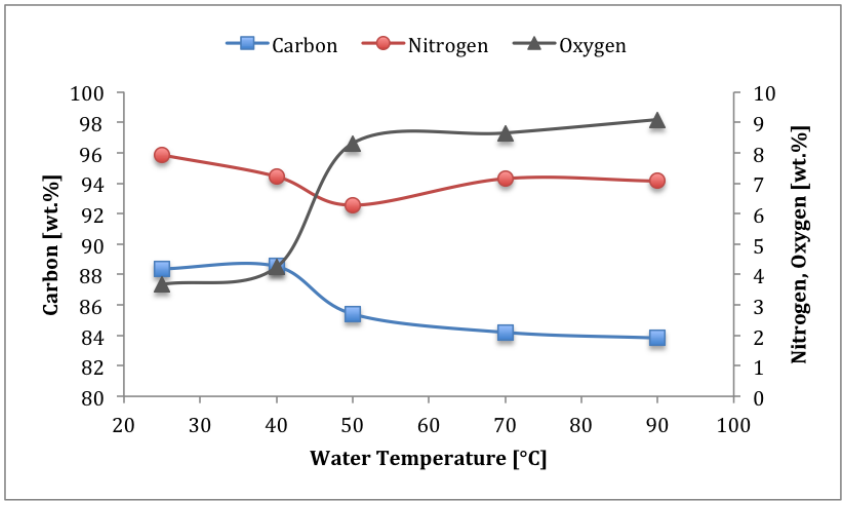

Figure 4.22: Elemental composition, estimated by EDX, as a function of water temperature for activated carbon fibers derived from PANI. The carbonization temperature, activation temperature and the activation time were 650°C, 950°C and 3 hours, respectively.

Figure (4.22) shows that the oxygen content increases with increasing water temperature, while the nitrogen content remains approximately constant. This result suggest that the doping of oxygen from the oxidation reaction between steam and carbon is more significant than the release of oxygen through thermal breakage of chemical bonds.

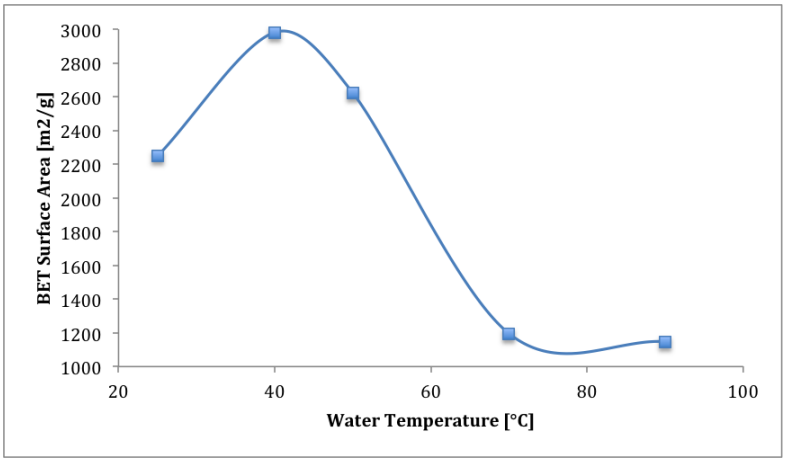

(a) BET surface area as a function of the water temperature.

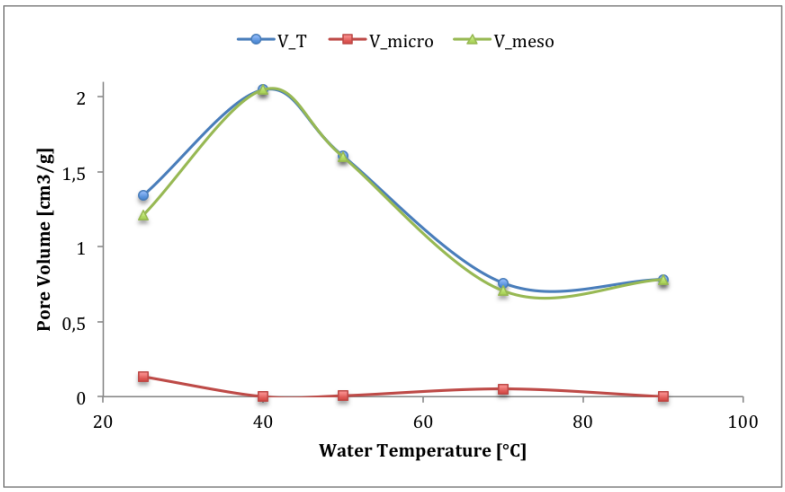

(b) Total pore volume, micropore volume and mesopore volume as a function of the water temperature.

Figure 4.23: Physical properties of activated carbon derived from polyaniline through a carbonization temperature and an activation temperature of 650 and 950°C, respectively. The water temperature was varied from 25 to 90°C and the activation time was 3 hours.

As seen from Figure (4.23a), the BET surface area goes through a maximum at a water temperature of 40°C, reaching a value of 2981.6 $m^2\ g^{-1}$. As more steam is introduced to the activation process, the BET surface area decreases. As seen from Table (B.1) in appendix B, with water temperatures of 70 and 90°C, the BET surface area becomes 1196.1 and 1148.2 $m^2\ g^{-1}$, respectively. Table (A.3) shows that the CO_2 activation process with equal activation temperature, activation time and flow rate of CO_2 as the combined CO_2 and steam activation process, results in a

BET surface area of 1570.4 m^2 g^{-1}. Hence, the optimum water temperatures for the combined CO_2 and steam activation process are water temperatures up to 50°C. The relatively small BET surface area obtained with water temperatures above 50°C, could be due to the high amount of steam entering the process. The high amount of steam does not only destroy the fiber structure, but since steam is a stronger activation agent than CO_2, it may produce pores having a very large diameter, which will reduce the BET surface area. This assumption could be supported by the pore size distribution obtained with various water temperatures, displayed in Figure (4.24). As can be seen, water temperatures of 70 and 90°C generate the smallest amount of pores with a diameter ranging from 1.5 to about 4 nm, which could suggest that larger pores have been formed.

Figure (4.23b) shows that the total pore volume and mesopore volume follow the same trend as the BET surface area. Also, it can be seen that the total pore volume is mainly composed by mesopores. This is in accordance with the pore size distribution displayed in Figure (4.24), in which mostly mesopores is generated. As can be seen, a water temperature of 40°C generates pores that have a diameter ranging from 1.5 to about 4.5 nm, where the largest pore volume consist of pores having a diameter larger than 2 nm. With a higher water temperature of 50°C, the range in which pores are generated has decreased to about 1.5 to 4 nm. With a lower water temperature of 25°C, the range in which pores are formed is from 1.5 to about 3.8 nm.

The pore size distribution obtained with various water temperatures, is in accordance with the literature, as steam activation provides larger development of wide micropores and mesopores [4]. By comparing the pore size distribution obtained with CO_2 activation (Figure (4.20)) and the pore size distribution obtained with the combined steam and CO_2 activation process, at equal activation conditions, it is clear that the pore size distribution is wider after the combined steam and CO_2 activation process. This is consistent with the literature, as the generation of mesopores greatly increases the pore size distribution [4].

As seen from Table (B.1), the burn-off during the combined CO_2 and steam activation process with an activation temperature and an activation time of 950°C and 3 hours, is around 90 %. This burn-off is very high and can be related to the complete removal micropores. In commercial activation processes, this burn-off is way too high and in addition to this burn-off, the carbonization yield has to be considered.

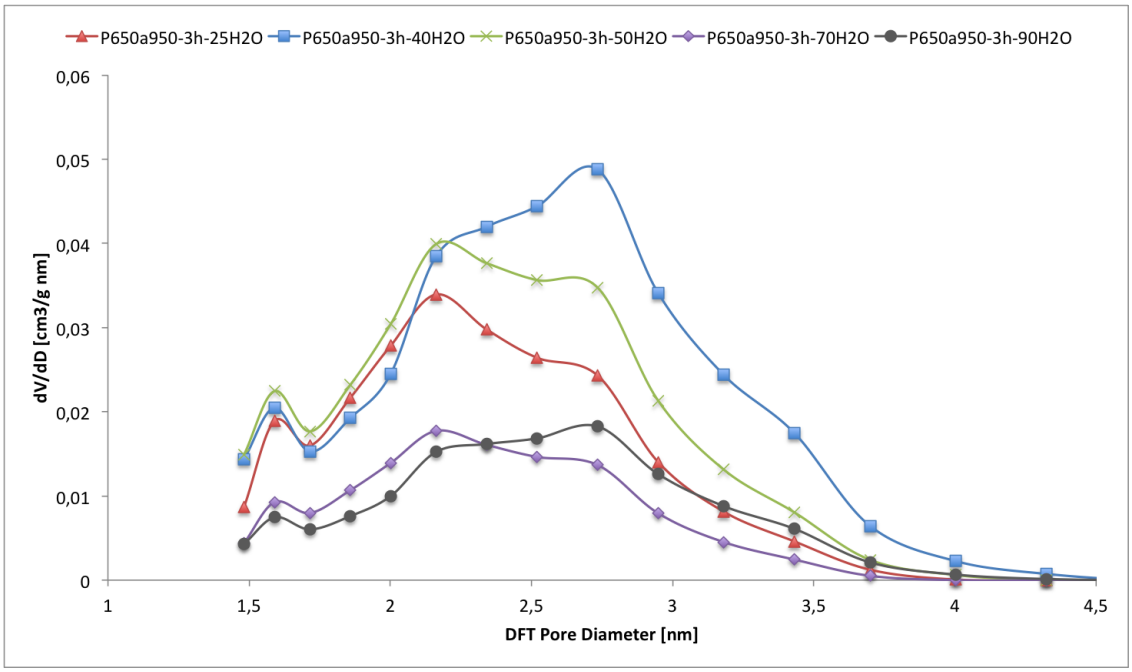

Figure 4.24: Pore size distribution, determined by NLDFT, of activated carbon derived from PANI through a carbonization temperature and an activation temperature of 650 and 950°C, respectively. The water temperature was varied from 25 to 90°C and the activation time was 3 hours.

4.3.2 Activation time

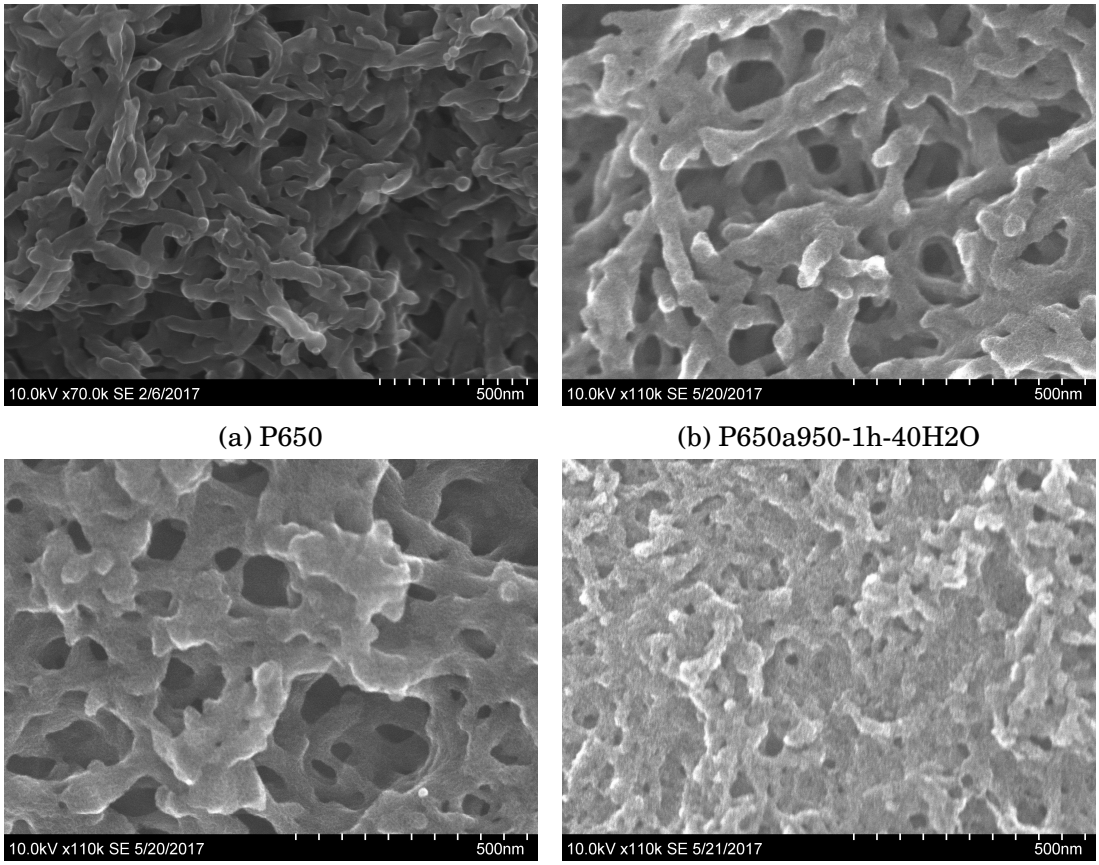

(a) P650

(b) P650a950-1h-40H2O

(c) P650a950-2h-40H2O

(d) P650a950-3h-40H2O

Figure 4.25: SEM images of activated carbon fibers derived from PANI through a carbonization temperature and an activation temperature of 650 and 950°C, respectively. The water temperature was 40°C and the activation time was varied from 1 to 3 hours.

As can be seen from Figure (4.25), during the combined CO_2 and steam activation process, the nanofiber structure is gradually destroyd with increasing activation time. Figure (4.25b) shows that the fiber structure is mostly retained after an activation time of one hour. However, as seen from Figure (4.25c), the fiber structure becomes almost completely broken after an activation time of two hours. Finally, the fiber structure is completely destroyd after an activation time of three hours, which results in a large decrease in macropore volume, as can be seen from Figure (4.25d).

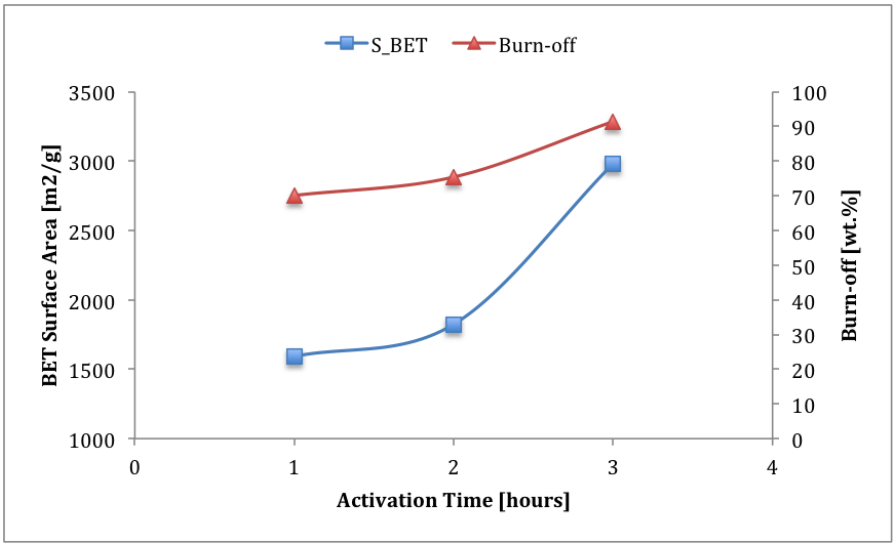

Figure 4.26: BET surface area and burn-off as function of activation time for activated carbon fibers derived from PANI through a carbonization temperature and an activation temperature of 650 and 950°C, respectively. The water temperature was 40°C and the activation time was varied from 1 to 3 hours.

Figure (4.26) shows that the BET surface area increases with activation time. It can be seen from Table (B.2) in appendix B, that the BET surface area becomes 1592.9, 1823.9 and 2981.6 m^2g^{-1} after an activation time of one, two and three hours, respectively. As expected, Figure (4.26), also shows that the burn-off increases with increasing activation time, ranging from 70.1, 75.4 and 91.4 wt.%. The increase in BET surface area with increaing activation time is reasonable, because a longer activation time results in more removal of volatile pyrolysis products, in addition to more release of carbon as CO, which is generated from the oxidation reactions involving both CO_2 and steam [21]. The release of volatile pyrolysis products and the oxidation reactions are also the reason why the yield decreases with increasing reaction time [21].

During this activation process, both micropores and small mesopores are generated from the oxidation reaction between CO_2 and carbon, as well as from the oxidation reaction between steam and carbon. It is reasonable to assume that most of the pores generated during this activation process is created by the reaction between steam and carbon, due to the fact that the oxidation reaction between CO_2 and carbon is more endothermic than the oxidation reaction between steam and carbon [27]. This means that a higher reactivity is achieved for the reaction between steam and carbon, compared to the reaction between CO_2 and carbon in this activation process. Another reason why CO_2 is less reactive than

steam, is due to the fact that CO_2 has a larger molecular size compared to H_2O [27]. Hence, by having a higher reactivity, the oxidation reaction between steam and carbon is contributing more to the development in pore structures, than the reaction between CO_2 and carbon.

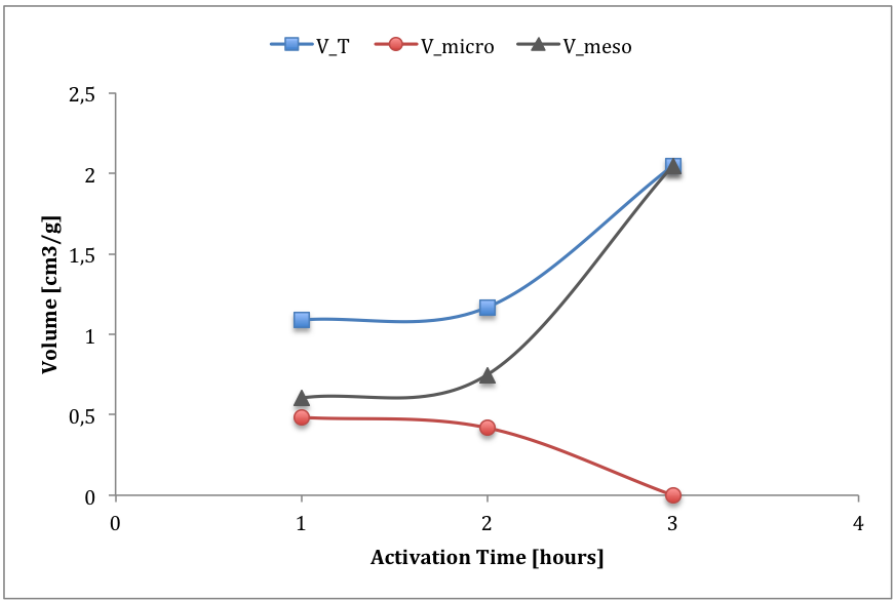

Figure 4.27: Total pore volume, micropore volume and mesopore volume as function of activation time for activated carbon fibers derived from PANI through a carbonization temperature and an activation temperature of 650 and 950°C, respectively. The water temperature was 40°C and the activation time was varied from 1 to 3 hours.

Figure (4.27) shows the total pore volume, micropore volume and mesopore volume as function of activation time in the combined CO_2 and steam activation process. It can be seen that the total pore volume increases with increasing activation time, as a result of increasing mesopore volume. These results also suggest that mesopores are created at the expense of micropores, as the micropore volume decreases with activation time. This is reasonable due to the presence of steam, in which steam mainly produces small mesopores [4]. In the CO_2 activation process, the micropore volume increases with increasing activation time up to 3 hours, as shown in Figure (4.8b).

Figure (4.28) shows the pore size distribution of activated carbons prepared with the combined CO_2 and steam activation process with various activation times. These results indicate that the pore size distribution increases with increasing activation time, where an activation time of 1, 2 and 3 hours generates pores with

a pore diameter ranging from about 1.5 to 3, 1.5 to 3.5 and 1.5 to 4.5 nm, respectively. Also, the pore volume generated increases with increasing activation time, where an activation time of 3 hours, mainly creates mesopores with a diameter ranging from 2.2 to 3.5 nm. This is reasonable, because more steam is able to react with carbon as the activation time increases.

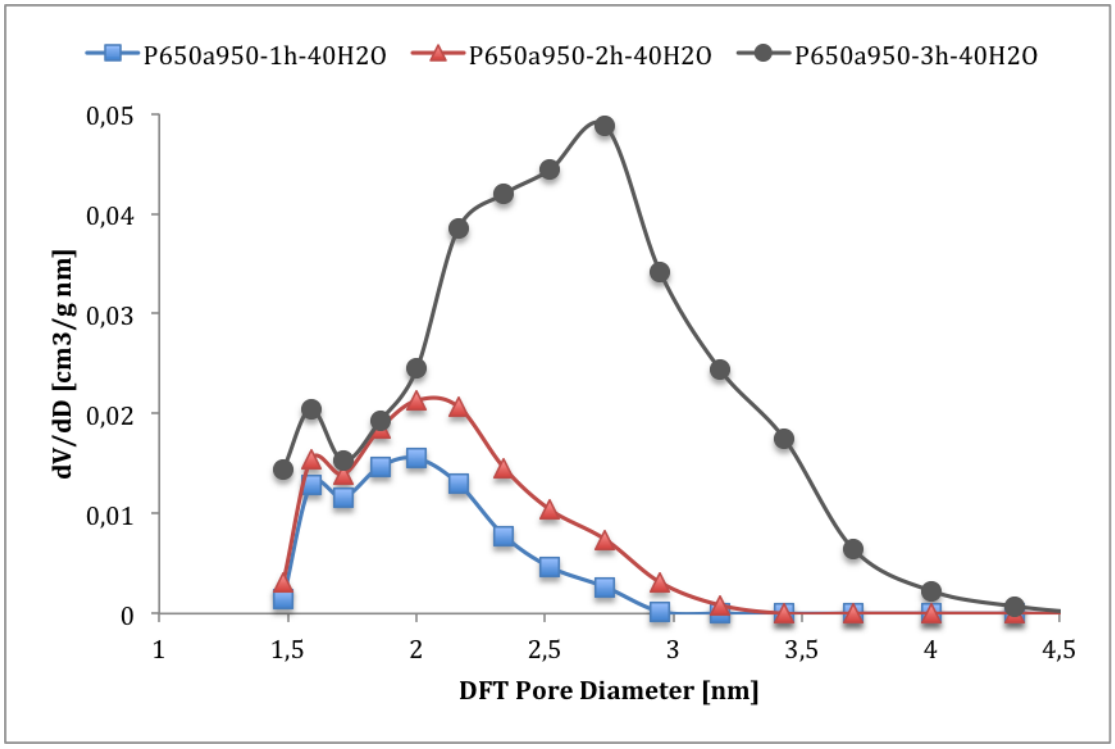

Figure 4.28: Pore size distribution, determined by NLDFT, of activated carbon derived from PANI through a carbonization temperature and an activation temperature of 650 and 950°C, respectively. The water temperature was 40°C and the activation time was varied from 1 to 3 hours.

4.3.3 Activation temperature

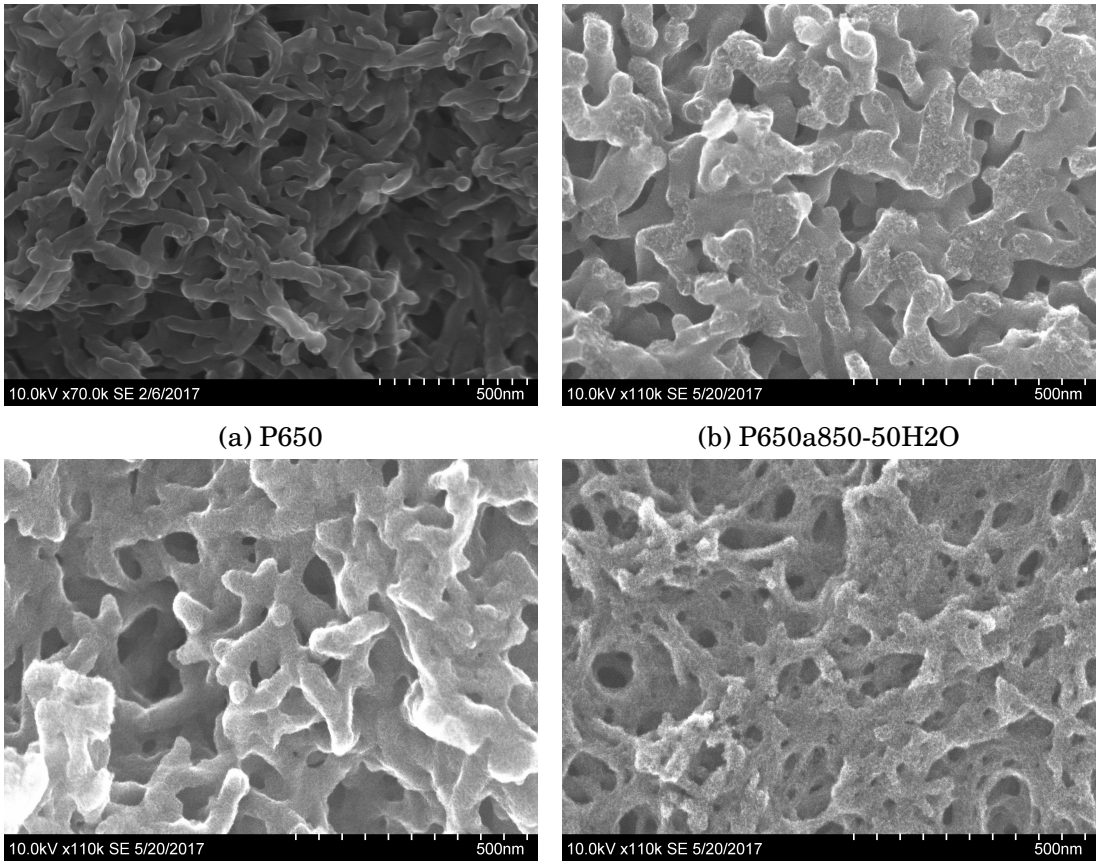

(a) P650

(b) P650a850-50H2O

(c) P650a900-50H2O

(d) P650a950-50H2O

Figure 4.29: SEM images of activated carbon fibers derived from PANI through a carbonization temperature and an activation time of 650°C and three hours, respectively. The water temperature was 50°C and the activation temperature was varied from 850 to 950°C.

Figure (4.29) shows that the nanofiber structure is gradually destroyd with increasing activation temperature after the combined CO_2 and steam activation process at a duration of three hours. The destruction of fiber structure is evident at an activation temperature of 850°C. Moreover, the fiber structure seems to be even more destroyd when using activation temperatures of 900 and 950°C, however some of the macroporous structure is maintained.

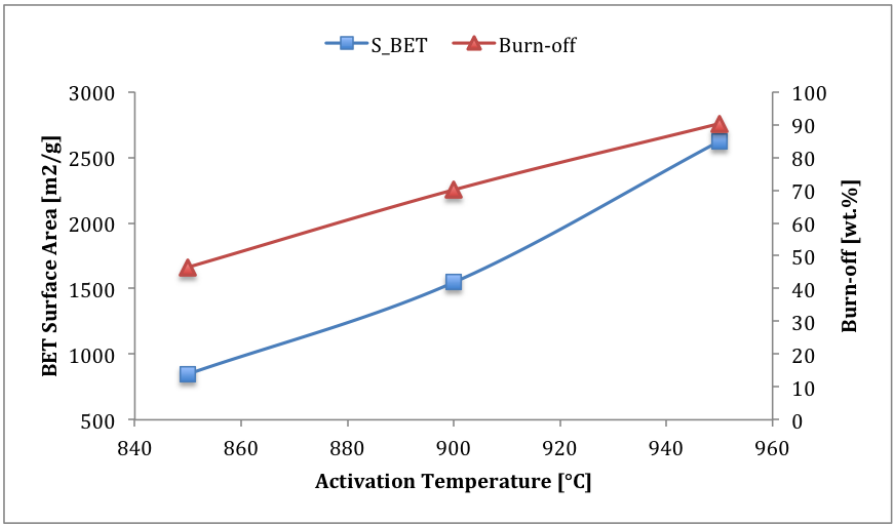

Figure 4.30: BET surface area and burn-off as function of activation temperature for activated carbon fibers derived from PANI through a carbonization temperature and an activation time of 650°C and three hours, respectively. The water temperature was 50°C and the activation temperature was varied from 850 to 950°C.

Figure (4.30) shows that the BET surface area, as well as the burn off, increases with increasing activation temperature. The BET surface area is 848.0, 1547.1 and 2622.6 m^2g^{-1} after an activation temperature of 850, 900 and 950°C, respectively. The corresponding burn-off is 46.5, 70.1 and 90.3 wt.%. An activation temperature of 950°C provides a very high BET surface area, but due to the trade-off with decrease in yield, the burn-off is very high [21]. As previously described, both the oxidation reaction between CO_2 and carbon and the oxidation reaction between steam and carbon are endothermic reactions, which means that both are thermodynamically favored at higher temperatures. Hence, as the activation temperature increases, the reactivity of both oxidation reactions increases [3].

Considering the extremely high burn-off after an activation temperature of 950°C, the optimum activation temperature in the combined CO_2 and steam activation process is probably 900°C. It can be seen from Figure (4.30) that the rate of increase in burn-off is higher than the rate of increase in BET surface area at an activation temperature ranging from 900 to 950°C. This means that the gain in BET surface area is small compared to the increase in burn-off.

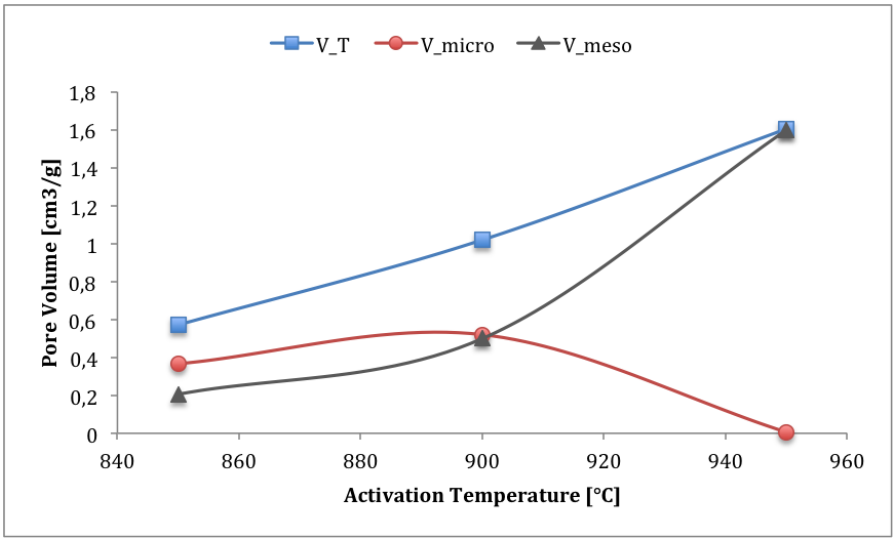

Figure 4.31: Total pore volume, micropore volume and mesopore volume as function of activation temperature for activated carbon fibers derived from PANI through a carbonization temperature and an activation time of 650°C and three hours, respectively. The water temperature was 50°C and the activation temperature was varied from 850 to 950°C.

Figure (4.31) shows that both the total pore volume and mesopore volume increase with increasing activation temperature. The rate of increase in total pore volume corresponds with the rate of increase in the BET surface area. As seen from Table (B.3) in appendix B, the total pore volume obtained is 0.570, 1.019 and 1.604 cm^3g^{-1} after an activation temperature of 850, 900 and 950°C, respectively. The rate of increase in mesopore volume is significantly larger after an activation temperature of 900°C, going from 0.499 to 1.598 cm^3g^{-1} after an activation temperature of 900 and 950°C, respectively. An activation temperature of 950°C yields a total pore volume that almost exclusively consists of mesopores.

The micropore volume goes through a maximum at an activation temperature of 900°C. The micropore volume is 0.364, 0.520 and 0.006 cm^3g^{-1} after an activation temperature of 850, 900 and 950°C, respectively. Both micropores and mesopores are created at activation temperatures up to 900°C, however at higher activation temperatures the reactivity of both CO_2 and steam is too high to create micropores. Hence, almost all micropores created after the carbonization process (0.109 cm^3g^{-1}) are enlarged to mesopores.

An activation temperature of 900°C is also the optimum activation temperature in regards to the micropore volume.

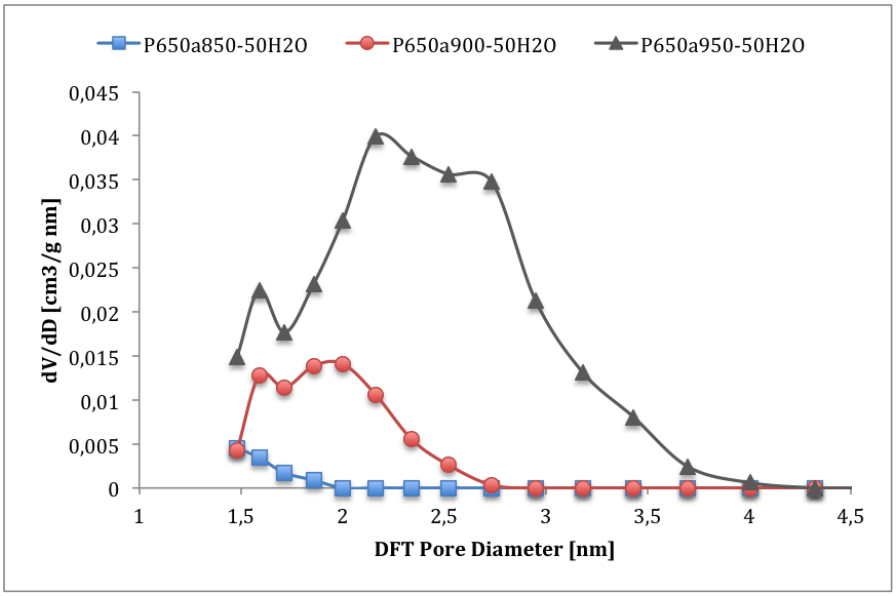

Figure 4.32: Pore size distribution, determined by NLDFT, of activated carbon fibers derived from PANI through a carbonization temperature and an activation time of 650°C and three hours, respectively. The water temperature was 50°C and the activation temperature was varied from 850 to 950°C.

Figure (4.32) shows the pore size distribution obtained after the combined CO_2 and steam activation process at an activation temperature of 850, 900 and 950°C. It can be seen that the pore size distribution greatly increases with activation temperature, where an activation temperature of 900°C mainly generates pores having a pore diameter between about 1.5 to 2.75 nm and an activation temperature of 950°C mainly produces pores in the range of about 1.5 to 4.2 nm. The large pore size distribution obtained with high activation temperatures is due to the additional oxidation reaction between steam and carbon. In general, steam activation generates a wider pore size distribution compared to CO_2 activation [4]. With an increasing activation temperature, the reactivity between steam and carbon increases, which increases the development of small mesopores.

t-plot method vs NLDFT

4.3.4 Partial pressure of CO_2

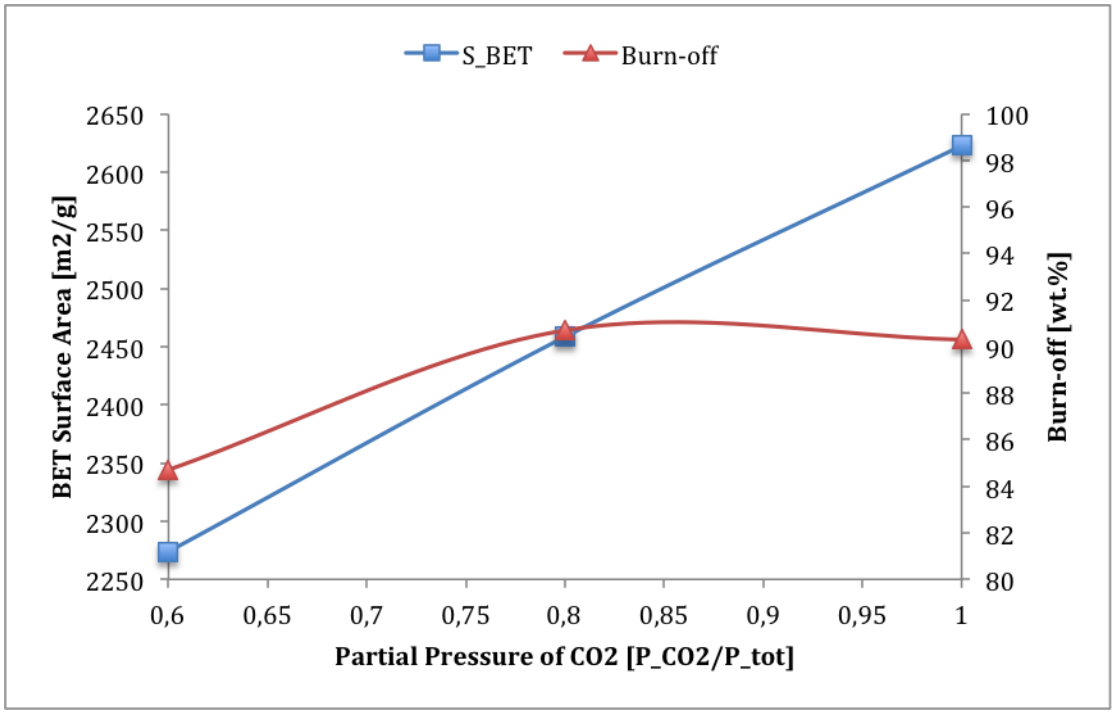

Figure 4.33: BET surface area and burn-off as function of the partial pressure of CO_2 for activated carbon fibers derived from PANI through a carbonization temperature and an activation temperature of 650 and 950°C, respectively. The activation time was set to be 3 hours and the water temperature was 50°C.

Figure (4.33) shows the BET surface area and burn-off as function of the partial pressure of CO_2 in the combined CO_2 and steam activation process. The BET surface area increases with increasing partial pressure of CO_2, while the burn-off increases with the patial pressure of CO_2 up to 0.8 P_{CO_2}/P_{tot}. The increase in BET surface area is reasonable, because the degree of activation increases with the amount of activation agents present in the activation process. The partial pressure of argon, which is inert during the activation process, decreases as the partial pressure of CO_2 increases. This leads to more CO_2 molecules being introduced together with steam, which enhances the degree of activation. A decrease in density and pore widening occurs, as the degree of activation increases [21].

It can be seen from Table (B.4) in appendix B that the resulting BET surface area is 2273.6, 2458.4 and 2622.6 m^2g^{-1} at a partial pressure of CO_2 equal to 0.6, 0.8 and 1.0 P_{CO_2}/P_{tot}, respectively. The burn-off ranges from 84.7, 90.7 and 90.3 wt.%

at the corresponding partial pressures. This indicates that a partial pressure of CO_2 equal to 1.0 P_{CO_2}/P_{tot} is favorable in the combined CO_2 and steam activation process, since it provides the largest BET surface area without an increase in burn-off compared to a partial pressure at 0.8 P_{CO_2}/P_{tot}. However, a burn-off at 90.3 wt.% is way too large in any commercial activation process, which means that the burn-off has to be decreased with a decrease in activation time or activation temperature [21].

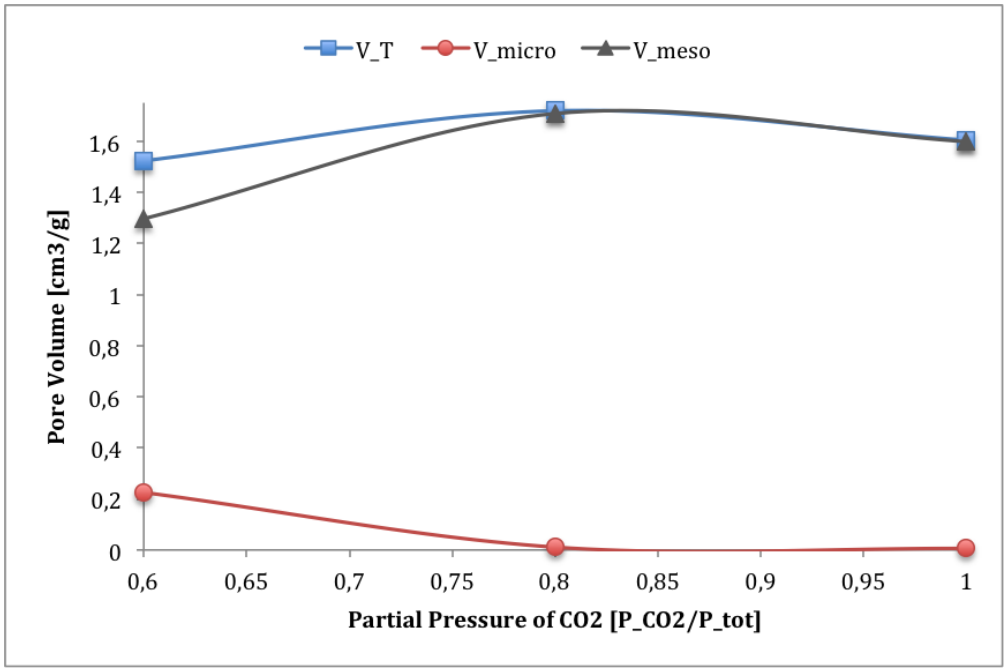

Figure 4.34: Total pore volume, micropore volume and mesopore volume as function of the partial pressure of CO_2 for activated carbon fibers derived from PANI through a carbonization temperature and an activation temperature of 650 and 950°C, respectively. The activation time was set to be 3 hours and the water temperature was 50°C.

Figure (4.34) shows the total pore volume, micropore volume and mesopore volume as function of the partial pressure of CO_2 in the combined CO_2 and steam activation process. The total pore volume and mesopore volume goes through a maximum of 1.719 and 1.708 cm^3g^{-1} at a partial pressure of CO_2 equal to 0.8 P_{CO_2}/P_{tot}. However, the micropore volume decreases with increasing partial pressure of CO_2, where a partial pressure of 0.6, 0.8 and 1.0 results in a micropore volume of 0.227, 0.011 and 0.006 cm^3g^{-1}, respectively. These values can be seen from Table (B.4) in appendix B.

Figure (4.35) shows the pore size distribution of activated carbons obtained with different partial pressure of CO_2 in the combined CO_2 and steam activation process. It can be seen that as the partial pressure of CO_2 increases, the pore size distribution becomes larger, where a partial pressure of 0.6 P_{CO_2}/P_{tot} generates pores having a diameter ranging from about 1.5 to 3.7 nm and a partial pressure of 0.8 and 1.0 P_{CO_2}/P_{tot} creates pores having a diameter ranging from about 1.5 to 4 nm. The widening of pores with increasing partial pressure of CO_2 indicated by the pore size distribution, is reasonable due to an increase in the level of activation [21]. Also, it can be seen that mostly mesopores having a diameter ranging between about 2 and 4 nm are developed with increasing partial pressure of CO_2 from 0.6 to 1.0 P_{CO_2}/P_{tot}. This is unexpected as CO_2 mainly generates micropores [38]. However, this could be due to different amounts of steam entering the activation process, as the amount of CO_2 and argon, which are carrying the water, changes.

Also, the high activation temperature of 950°C could influence the ability of CO_2 to diffuse into the interior of the carbon, as the CO_2 and carbon become more reactive with increasing temperature. This could result in CO_2 reacting with the carbon on the surface before diffusing into the interior, which limits development of micropores. The activation temperature plays an important role in controlling the reaction kinetics, where the reaction can go from being chemically controlled to become diffusionally controlled at high temperatures [11]. When the reaction is diffusionally controlled, CO_2 reacts on the surface of the particles, which does not provide net porosity [11]. To observe this change from chemically to diffusionally controlled reaction conditions, the variation of the reaction rate with the temperature can be determined using the Arrhenius equation [11]. At temperatures between 850 and 950°C, the diffusion towards and from the particle surface is much faster compared to the oxidation reaction between CO_2 and carbon. At temperatures between 950 and 1050°C, the speed of the activation process is determined by a combination of the diffusion of CO_2 inside the pores and the reaction rate. Finally, at temperatures between 1050 and 1100°C, the reaction rate of the oxidation reaction is so fast that the diffusion of CO_2 towards the particle surface is what limits the speed of the activation process [11]. Hence, because the activation temperature was set at 950°C, it could be assumed that the speed of the activation process is determined by a combination of the diffusion of CO_2 inside the pores and the reaction rate. This could be the reason why mostly mesopores are generated as the amount of CO_2 increases, since the CO_2 molecules are not able to properly diffuse into the interior, which results in widening of existing pores.

It is important to know that these temperature intervals in the activation process were determined based on a different precursor and carbonization temperature than that used in this work. The carbonization temperature effects the reactivity of the carbonized material with CO_2, where material carbonized at higher temperatures shows less reactivity [11]. Hence, these temperature intervals should only be used as a guidance in regard to this work.

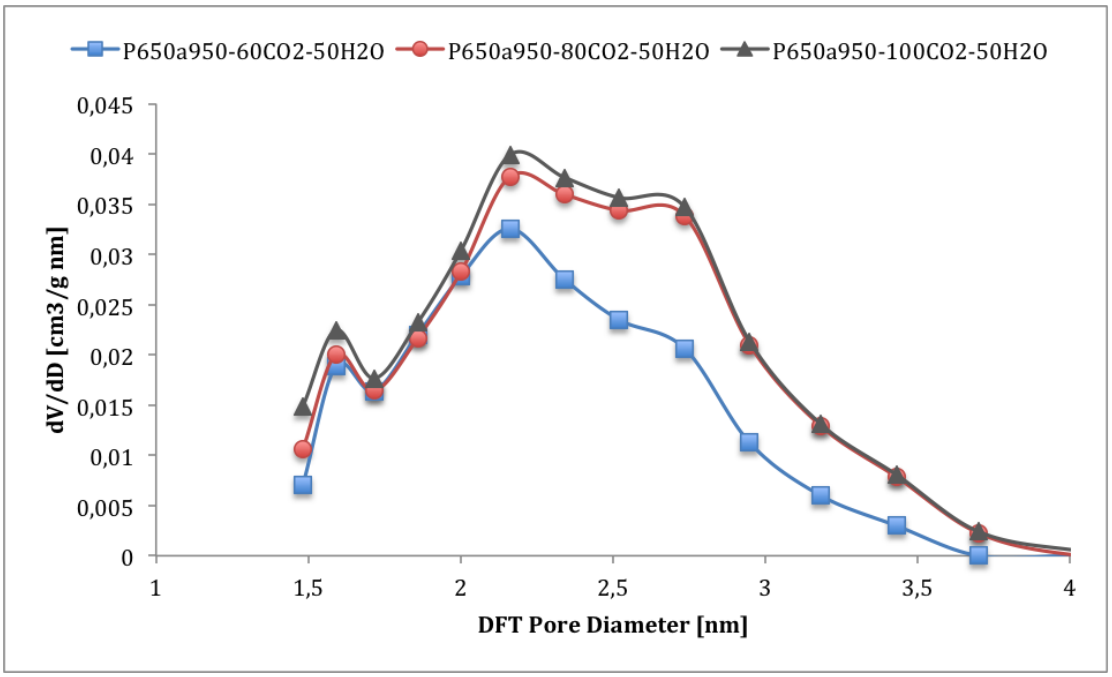

Figure 4.35: Pore size distribution, determined by NLDFT, of activated carbon fibers derived from PANI through a carbonization and an activation temperature of 650 and 950°C, respectively. The activation time was set to be 3 hours and the water temperature was 50°C. The partial pressure of CO_2 was varied from 0.6 to 1.0 P_{CO_2}/P_{tot}.

4.4 The effects of activation agent

4.4.1 Activation time

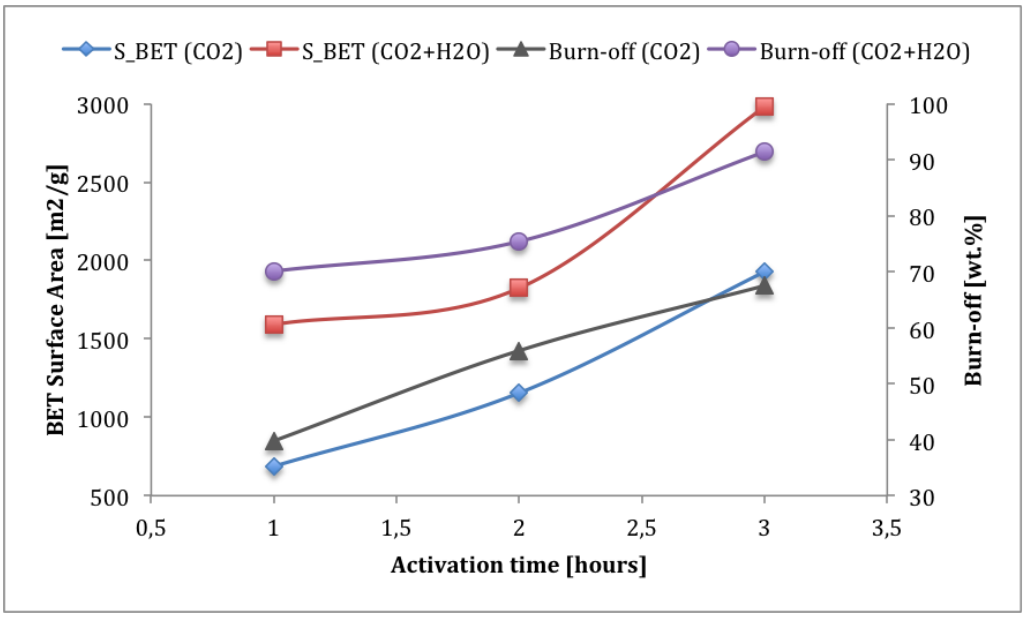

Figure 4.36: BET surface area and burn-off as function of activation time for activated carbon fibers derived from PANI through a carbonization temperature and an activation temperature of 650 and 950°C, respectively. The activation time was varied from 1 to 3 hours. In the combined CO_2 and steam activation process, the water temperature was set to be 40°C.

Figure 4.36 shows the BET surface area and burn-off as function of the activation time. As previously discussed, both the BET surface area and the burn-off increases with increasing activation time in both the CO_2 activation process and the combined CO_2 and steam activation process. It can be seen that for each activation time, both the BET surface area and the burn-off is larger after the combined CO_2 and steam activation process, combared to that after the CO_2 activation process. This is reasonable due to the presence of steam in the combined activation process.

In the combined CO_2 and steam activation process, an activation time of two hours is probably the optimum activation time, due to the very high burn-off of 91.4 wt.% with an activation time of three hours. In this activation process, an activation time of two hours results in a BET surface area of 1823.9 m^2g^{-1}, while the burn-off is 75.4 wt.%. It can be seen that by using the CO_2 activation process

with a duration of three hours, a BET surface area of 1927.7 can be obtained, while the burn-off is 67.5 wt.%. This means that a larger BET surface area can be produced with a smaller burn-off, by using the CO_2 activation process, compared with using the combined activation process. This can be achieved by running the CO_2 activation process one hour longer than the combined CO_2 and steam activation process. A higher BET surface area accompanied with a smaller burn-off is possible due to the difference in the development of pore structure.

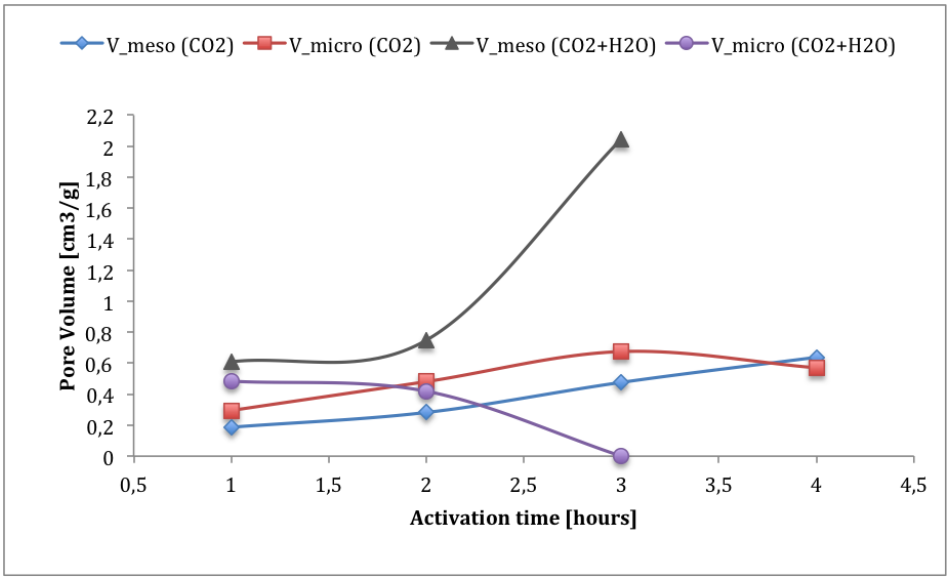

Figure 4.37: Micropore volume and mesopore volume as function of activation time for activated carbon fibers derived from PANI through a carbonization temperature and an activation temperature of 650 and 950°C, respectively. The activation time was varied from 1 to 3 hours. In the combined CO_2 and steam activation process, the water temperature was set to be 40°C.

Figure (4.37) shows the micropore volume and the mesopore volume as function of activation time. For both the CO_2 activation process and the combined CO_2 and steam activation process, the mesopore volume increases with increasing activation time. However, at each activation time, the mesopore volume achieved is higher for the combined CO_2 and steam activation process. This is reasonable due to the presence of steam in the combined CO_2 and steam activation process, as steam mainly creates mesopores [4]. The micropore volume decreases with increasing activation time in the combined CO_2 and steam activation process. However, in the CO_2 activation process, the micropore volume goes through a maximum at three hours of activation. The high content of micropores (58.6 % of the total pore volume) produced with the three hours long CO_2 activation

process, is the reason why a larger BET surface area is obtained with a smaller burn-off, compared to that obtained with the two hour long combined CO_2 and steam activation process. This is reasonable, due to the fact that micropore volume contributes more to the BET surface area than mesopore volume. This is because, in two equally large volumes where one consists of micropores and the other consists of mesopores, the volume consisting of micropores would have more pore walls which creates a larger surface, due to the smaller pore diameter of micropores. Also, the high amount of micropores is most likely the reason why the burn-off is smaller, as less carbon has to be removed when creating a micropore versus creating a mesopore.

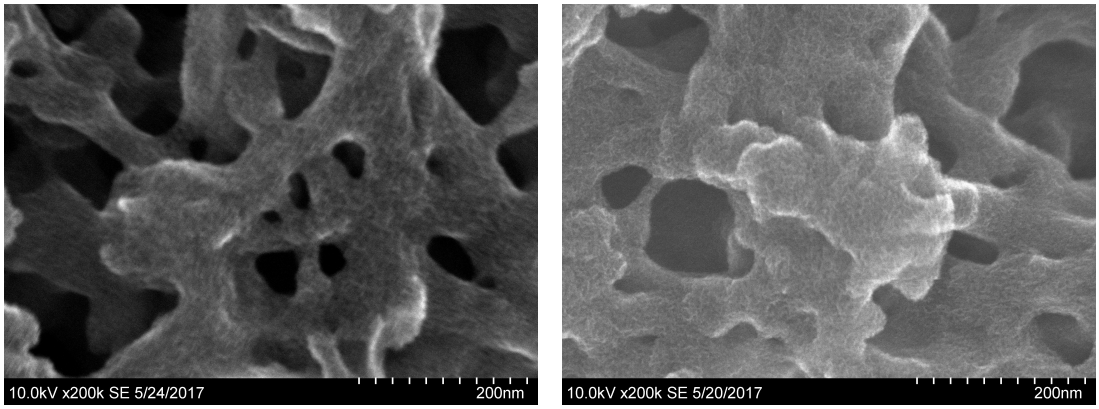

(a) P650a950-2h (b) P650a950-2h-40H2O

Figure 4.38: SEM images of activated carbon fibers derived from PANI through a carbonization temperature and an activation temperature of 650 and 950°C, respectively. In the combined CO_2 and steam activation process, the water temperature was set to be 40°C. The activation time was two hours for both the CO_2 activation process and the combined CO_2 and steam activation process.

As seen from Figure (4.38), the nanofiber structure is retained after the CO_2 activation process with an activation temperature and a duration of 950°C and two hours. However, the combined CO_2 and steam activation process carried out with identical conditions as the CO_2 activation process, partially destroys the nanofiber structure. Also the macropore volume is smaller after the combined CO_2 and steam activation process, which is a result of the destruction of the fiber network. It can also be seen that the surface obtained with the combined CO_2 and steam activation process is more rough compared to the surface obtained with the CO_2 activation process. This could indicate that more small mesopores are formed during the combined CO_2 and steam activation process, which is consistent with the results from Figure (4.37).

4.4.2 Activation temperature

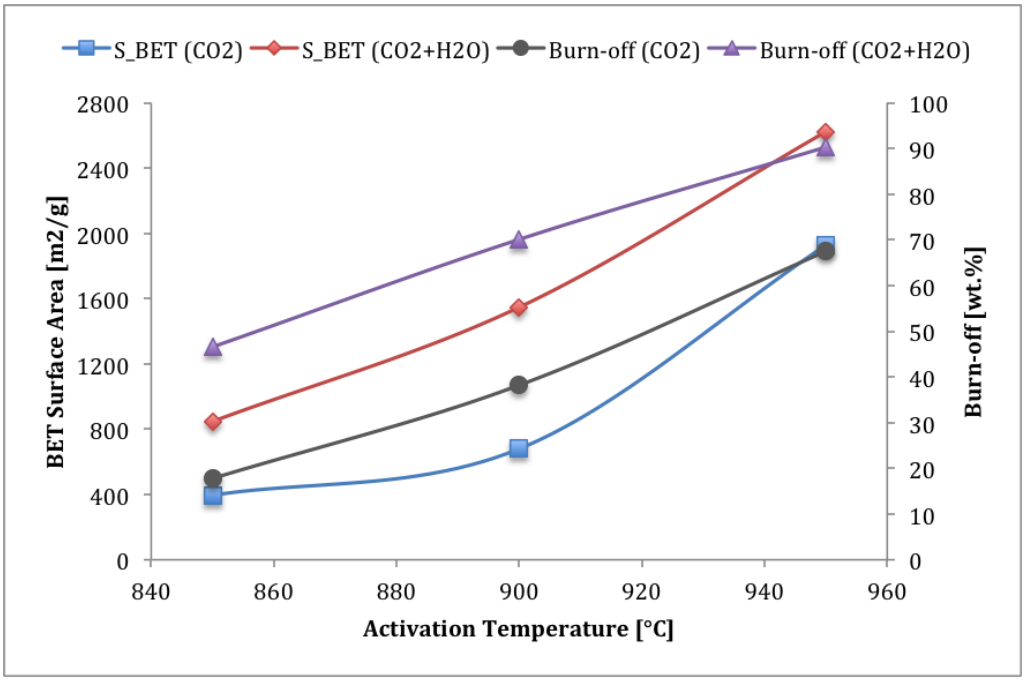

Figure 4.39: BET surface area and burn-off as function of activation temperature for activated carbon fibers derived from PANI through a carbonization temperature and an activation time of 650°C and three hours, respectively. The activation temperature was varied from 850 to 950°C. In the combined CO_2 and steam activation process, the water temperature was set to be 50°C.

Figure (4.39) shows the BET surface area and burn-off as function of activation temperature for both the CO_2 activation process and the CO_2 and steam activation process. As previously described, both the BET surface area and burn-off increases with increasing activation temperature. At each activation temperature, both the BET surface area and the burn-off is larger after the combined CO_2 and steam activation process, compared to that of the CO_2 activation process. This is due to the presence of steam in the combined CO_2 and steam activation process, as steam is a more reactive activation agent compared to CO_2 [27]. Another factor is that two activation agents are introduced in the combined CO_2 and steam activation process, which means that more activating molecules that are able to remove carbon are present during the activation. Also, at activation temperatures below 900°C, the BET surface area obtained after the combined CO_2 and steam activation process is much higher compared to that obtained after pure CO_2 activation. This could be due to the fact that the reaction between CO_2 and carbon

has a slow reaction rate at temperatures around 800°C, while the reaction rate of the reaction between steam and carbon is high [10]. Hence, at low temperatures the reaction between CO_2 and carbon is slow and have to be maintained for a long time. In these conditions, the slow reaction rate allows for better controllability of the activation process, where CO_2 is able to penetrate inside of the carbon particles via superficial groups or structural defects and the gasification occurs inside the carbonized material, which creates porosity [11].

It can be seen that the rate of increase in BET surface area is higher in the combined CO_2 and steam activation process compared to the CO_2 activation process at activation temperatures from 850 to 900°C. This is most likely due to the reactivity of the oxidation reaction between steam and carbon, which is more affected by the reaction temperature than the reaction between CO_2 and carbon. As the activation temperature increases to 950°C, the difference in BET surface area is smaller compared to the difference in BET surface area at 900°C. This could be related to the difference in pore structure produced by the two activation processes.

It can be seen that the CO_2 activation process carried out with an activation temperature of 950°C produces a higher BET surface area with a smaller burn-off, compared to that produced with the CO_2 and steam activation process performed at 900°C. As previously discussed, this could be due to differences in pore structure development.

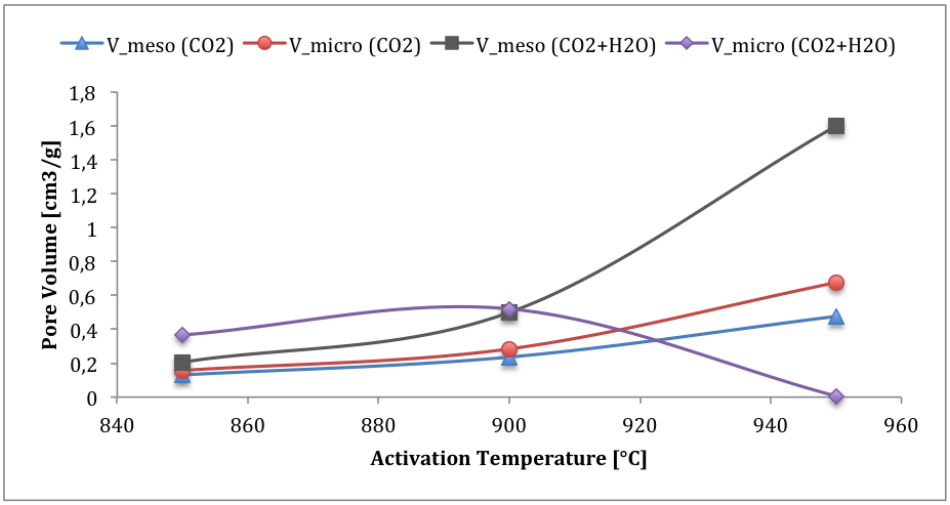

Figure 4.40: Micropore volume and mesopore volume as function of activation temperature for activated carbon fibers derived from PANI through a carbonization temperature and an activation time of 650°C and three hours, respectively. The activation temperature was varied from 850 to 950°C. In the combined CO_2 and steam activation process, the water temperature was set to be 50°C.

Figure (4.40) shows that the mesopore volume increases with increasing activation temperature. In the CO_2 activation process, the micropore volume increases with activation temperature, while in the combined CO_2 and steam activation process, the micropore volume goes through a maximum at 900°C. This indicates that an activation temperature of 950°C is too severe in order to produce micropores by the combined CO_2 and steam activation process. The continuous increase in micropore volume by the CO_2 activation process, even at a high activation temperature of 950°C, is due to the better control of the activation process, where carbon atoms are removed from the particle inside [27]. This enhances the creation of micropores.

As seen from Figure (4.40), the rate of increase in both micropores and mesopores is higher in the CO_2 and steam activation process compared to that in the CO_2 activation process, between activation temperatures of 850 and 900°C. This could be the reason why the rate of increase in BET surface area was higher for the combined CO_2 and steam activation process at these temperatures. Also, the fact that the CO_2 activation process carried out with an activation temperature of 950°C produced a higher BET surface area with a smaller burn-off than that obtained with CO_2 and steam activation performed at 900°C, could be due to the higher content of micropores produced in the CO_2 activation process.

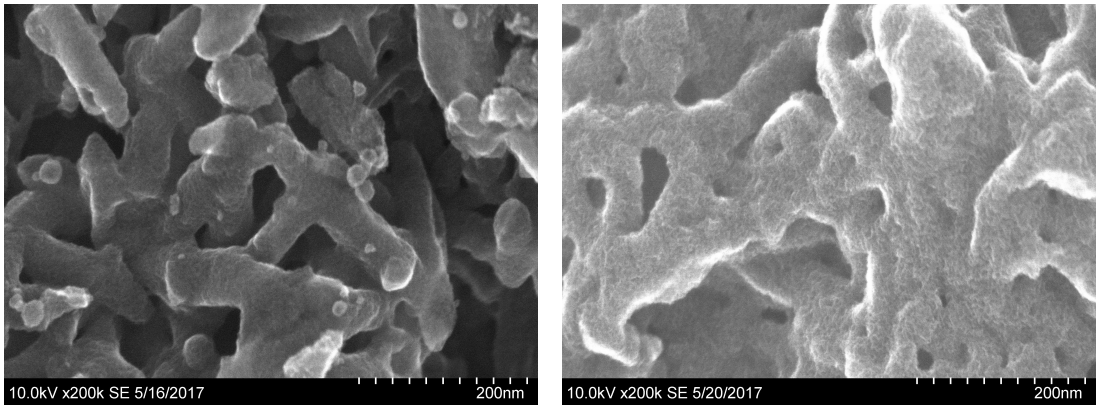

(a) P650a900 (b) P650a900-50H2O

Figure 4.41: SEM images of activated carbon fibers derived from PANI through a carbonization temperature and an activation time of 650°C and three hours, respectively. In the combined CO_2 and steam activation process, the water temperature was set to be 50°C. The activation temperature was 900°C for both the CO_2 activation process and the combined CO_2 and steam activation process.

As seen from Figure (4.41), the nanofiber structure is retained after the CO_2 activation process with an activation temperature and a duration of 900°C and three hours. However, the combined CO_2 and steam activation process carried out with identical conditions as the CO_2 activation process, destroys the nanofiber structure to a certain extent. As can be seen, the destruction of the fiber network results in a smaller macropore volume after the combined CO_2 and steam activation process. The surface obtained with the combined CO_2 and steam activation process is more coarse than the surface obtained with the CO_2 activation process. This indicates that more small mesopores are formed during the combined CO_2 and steam activation process, which is in agreement with the results from Figure (4.40).

4.5 Optimization

Properties	P650a950-5h-0.2CO_2	P650a950-1h-40H_2O-2h-1CO_2
S_{BET} [m^2/g]	1273.4	2552.6
V_T [cm^3/g]	0.793	1.662
V_{micro} [cm^3/g]	0.524	0.285
V_{meso} [cm^3/g]	0.269	1.377
V_{meso}/V_T [%]	33.9	82.9
V_{micro}/V_T [%]	66.1	17.1
Burn-off [wt.%]	56.1	83.6

Table 4.4: Physical properties of activated carbon fibers derived from PANI carbonized at 650°C. P650a950-5h-0.2CO_2 corresponds to CO_2 activation at 950°C for a duration of 5 hours. The partial pressure of CO_2 was 0.2. P650a950-1h-40H_2O-2h-1CO_2 corresponds to 1 hour of the combined CO_2 and steam activation process followed by 2 hours of CO_2 activation at 950°C. The water temperature was 50°C and a flow rate of CO_2, excluding argon, was used.

It can be seen from Table (4.4) that activated carbon fibers prepared with CO_2 activation at 950°C for a duration of 5 hours exhibit a high fraction of micropores equal to 66.1 %. A long activation time of 5 hours was chosen, since the previous results indicate that the BET surface area increases with increasing activation time. However with an activation time of 4 hours and a partial pressure of CO_2 equal to 0.8, the burn-off was high, having a value of 80.6 wt.%, as seen from Table (A.1) in appendix A. Therefore, a lower partial pressure of CO_2 at 0.2 was applied in order to decrease the burn-off. The results show that with these reaction conditions, the obtained BET surface area is not significantly large, however the burn-off is moderate with a value of 56.1 wt%. Hence, in the future work, the CO_2 activation process could be carried out with a increased partial pressure of CO_2 of 0.4 and 0.6, in order to increase the BET surface area. It is reasonable to assume an increase in burn-off with increasing partial pressure of CO_2, however the increase in burn-off is most likely small, since CO_2 generates mostly microporosity [38].

The combined CO_2 and steam activation process was followed by activation with pure CO_2 in order to exploit the high reactivity of steam. The combined CO_2 and steam activation process with a reaction time of 1 hour at 950°C was shown to generate a significantly larger BET surface area than the CO_2 activation process under these conditions. It was shown that the micropore volume was reduced

when increasing the activation time in the combined CO_2 and steam activation process, as seen from Table (B.2). Therefore an activation time of 1 hour was chosen followed by 2 hours of CO_2 activation at the same temperature, in order to further increase the BET surface area. The resulting activated carbon fibers showed a high BET surface area of 2552.6 m^2g^{-1}. It can be seen from Table (B.1) that by this method it is possible to obtain a larger BET surface area with a smaller burn-off, compared to most of the BET surface areas obtained during the three hour combined CO_2 and steam activation process. However, a burn-off at 83.6 wt% is still very high, hence it is necessary to further optimize the activation process in the future.

Properties	CS650	CS650a950-3h-50H_2O
S_{BET} [m^2/g]	509.9	3042.2
V_T [cm^3/g]	0.284	1.768
V_{micro} [cm^3/g]	0.221	0.021
V_{meso} [cm^3/g]	0.063	1.747
V_{meso}/V_T [%]	22.2	98.8
V_{micro}/V_T [%]	77.8	1.2
Burn-off [wt.%]	60.6	92.1

Table 4.5: Physical properties of carbon spheres and activated carbon spheres derived from RF polymer spheres through a carbonization temperature and an activation temperature of 650 and 950°C, respectively. The duration of the carbonization and activation process was 2 and 3 hours, respectively. The carbon spheres were subjected to the combined CO_2 and steam activation process, where the water temperature was set to be 50°C.

Table (4.5) shows the BET surface area and pore volume of carbon spheres and activated carbon spheres through the combined CO_2 and steam activation process. By comparing the properties of carbon spheres with the properties of carbonized PANI fiber (P650, shown i Table A.1), it can be seen that the carbon spheres have a larger BET surface area of 509.9 m^2g^{-1}. Also, the carbon spheres are more microporous, having a micropore volume fraction of 77.8 %, compared to 54.0 % for the carbonized PANI fibers. The activated carbon spheres possess a very large BET surface area of 3042.2 m^2g^{-1} with a high fraction of mesopores, which makes the carbon material promising for electrode material in supercapacitiors. Compared to carbonized PANI fibers activated under identical conditions as the carbon spheres (Table B.1), a smaller BET surface area of 2622.6 m^2g^{-1} is obtained. This difference in BET surface area is most likely due to the different pore structure of the precursors.

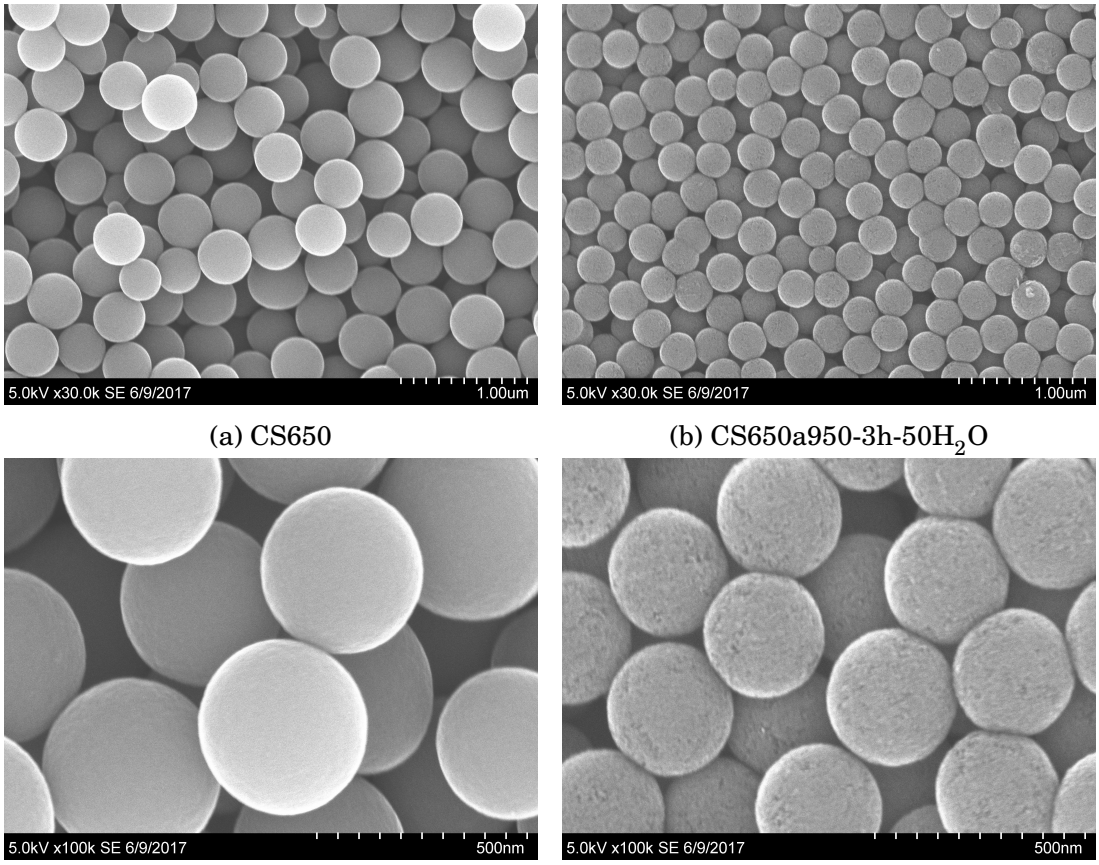

(a) CS650 (b) CS650a950-3h-50H_2O

(c) CS650 (d) CS650a950-3h-50H_2O

Figure 4.42: SEM images of carbon spheres and activated carbon spheres. Carbonization and activation temperature were 650 and 950°C, respectively. The duration of the carbonization and activation process were 2 and 3 hours, respectively. The carbon spheres were subjected to the combined CO_2 and steam activation process, where the water temperaure was 50°C.

As seen from Figure (4.42a), the slow heating carbonization process to a temperature of 650°C for a duration of two hours, does not change the spherical morphology of the RF polymer spheres. Also, it can be seen that the size distribution of carbon spheres is very small, which indicates that the carbonization process does not effect the distribution of particle size. This is in accordance with literature, where it was found that the spherical shape of RF polymer spheres was completely retained after carbonization processes up to 900°C [7].

Figure (4.42c) shows a very smooth particle surface, which indicates that the surface smoothness does not change during the carbonization process. This result is

also obtained in the literature [7]. Figure (4.42b) shows that the spherical morphology is retained even after a combined CO_2 and steam activation process at 950°C, which indicates the high thermal stability of the carbon spherical structure. However, by comparing Figure (4.42a) and (4.42b), it can be seen that the size of the carbon spheres has become smaller after the activation process. This decrease in particle size is most likely a result of the release of volatile materials and the release of carbon through the oxidation reactions. In addition, it can be seen from Figure (C.1) and (C.2) in appendix C, that the average particle diameter after carbonization is about 400 nm, while the average particle diameter after activation is about 300 nm. By comparing Figure (4.42c) and (4.42d), it can be seen that the very smooth surface of carbon spheres has become rough after the activation process. This result indicates the creation of mesopores during the activation process, by the release of volatile material and release of carbon through the oxidation reactions.

4.5.1 Surface oxygen groups

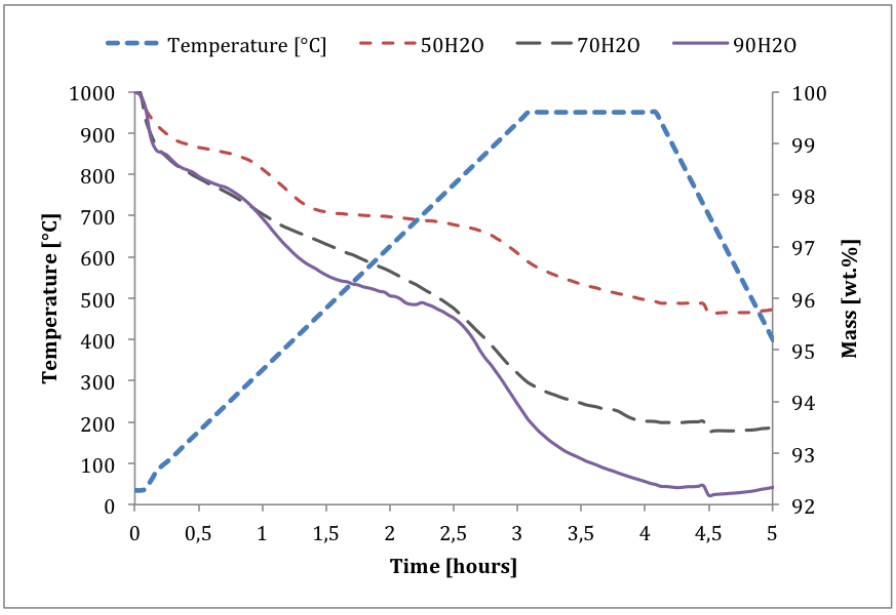

Figure 4.43: Thermal gravimetric analysis where activated carbons derived from PANI were exposed to one hour of heat treatment at 950°C in an argon atmosphere. The combined CO_2 and steam activation process with an activation temperature and an activation time of 950°C and three hours was used to obtain the activated carbons. The water temperature in the activation process was 50, 70 and 90°C.

Figure (4.43) shows the mass loss during one hour of heat treatment at 950°C in an inert atmosphere, for carbons activated with the combined CO_2 and steam activation process. Several water temperatures were used in order to vary the amount of steam present in the activation process. It can be seen that the total mass loss increases with increasing water temperature, which indicates that higher water temperatures gives activated carbons with more volatile materials. This is reasonable because the amount of steam present during the activation process increases with increasing water temperature, hence more oxygen atoms are introduced into the carbon network.

During the heat treatment in an inert atmosphere, oxygen atoms are released as CO and CO_2. At relatively low temperatures, oxygen is mainly released as CO_2 from functional groups such as -COOH. Oxygen gets released as CO from groups such as C-OH, C=O and COC as the temperature increases. The increase in total mass loss with increasing amount of steam present during the activation process, indicates that the oxygen content of activated carbons increases. As shown in Figure (4.22), this is consistent with the oxygen content measured by EDX, where the oxygen content was determined to be 8.31, 8.65 and 9.09 wt.% with water temperatures of 50, 70 and 90°C respectively. As can be seen from Figure (4.43), the three curves are similar in shape, in which all exhibit significant drop in mass at the beginning of the heat treatment and after about 1 hour and 2.5 hours.

As seen from Figure (C.3c) and (C.3d) in appendix C, the presence of oxygen atoms on the surface of activated carbon spheres obtained by the combined CO_2 and steam activation process, indicates the introduction of oxygen through the oxidation reaction between steam and carbon.

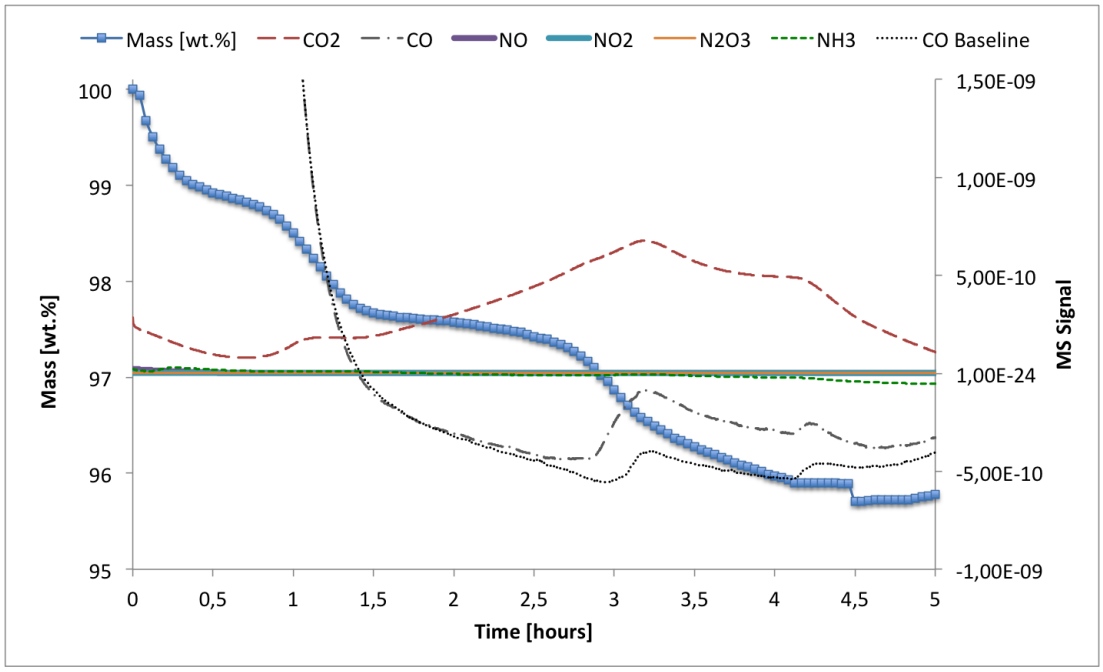

Figure 4.44: TGA combined with MS where activated carbons derived from PANI were exposed to one hour of heat treatment at 950°C in an argon atmosphere. The combined CO_2 and steam activation process with an activation temperature and an activation time of 950°C and three hours was used to obtain the activated carbons. The water temperature in the activation process was 50°C.

Figure (4.44) shows the mass loss and the formation of CO_2, CO and different nitrogen-containing gases during one hour of heat treatment at 950°C in an inert atmosphere, for carbons activated with the combined CO_2 and steam activation process with a water temperature of 50°C. The initial weight drop occuring at a temperature of about 100°C is most likely connected the the release of volatile materials, such as water. The second significant weight drop occurs after about 1 hour and at a temperature of about 350°C, which is most likely due to the release of oxygen through CO_2. More CO_2 is generated as the temperature increases, resulting in a slight decrease in weight. The final significant weight drop occurs after about 2.8 hours and at a temperature of about 900°C. This weight drop is most likely connected to the release of oxygen through the formation of CO. It can be seen that both CO_2 and CO are formed at a temperature of 950°C.

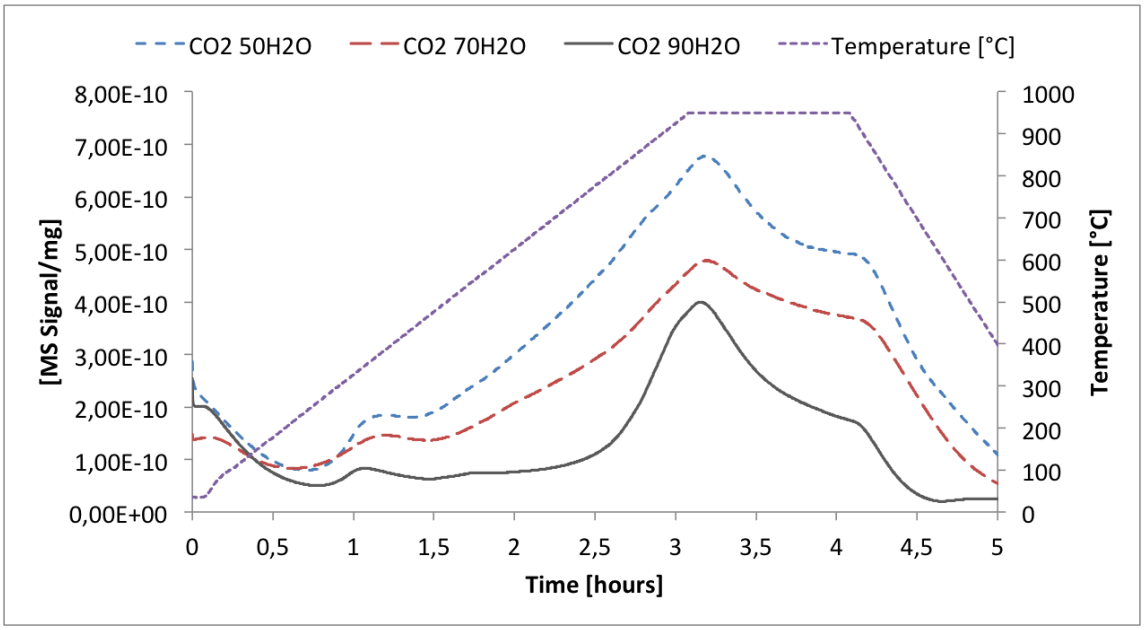

Figure 4.45: MS results during the one hour heat treatment, at 950°C in an argon atmosphere, of activated carbons derived from PANI. The combined CO_2 and steam activation process with an activation temperature and an activation time of 950°C and three hours was used to obtain the activated carbons. The water temperature in the activation process was 50, 70 and 90°C.

Figure (4.45) shows the formation of CO_2 during the heat treatment of activated carbons obtained after the combined CO_2 and steam activation process with various amount of steam. As previously discussed, the oxygen content of activated carbons increases with the water temperature used in the activation process. Hence, it could be expected that the release of oxygen in the form of CO_2 increases with water temperature. This assumption is not met, as the results indicate that the formation of CO_2 decreases with water temperature.

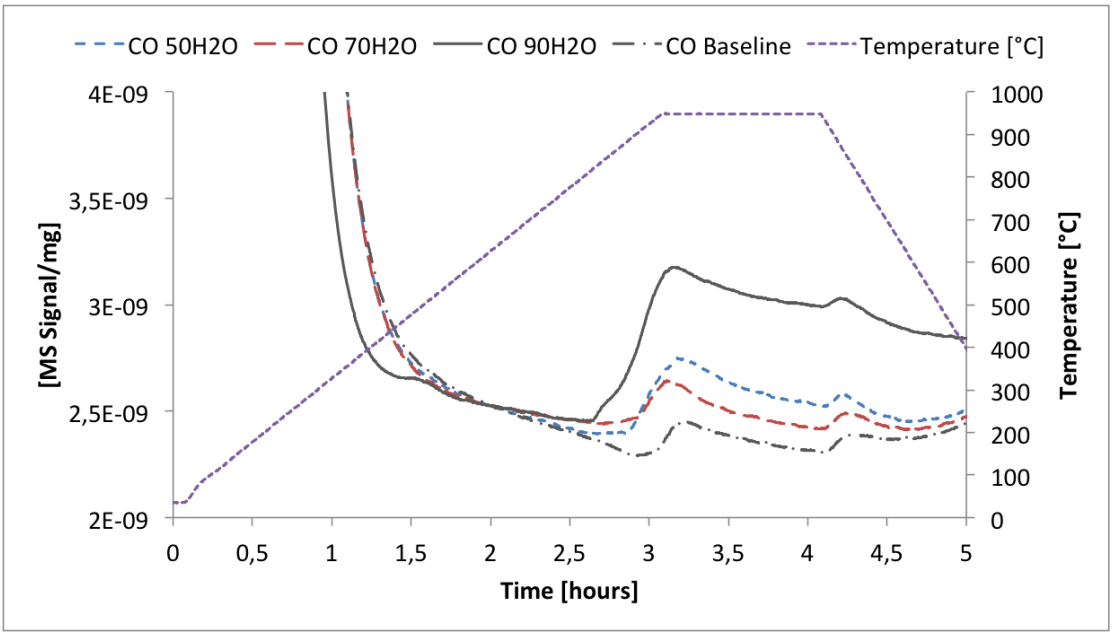

Figure 4.46: MS results during the one hour heat treatment, at 950°C in an argon atmosphere, of activated carbons derived from PANI. The combined CO_2 and steam activation process with an activation temperature and an activation time of 950°C and three hours was used to obtain the activated carbons. The water temperature in the activation process was 50, 70 and 90°C.

Figure (4.46) shows the formation of CO during the heat treatment of activated carbons obtained after the combined CO_2 and steam activation process with various amount of steam. The formation of CO is considerably highest for the activated carbons obtained with a water temperature of 90°C. As determined by EDX, a water temperature of 90°C gives activated carbons with the highest oxygen content. Hence, it is reasonable that the formation of CO is highest when using a water temperature of 90°C, since more oxygen is present in the activated carbon, which can be released during the heat treatment. It can also be seen that activated carbons obtained with a water temperature of 50°C in the activation process, release a slightly larger amount of CO during the heat treatment, compared to the activated carbons obtained with a water temperature of 70°C. This is unexpected, due to the fact that an increase in water temperature results in an increase in oxygen content.

4.6 Supercapacitors

4.6.1 Activation time

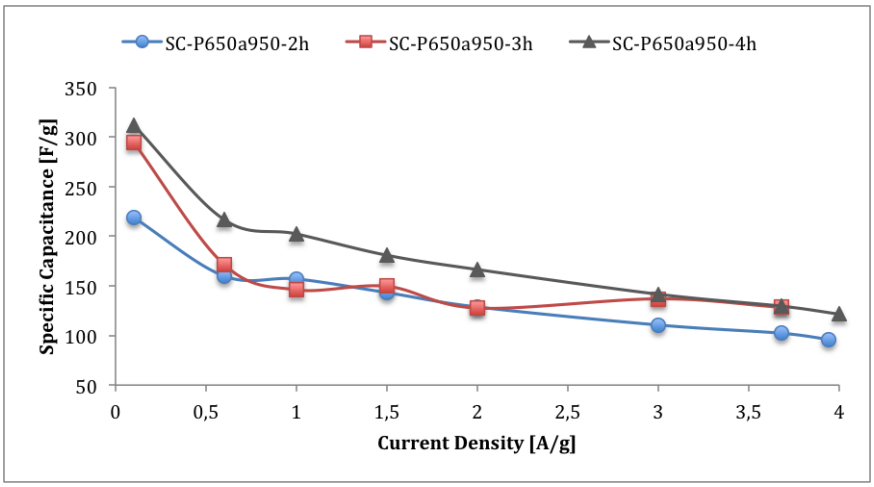

Figure 4.47: Rate capability (current density versus specific capacitance) of supercapacitors composed of activated carbons derived from PANI through a carbonization temperature and an activation temperature of 650 and 950°C. The duration of the CO_2 activation process was 2, 3 and 4 hours and the partial pressure of CO_2 was 0.8.

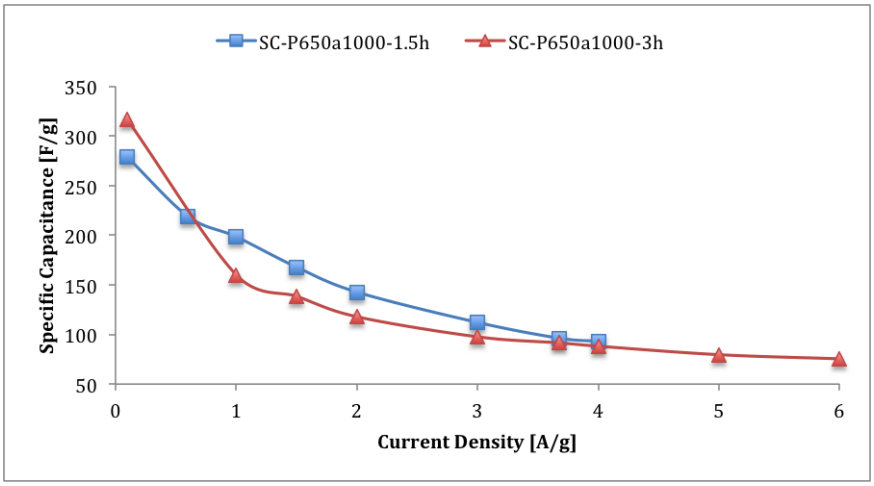

Figure 4.48: Rate capability of supercapacitors composed of activated carbons derived from PANI through a carbonization temperature and an activation temperature of 650 and 1000°C. The duration of the CO_2 activation process was 1.5 and 3 hours and the partial pressure of CO_2 was 0.8.

Figure (4.47) shows the rate capabilities of SC-P650a950-2h, SC-P650a950-3h and SC-P650a950-4h. The results show that at a low current density of 0.1 A/g, the specific capacitance increases with activation time, where an activation time of 2, 3 and 4 hours provide a high specific capacitance of 218.4, 294.2 and 311.9 F/g, respectively. Also, the results show that the rate capability decreases with activation time, where an activation time of 2 hours showed the best rate capability with a 46.8 % capacitance retention at a current density of 3.68 A/g. Activation times of 3 and 4 hours showed worse rate capabilities with a 43.6 and 41.5 % capacitance retention at a current density of 3.68 A/g, respectively.

Figure (4.48) shows the rate capabilities of SC-P650a1000-1.5h and SC-P650a1000-3h. As the previous results were for an activation temperature of 950°C, the same trend in rate capability is obtained with an activation temperature of 1000°C. At a low current density of 0.1 A/g, an activation time of 1.5 and 3 hours provide a specific capacitance of 278.4 and 316.7 F/g, respectively. However, an activation time of 1.5 hours shows the best rate capability with a 34.6 % capacitance retention at a current density of 3.68 A/g. An activation time of 3 hours shows a 27.8 % capacitance retention at a current density of 3.68 A/g.

Compared to the rate capability obtained in the literature, all of the rate capabilities obtained in this work are poor. It has been reported that activated carbons obtained from PANI through a chemical activation process with KOH at an activation temperature of 850°C, exhibit a very good rate capability with a 72 % retention in the capacitance at 5 A/g [26]. It was suggested that the macroporous structure plays a more important role on the rate capability, than the chemical properties of the electrode material [26]. As seen from Figure (4.6), the SEM images show that the fiber structure gradually is destroyd with increasing activation time. It can be seen that the destruction of fibers greatly effects the macropore volume, as the macropore volume has been significantly reduced after an activation time of 4 hours. Hence, the decrease in rate capability with increasing activation time is consistent with literature, as the macroporous structure gradually breakes down.

However, the activated carbon prepared with KOH activation showed a specific capacitance of a single electrode of 297 F/g [26], which is less than the specific capacitance obtained in this work, despite having a larger BET surface area of 3014 m^2g^{-1}. This suggests that other properties, such as the total pore volume and the pseudocapacitance generated from oxygen groups, plays an important role on the specific capacitance [23].

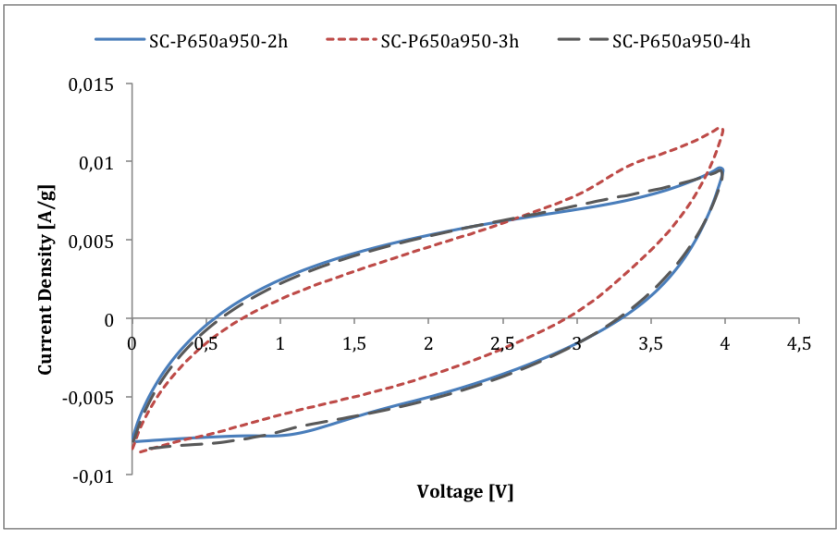

(a)

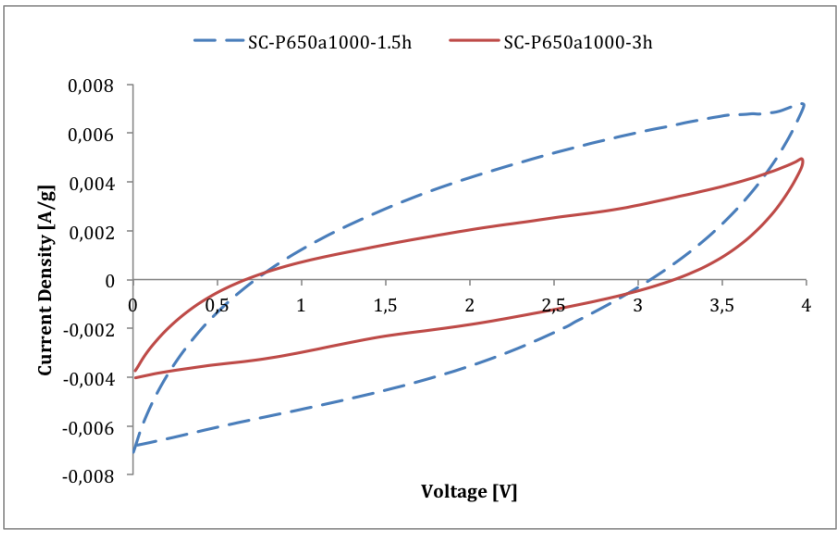

(b)

Figure 4.49: CV curves at a scan rate of 50 mVs^{-1} of supercapacitors composed of activated carbons derived from PANI through a carbonization temperature of 650°C. a) An activation temperature of 950°C and a CO_2 activation time of 2, 3 and 4 hours. b) An activation temperature of 1000°C and a CO_2 activation time of 1.5 and 3 hours.

Figure (4.49a) and (4.49b) show the CV curves of activated carbons prepared by the CO_2 activation process at 950°C and 1000°C, respectively. All of the CV curves obtained with different activation time exhibit a leaf-like shape, which is not associated with ideal capacitive performance. An ideal capacitve behavior is

represented with a rectangular-shaped CV curve [26]. The CV curve has a rectangular shape when only the electrical double-layer constitutes the capacitance. In this case the capacitance is purely electrostatic and the current is independent of potential. Also, upon a reversal of the potential sweep, the sign of the current is immediately reversed [24]. It is clear that in all of these CV curves, the current is not independent of potential. However, when pseudocapacitance contributes to the capacitance, the CV curve is not always rectangular in shape. In this case, the CV curve becomes distorted and more asymmetric when the scan rate is increased [25]. As seen from Figure (4.49), the CV curves are distorted, which implies that pseudocapacitance contributes to the capacitance. As can be seen from Figure (4.7), the EDX results show that the activated carbons prepared with the CO_2 activation process contain both nitrogen and oxygen, in which both the nitrogen and oxygen content decreases with activation time. These nitrogen and oxygen groups can provide pseudocapacitance by reacting chemically with the electrolyte [23]. As seen from Figure (2.5), due to the leaf-like shape, the CV curves obtained in this work indicate that the supercapacitors have resistivity. Also, all of the CV curves exhibit a small peak at the end of the charging section (4 V), which is characteristic for supercapacitors with carbon material [24]. In addition, the CV curves of sample SC-P650a950-2h and SC-P650a1000-3h, show a small peak at approximately 1 V on the discharge section. This also indicates the presence of pseudocapacitance through redox reactions [26]. Figure (4.50) and (4.51) show GCD curves of activated carbons prepared by the CO_2 activation process at 950°C and 1000°C, respectively. All of the GCD curves show an almost triangular shape, which indicates good performance. However, the voltage drop at the beginning of the discharge process is quite large for all the supercapacitors. Especially, as seen from Figure (4.50b), sample SC-P650a950-3h shows a voltage drop of almost 1 V at the beginning of the discharge process, which implies a large resistance in the material due to ion diffusion resistance [26]. Also, when the capacitance originates from the electrical double-layer only, the potential changes linearly with time at constant current density. However, when pseudocapacitance contributes to the capacitance, the chronopotentiograms deviate from this linear trend [25]. This also implies that pseudocapacitance is present, as non of the GCD curves shows a linear change in potential with time. In addition, the small peak at approximately 1 V on the discharge section of the CV curves of sample SC-P650a950-2h and SC-P650a1000-3h corresponds to the small peaks at about 600 and 550 s in the GCD curves in Figure (4.50a) and (4.51b), respectively. In comparison, the activated carbons derived from PANI though KOH activation, exhibited a more ideal capacitive behavior, in which an almost rectangular shaped CV curve and a triangular shaped GCD curve were obtained [26].

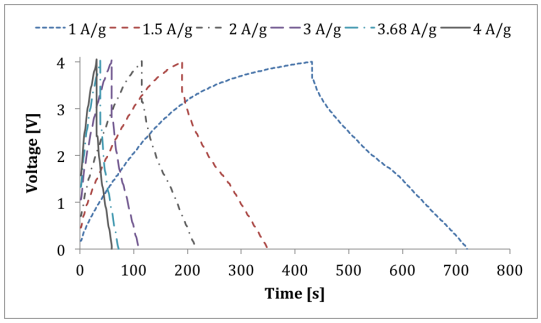

(a) SC-P650a950-2h

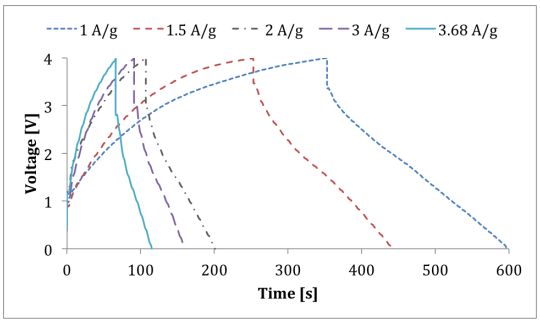

(b) SC-P650a950-3h

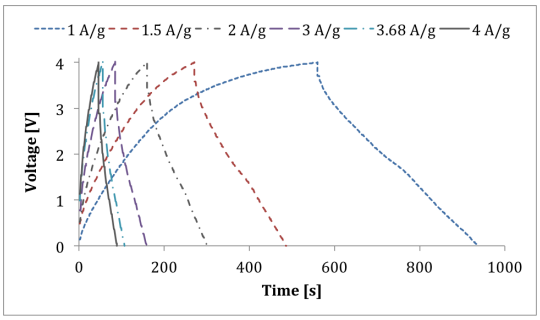

(c) SC-P650a950-4h

Figure 4.50: GCD curves of supercapacitors composed of activated carbons derived from PANI through a carbonization temperature and an activation temperature of 650 and 950°C. The duration of the CO_2 activation process was 2, 3 and 4 hours.

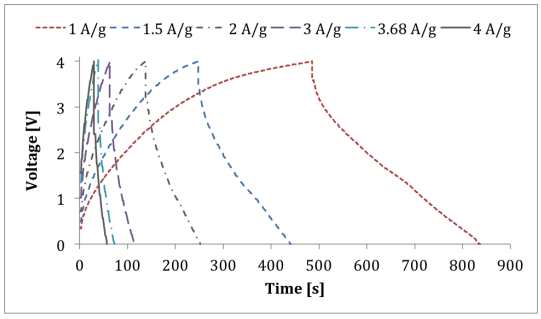

(a) SC-P650a1000-1.5h

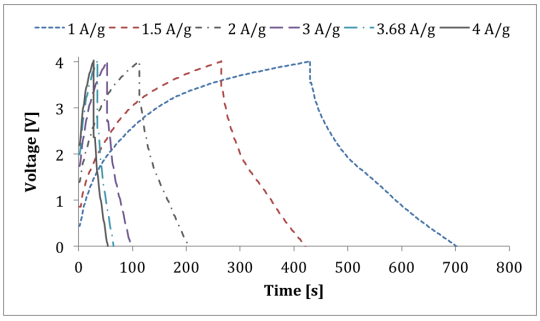

(b) SC-P650a1000-3h

Figure 4.51: GCD curves of supercapacitors composed of activated carbons derived from PANI through a carbonization temperature and an activation temperature of 650 and 1000°C. The duration of the CO_2 activation process was 1.5 and 3 hours.

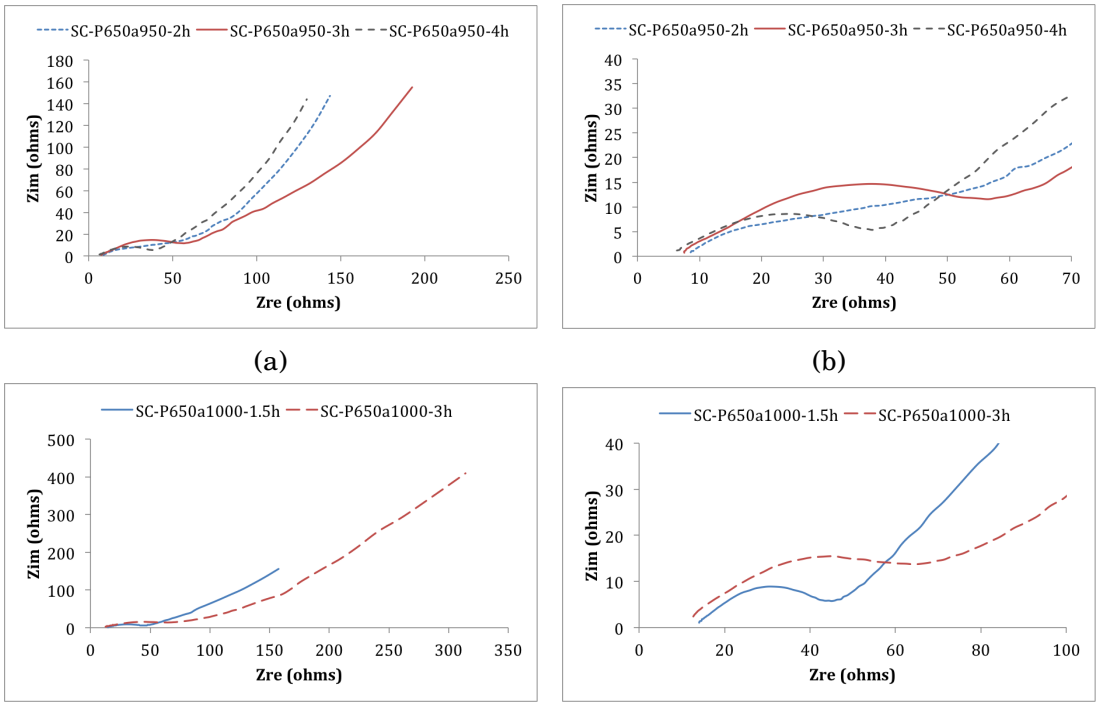

Figure 4.52: Nyquist plots of supercapacitors composed of activated carbons derived from PANI through a carbonization temperature of 650°C. a), b) An activation temperature of 950°C and a CO_2 activation time of 2, 3 and 4 hours. c), d) An activation temperature of 1000°C and a CO_2 activation time of 1.5 and 3 hours.

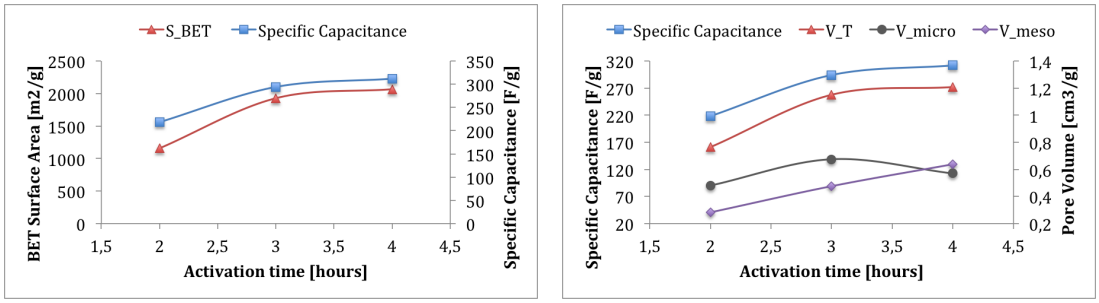

Figure 4.53: Specific capacitance versus physical properties of activated carbons derived from PANI through a carbonization temperature and an activation temperature of 650 and 950°C. The duration of the CO_2 activation process was 2, 3 and 4 hours. a) BET surface area. b) Total pore volume, micropore volume and mesopore volume.

Figure (4.52) shows the Nyquist plot obtained from electrochemical impedance spectroscopy (EIS) analysis of activated carbons prepared by CO_2 activation at various activation times. Active electrode materials that behave as ideal capacitors exhibit an almost vertical curve in the low-frequency region [26]. The diagram can be used to estimate the resistance of the electrode material, in which a charge transfer resistance is given by the diameter of a semicircle [25]. As shown in Figure (4.52b), the diameters of the semicircles indicate that an activation time of 3 hours at 950°C gives the largest charge transfer resistance, followed by an activation time of 4 hours. Figure (4.52d) indicates that an activation time of 3 hours at 1000°C gives a larger charge transfer resistance than an activation time of 1.5 hours. The slope of the 45° region of the Nyquist curve is referred to as the Warburg region. The length of the Warburg region reflects the frequency dependence of the ion diffusion from the electrolyte to the surface of the electrode [26]. As seen from Figure (4.52a), the Warburg region is largest for an activation time of 3 hours at 950°C, followed by an activation time of 2 hours. The Warburg region is smallest for an activation time of 4 hours, which indicates that the diffusion path is smallest for activated carbons prepared with an activation time of 4 hours. This is reasonable because, as seen from Figure (4.6), the macropore volume is greatly reduced after an activation time of 4 hours, which leads to short ion-diffusion distances when the macropores are filled with electrolyte [26].

Figure (4.53a) shows the specific capacitance of a single electrode and BET surface area as function of the activation time in the CO_2 activation process at 950°C. The specific capacitance was measured at a current density of 0.1 A/g. It can be seen that both the specific capacitance and and the BET surface increases with activation time. This is in accordance with literature, where it is stated that the surface area should be as large as possible to achieve a high specific capacitance. The specific capacitance increases with increasing BET surface area because the interface located between the electrodes and the electrolyte increases with increasing BET surface area [22]. A large interface is able to store a lot of electrical charges, which constitutes the capacitance of the supercapacitor.

Figure (4.53b) shows the specific capacitance of a single electrode, the total pore volume, micropore volume and mesopore volume as function of activation time. The specific capacitance, total pore volume and mesopore volume increase with increasing activation time, while the micropore volume goes through a maximum at 3 hours of activation. These results suggest that also the total pore volume contributes to the capacitance. In addition, it seems like the micropore volume effects the capacitance, as the rate of increase in capacitance is reduced when the micropore volume decreases. However, it can also be that the effect of micropore

volume on the capacitance, is actually coming from the effect of BET surface area on the capacitance, as the micropore volume has a great effect on the BET surface area. Generally, micropores does not contribute much to the size of the electrical double-layer and hence the capacitance, due to the fact that micropores do not provide enough space for the solvated ions in the electrolyte [30]. Therefore, the presence of mesopores is important for the capacitance, since they provide less resistance for transfering ions [30].

4.6.2 Water temperature

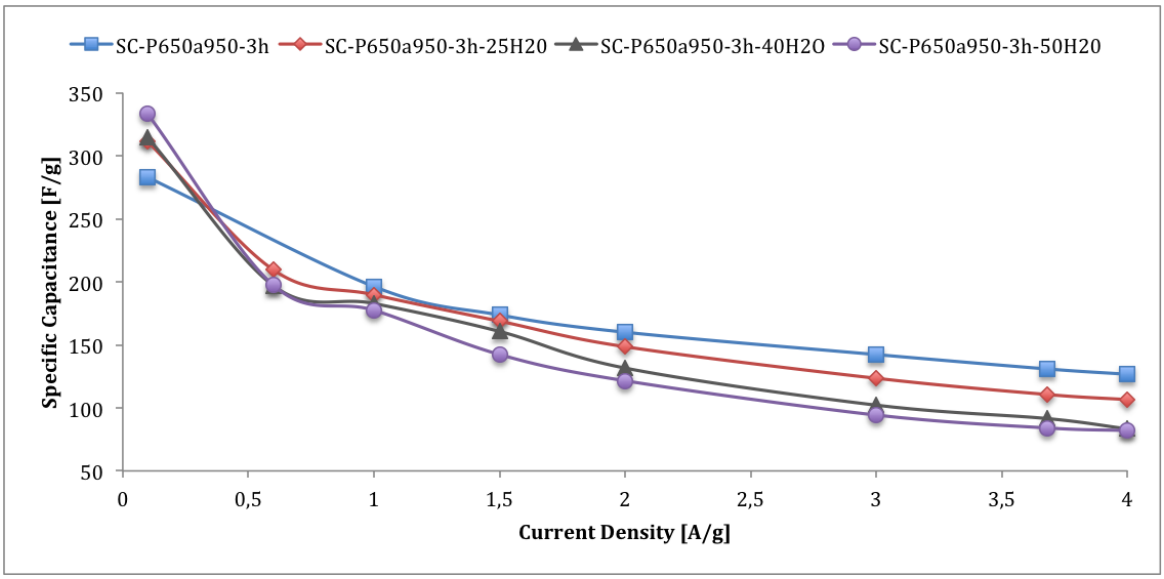

Figure 4.54: Rate capability of supercapacitors composed of activated carbons derived from PANI through a carbonization temperature and an activation temperature of 650 and 950°C. The duration of the combined CO_2 and steam activation process was 3 hours and the water temperature was varied.

Figure (4.54) shows the rate capabilities of activated carbon fibers prepared with the combined CO_2 and steam activation process, with various amount of steam. At a current density of 0.1 A/g, the specific capacitance of a single electrode is 311.5, 314.8 and 333.6 F/g with the use of a water temperature of 25, 40 and 50°C, respectively. However, the rate capability decreases with increasing amount of steam in the activation process, where water temperatures of 25, 40 and 50°C result in a capacitance retention of 35.5, 29.1 and 25.2 % at a current density of 3.68 A/g. These results are consistent with the literature, where it is stated that the macropore volume has an important effect on the rate capability [26]. As

seen from Figure (4.21), the destruction of the fiber structure increases with the amount of steam, where water temperatures of 70 and 90°C completely destroy the macroporous structure. Sample SC-P650a950-3h, which is prepared by the CO_2 activation process with a partial pressure of CO_2 equal to 1, has a better rate capability with a 46.3 % capacitance retention at 3.68 A/g. Based on the fiber structure obtained with a partial pressure of CO_2 of 0.8, shown in Figure (4.6), it is reasonable to assume that the macroporous structure is maintained after the CO_2 activation process. This could explain the better rate capability of sample SC-P650a950-3h, compared to the samples prepared with both CO_2 and steam.

The macroporous structure is important to achieve a good rate capability, because macropores with good connectivity to micropores and mesopores reduce the ion transportation resistance by minimizing the ion diffusion distances. This enhances the utilization of the mesopores on the interior surface, which provides better rate capability [26].

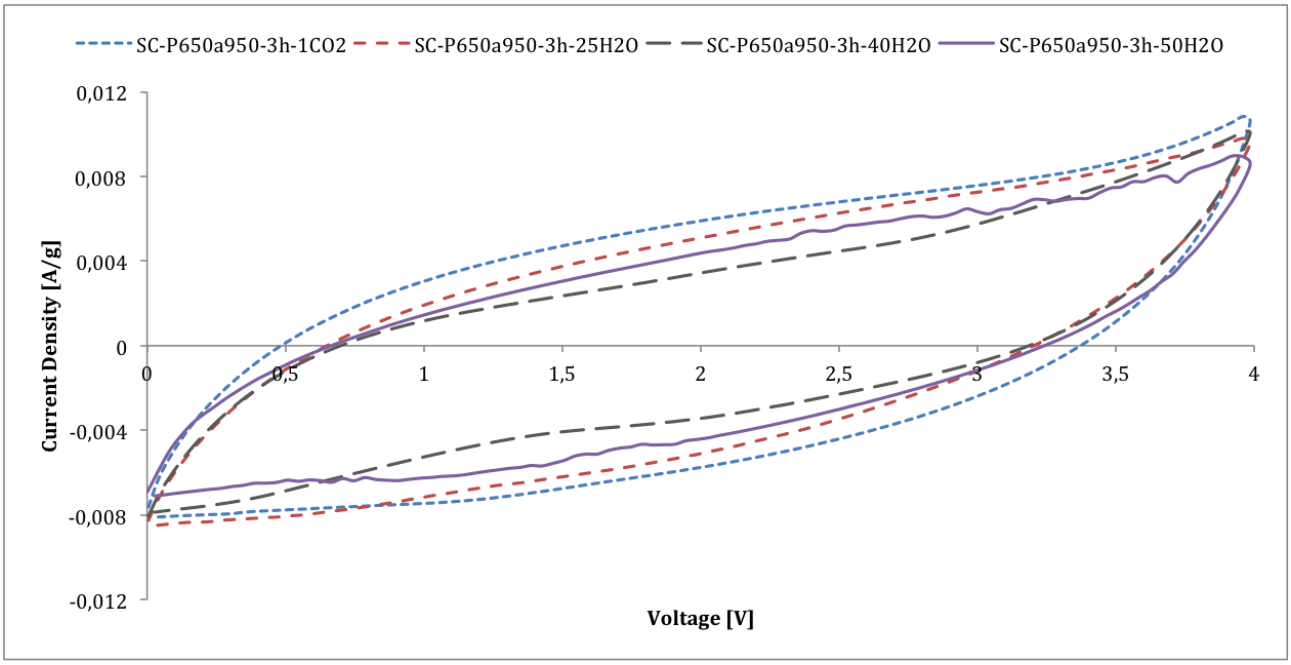

Figure 4.55: CV curves at a scan rate of 50 mVs^{-1} of supercapacitors composed of activated carbons derived from PANI through a carbonization temperature and an activation temperature of 650 and 950°C. The duration of the combined CO_2 and steam activation process was 3 hours and the water temperature was varied.

Figure (4.55) shows the CV curves of activated carbons prepared by the combined CO_2 and steam activation process, with different amount of steam. All of

the CV curves have a distorted shape, which suggests that pseudocapacitance contributes to the capacitance. In addition, a peak at the end of the charging process (4 V) can be observed for all the samples, which is characteristic for supercapacitors based on carbon materials [24]. As seen from Figure (4.22), the EDX results indicate that the oxygen content increases with the amount of steam present in the activation process, while the nitrogen content remains approximately constant. This increase in oxygen content could give rise to the pseudocapacitance, which is suggested by the CV curves. As can be seen, a water temperature of 50°C gives a CV curve with several small peaks located near the end of the charging and discharging section of the CV curve. These peaks could be due to redox reactions happening between the electrolyte and the oxygen and nitrogen containing groups in the electrode material [25].

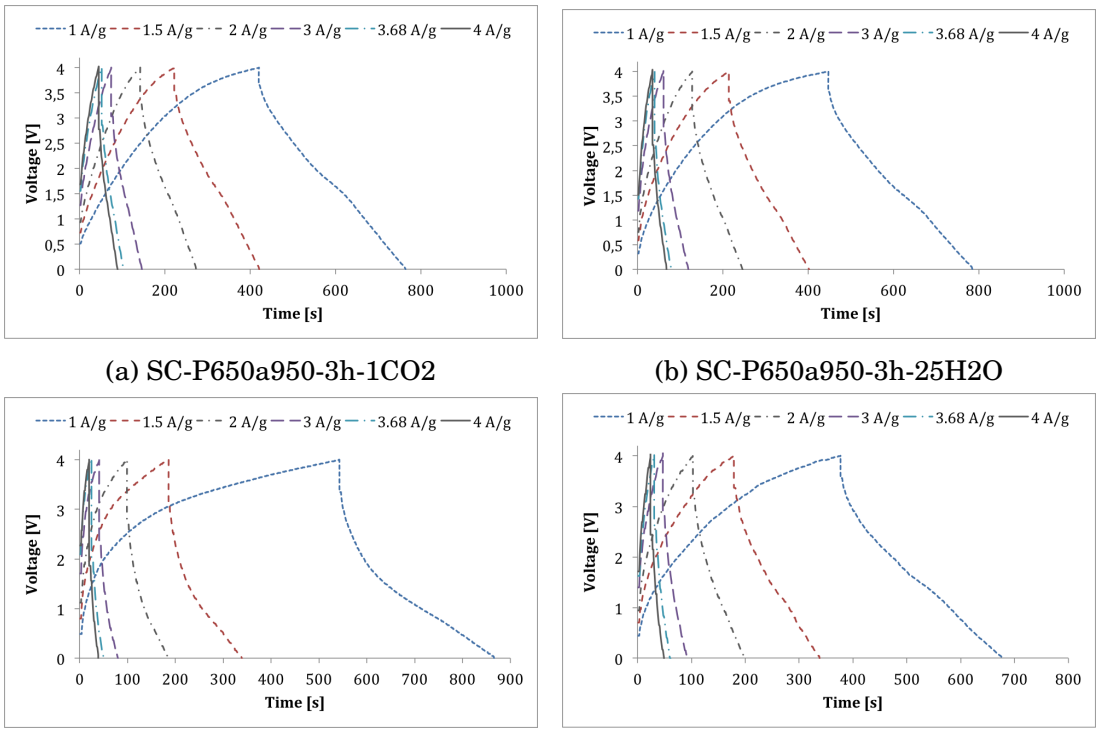

(a) SC-P650a950-3h-1CO2

(b) SC-P650a950-3h-25H2O

(c) SC-P650a950-3h-40H2O

(d) SC-P650a950-3h-50H2O

Figure 4.56: GCD curves of supercapacitors composed of activated carbons derived from PANI through a carbonization temperature and an activation temperature of 650 and 950°C. The duration of the combined CO_2 and steam activation process was 3 hours and the water temperature was varied.

Figure (4.56) shows the GCD curves at different current densities of activated carbons prepared by the combined CO_2 and steam activation process, with dif-

ferent amount of steam. As the previous samples obtained with CO_2 activation, these samples also have a quite large voltage drop at the beginning of the discharge process, which means that the ion diffusion resistance is large [26]. The contribution of pseudocapacitance to the capacitance is also visible from the GCD curves, as the effect of pseudocapacitance leads to a slower charge/discharge rate [26]. This is especially visible in the GCD curve of the activated carbon obtained with a water temperature of 40°C, shown in Figure (4.56c).

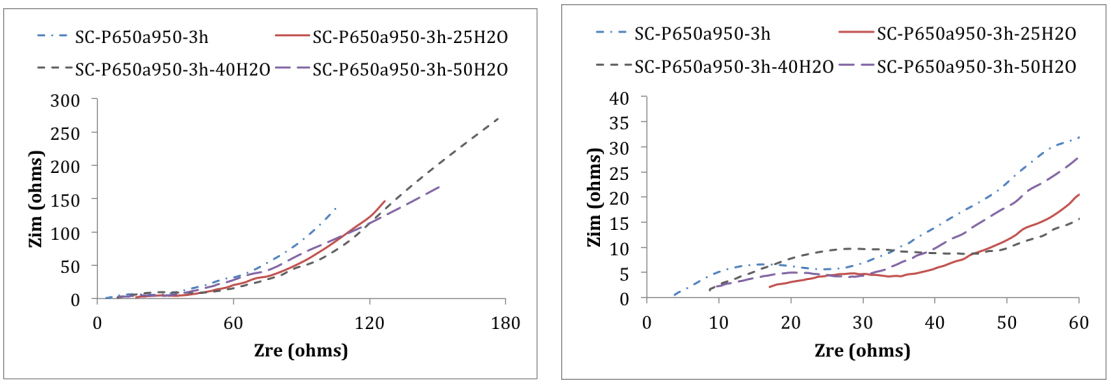

Figure 4.57: Nyquist plots of supercapacitors composed of activated carbons derived from PANI through a carbonization temperature and an activation temperature of 650 and 950°C. The duration of the combined CO_2 and steam activation process was 3 hours and the water temperature was varied.

As seen from Figure (4.57), no trend in the charge transfer resistance with the amount of steam in the activation process is observed. This could be expected as the nanofiber structure is destroyd during the combined CO_2 and steam activation process, as can be seen from Figure (4.21).

Figure (4.58) shows the specific capacitance of a single electrode and the BET surface area as function of the amount of steam present in the combined CO_2 and steam activation process. The result shows that with a water temperature below 40°C, the specific capacitance increases with increaing BET surface area, which is consistent with literature as an increase in BET surface area provides more space for storage of electrical charges [22]. However, at water temperatures higher than 40°C, the specific capacitance increases greatly, while the BET surface area decreases. This is unexpected, considering the importance of BET surface area on the size of the electrical double-layer, which is the largest contribution to the capacitance of an electrical double-layer capacitor [22]. It can be seen that also the total pore volume and the mesopore volume decreases at water temperatures

higher than 40°C, while the micropore volume remains approximately zero. This indicates that the increase in specific capacitance is not due to the total pore volume, mesopore volume and micropore volume. Thus, another property than the specific surface area and the pore structure is most likely the reason for the increase in capacitance. As seen from Figure (4.58), the increase in capacitance at water temperatures above 40°C could be due to an increase in oxygen content, which is estimated by EDX. This increase in oxygen content could result in an increased pseudocapacitance from redox reactions, which increases the total capacitance. However, it is difficult to assume that this is the case, because all of the properties changes with the water temperature. Ideally, the effect of oxygen content on the capacitance should be examined at both constant BET surface area and pore volume.

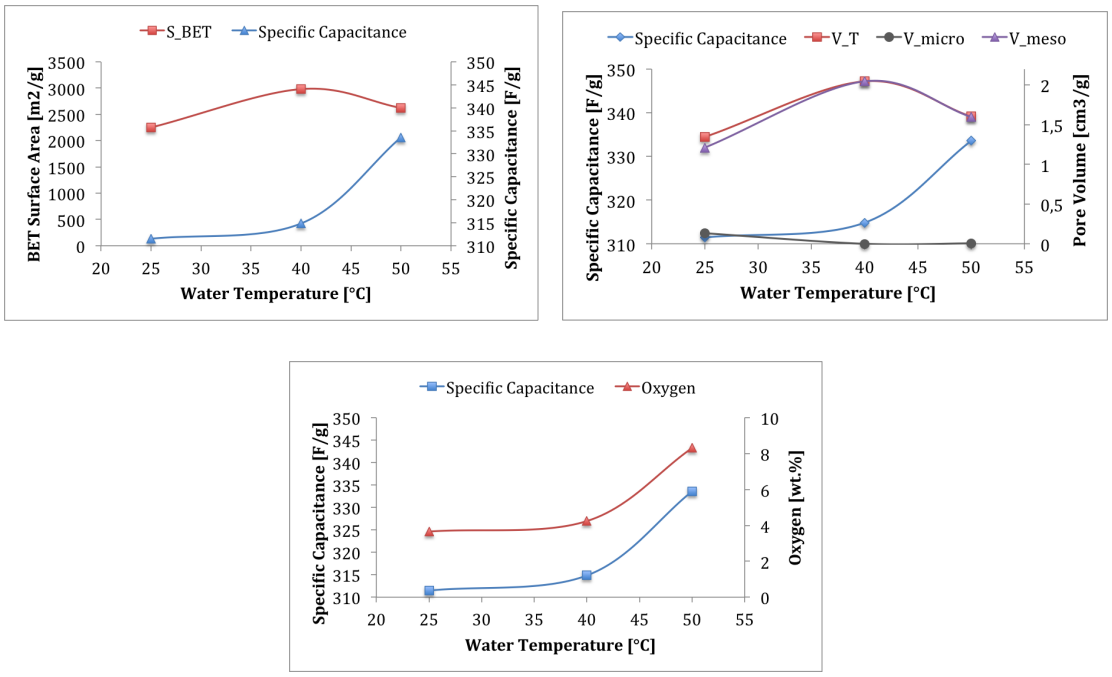

Figure 4.58: Specific capacitance versus physical properties of activated carbons derived from PANI through a carbonization temperature and an activation temperature of 650 and 950°C. The duration of the combined CO_2 and steam activation process was 3 hours and the water temperature was varied.

4.6.3 Carbon spheres

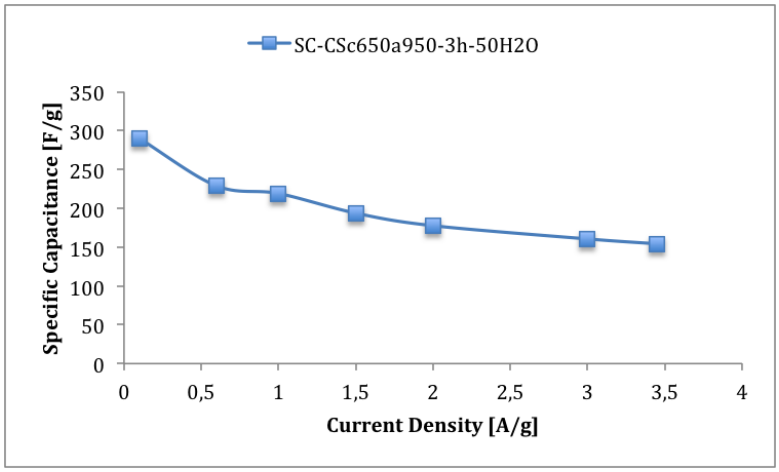

Figure 4.59: Rate capability of a supercapacitor composed of activated carbon spheres through a carbonization temperature and an activation temperature of 650 and 950°C. The duration of the combined CO_2 and steam activation process was 3 hours and the water temperature was 50°C.

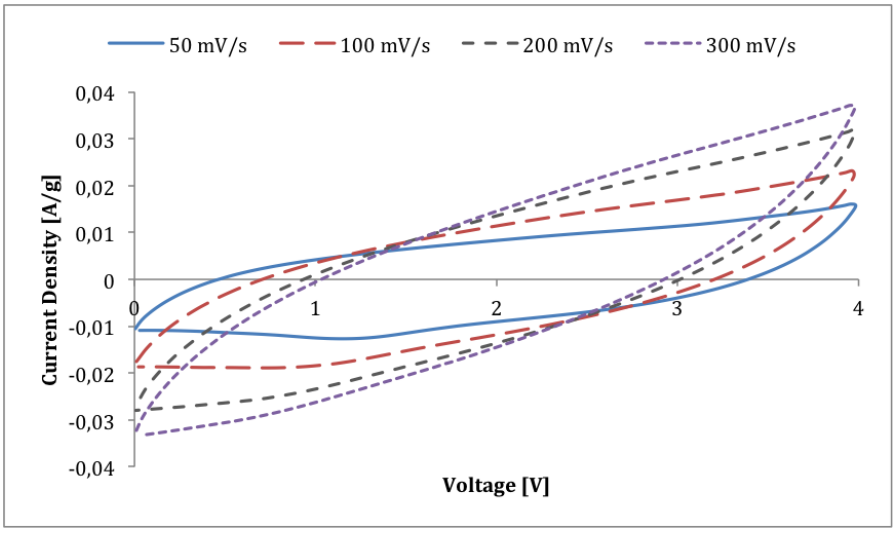

Figure 4.60: CV curves at scan rates ranging from 50 to 300 mVs^{-1} of a supercapacitor composed of activated carbon spheres through a carbonization temperature and an activation temperature of 650 and 950°C. The duration of the combined CO_2 and steam activation process was 3 hours and the water temperature was 50°C.

Figure (4.59) shows the rate capability of activated carbon spheres prepared with the combined CO_2 and steam activation process. At a current density of 0.1 A/g, the specific capacitance of a single electrode is 289.4 F/g. However, the activated carbon spheres shows the best rate capability obtained in this work, with a capacitance retention of 53.3 % at a current density of 3.45 A/g. The reason why the rate capability is higher for the activated carbon spheres than the rate capability for the activated carbons derived from PANI, could be that the spherical morphology of the carbon spheres is not effected by the activation process. As the fiber structure is somewhat destroyd in some of the activation processes, Figure (4.42b) shows that the spherical morphology of carbon spheres is retained after the activation step. Therefore the macroporous structure of carbon spheres is maintained. Still, this rate capability is low, compared to that obtained in the literature [26].

Figure (4.60) shows the CV curves at scan rates between 50 and 300 mV/s of activated carbon spheres prepared by the combined CO_2 and steam activation process. It can be seen that the CV curve has the most rectangular-like shape at the lowest scan rate of 50 mV/s. As the scan rate increases, the CV curve becomes distorted and more asymmetric, which is in accordance with literature [25]. This is due to the pseudocapacitance originated from the nitrogen and oxygen groups present on the carbon spheres. The presence of oxygen atoms on the surface of the activated carbon spheres is suggested by EDX mapping, showed in Figure (C.3c) and (C.3d) in appendix C. Also, a small peak at approximately 1.2 V in the discharge section of the CV curve suggest that redox reactions occur between the electrolyte and the electrode material [26]. This peak most likely correspond to the peak occuring at about 700 s in the discharge process of the GCD curve, shown in Figure (4.61). The GCD curve of activated carbon spheres shows a quite small voltage drop in the beginning of the discharge, compared to the other samples prepared in this work, which suggest a low resistance of ion diffusion [26].

Figure (4.62) shows the Nyquist diagram of activated carbon spheres prepared with the combined CO_2 and steam activation process. The diameter of the semicircle is small, which indicates a low charge transfer resistance in the material. However, the Warburg region is quite large, which indicates quite long ion-diffusion distances.

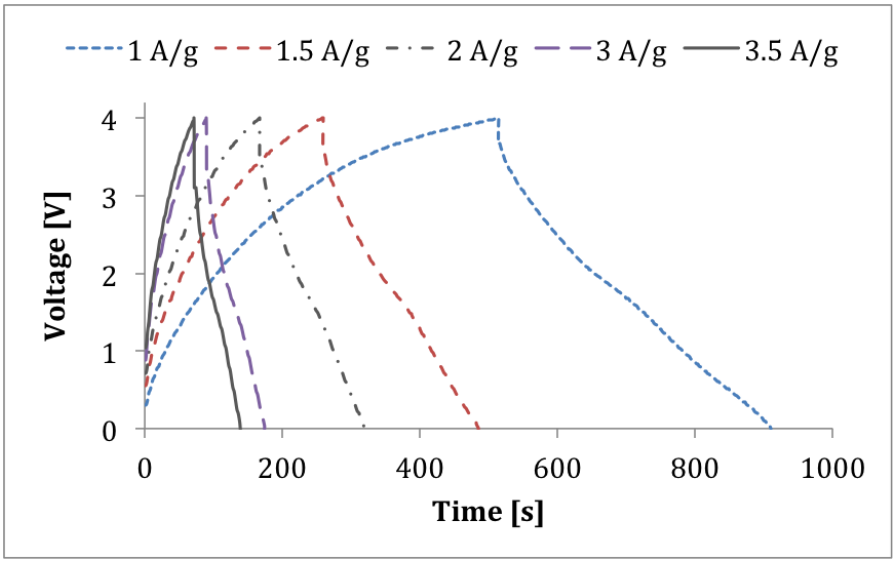

Figure 4.61: GCD curves of a supercapacitor composed of activated carbon spheres through a carbonization temperature and an activation temperature of 650 and 950°C. The duration of the combined CO_2 and steam activation process was 3 hours and the water temperature was 50°C.

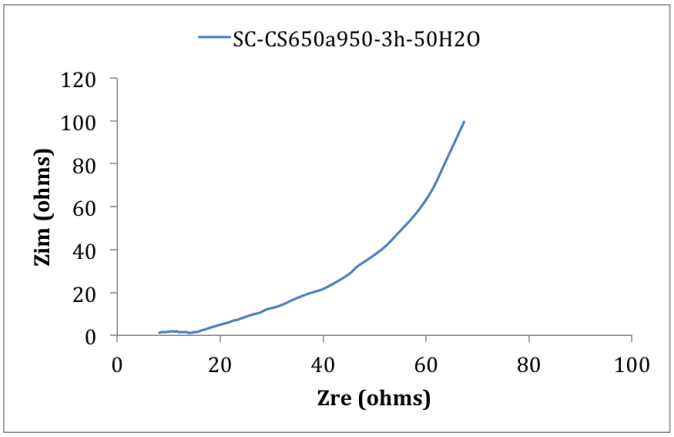

Figure 4.62: Nyquist plot of a supercapacitor composed of activated carbon spheres through a carbonization temperature and an activation temperature of 650 and 950°C. The duration of the combined CO_2 and steam activation process was 3 hours and the water temperature was 50°C.

4.6.4 The effects of surface oxygen groups

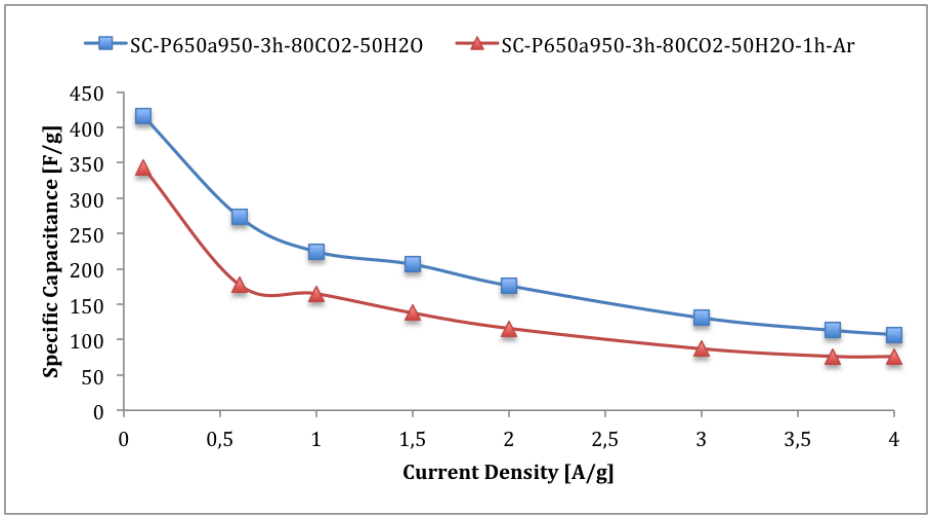

Figure 4.63: Rate capability of supercapacitors composed of activated carbons derived from PANI through a carbonization temperature and an activation temperature of 650 and 950°C. The duration of the combined CO_2 and steam activation process was 3 hours and the water temperature was 50°C. The partial pressure of CO_2 and argon was 0.8 and 0.2, respectively.

Figure (4.63) shows the rate capabilities of activated carbon fibers prepared with the combined CO_2 and steam activation process. In addition to the activation step, sample SC-P650a950-3h-80CO2-50H2O-1h-Ar was subjected to a one hour heat treatment at 950°C in an inert atmosphere, as carried out in section 4.5.1. As seen from Figure (4.22), the combined CO_2 and steam activation process introduces oxygen atoms to the carbon material, hence this heat treatment was carried out in order to remove the oxygen groups present on the carbon surface. As seen from Figure (4.63), at a current density of 0.1 A/g the specific capacitance of a single electrode is very high with a value of 416.5 and 342.7 F/g for the two materials. As the current density increases, the specific capacitance of the sample not subjected to the heat treatment, remains higher than the specific capacitance of the sample exposed to the heat treatment. This is reasonable, because the sample not subjected to the heat treatment contains more oxygen, which provides more pseudocapacitance. The capacitance can be increased by the pseudocapacitance provided by the oxidation-reduction reactions between the electrolyte and the oxygen functional groups [23]. The additional pseudocapacitance can make up about 5-10 % of the total capacitance [22].

Also, it can be seen that the rate capability curves are very similar in shape. This could suggest that the pore structure, more specifically the macropore structure, is very similar in the two carbon materials. It is reasonable to assume a very similar pore structure in the two samples, because the BET results showed just a small increase in BET surface area, micropore volume and mesopore volume for the sample subjected to the heat treatment. This can be seen from Table (D.1) in appendix D. This is reasonable, because the pore volume is expected to increase when oxygen groups are removed from the surface. The rate capability of sample SC-P650a950-3h-80CO2-50H2O and SC-P650a950-3h-80CO2-50H2O-1h-Ar are very poor, with a capacitance retention of 27.1 and 22.3 % at a current density of 3.68 A/g, respectively. The BETTER RATE ...

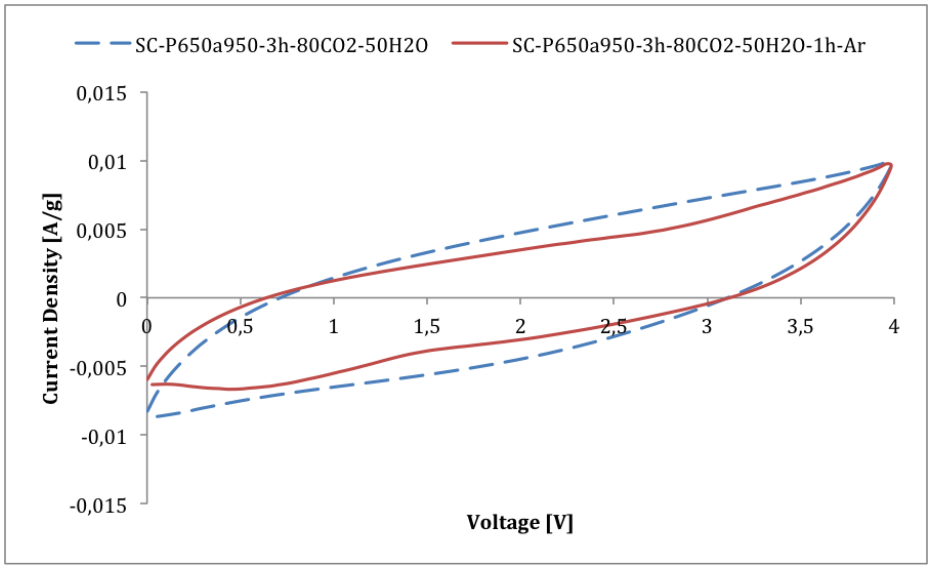

Figure 4.64: CV curves at a scan rate of 50 mVs^{-1} of supercapacitors composed of activated carbons derived from PANI through a carbonization temperature and an activation temperature of 650 and 950°C. The duration of the combined CO_2 and steam activation process was 3 hours and the water temperature was 50°C. The partial pressure of CO_2 and argon was 0.8 and 0.2, respectively.

As seen from Figure (4.64) the distorted shape of the CV curves indicates the contribution of pseudocapacitance in both of the supercapacitors. This implies that the one hour heat treatment at a temperature of 950°C in an inert atmosphere was not able to remove all of the oxygen and nitrogen present in the activated carbon material. Also, the GCD curve shown in Figure (4.65) indicates the presence of pseudocapacitance, as the effect of pseudocapacitance results in a slower discharge rate [26].

Figure (4.66) shows the Nyquist diagram of activated carbons obtained with the combined CO_2 and steam activation process. The activated carbon subjected to the heat treatment and the activated carbon not subjected to the heat treatment, shows a similar curve in the Nyquist diagram. The peak appearing for the activated carbon not exposed to the heat treatment could be due to a disturbance during the measurement. The similar rate of increase suggests that the ion-diffusion distances are similar for the two electrode materials. This is reasonable because both materials exhibit similar pore structures, as can be seen from Table (D.1) in appendix D.

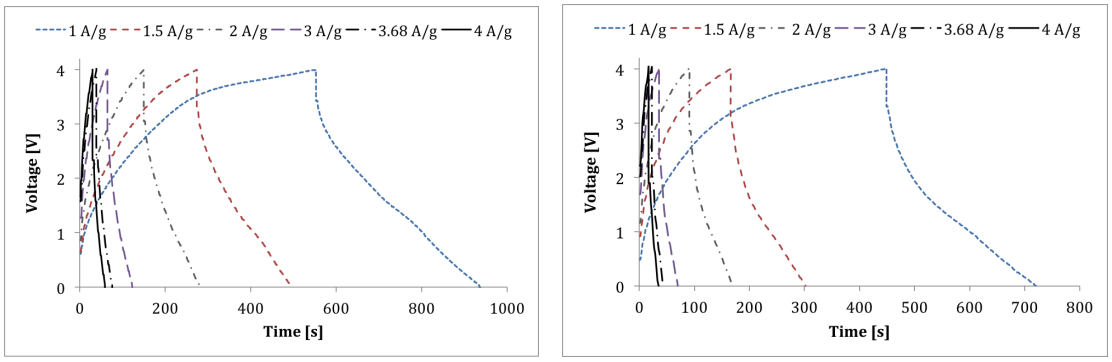

(a) SC-P650a950-3h-80CO2-50H2O (b) SC-P650a950-3h-80CO2-50H2O-1h-Ar

Figure 4.65: GCD curves of supercapacitors composed of activated carbons derived from PANI through a carbonization temperature and an activation temperature of 650 and 950°C. The duration of the combined CO_2 and steam activation process was 3 hours and the water temperature was 50°C. The partial pressure of CO_2 and argon was 0.8 and 0.2, respectively.

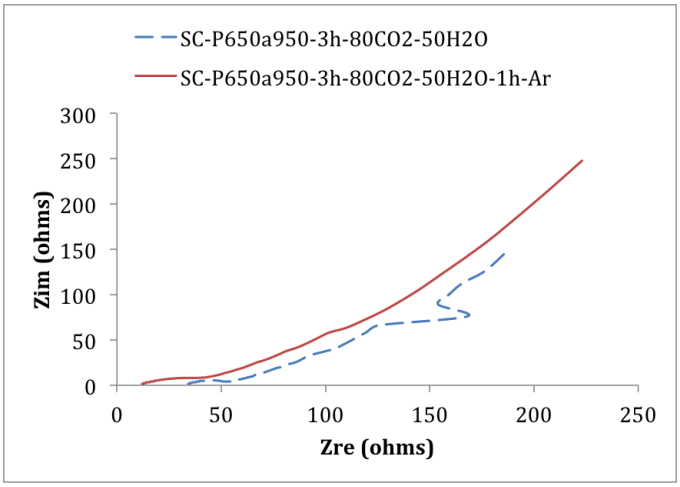

Figure 4.66: Nyquist plot of supercapacitors composed of activated carbons derived from PANI through a carbonization temperature and an activation temperature of 650 and 950°C. The duration of the combined CO_2 and steam activation process was 3 hours and the water temperature was 50°C. The partial pressure of CO_2 and argon was 0.8 and 0.2, respectively.

4.6.5 The effects of properties on performance

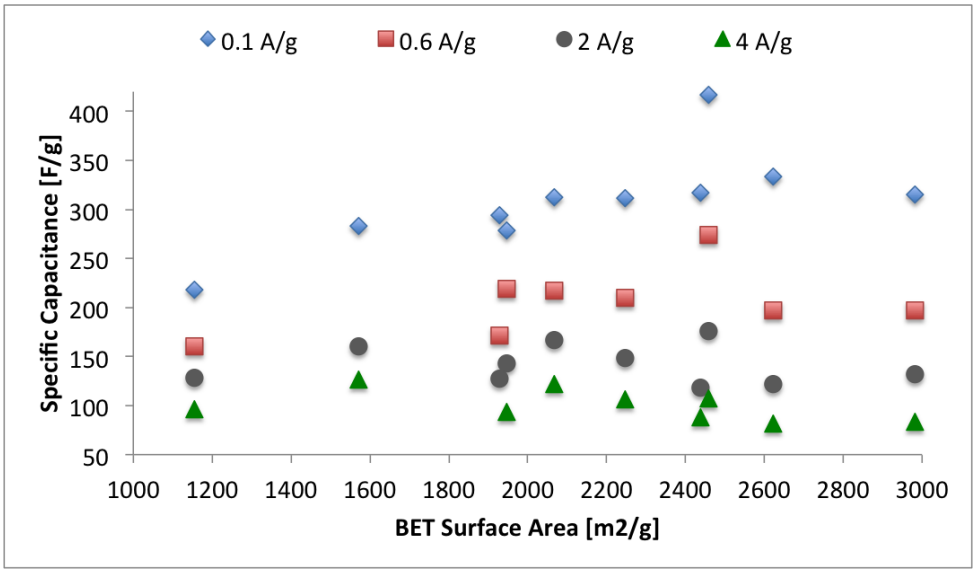

Figure 4.67: Specific capacitance of a single electrode versus BET surface area for electrode materials prepared from activated carbons derived from PANI, excluding the electrode material prepared from carbon spheres and sample P650a950-3h-80CO2-50H2O-1h-Ar.

Figure (4.67) shows the dependency of BET surface area on the specific capacitance of a single electrode. At a low current density of 0.1 A/g, a trend where the specific capacitance increases with increasing BET surface area can be observed. This trend also appear to a degree at a current density of 0.6 A/g. The influence of the BET surface area on the specific capacitance seems to disappear as the current density increases to 2 and 4 A/g. This is consistent with literature, as an increase in BET surface area results in a larger interface, which is able to store more electrical charges [22]. The BET surface area of the electrode material is considered to be the most important property in order to obtain electrical-double layer capacitors with high specific capacitance [30]. This is because the storage of electrical charges at the inteface between the electrodes and the electrolyte is the main contribution to the capacitance in electrical double-layer capacitors based on activated carbon. In these supercapacitors, pseudocapacitance generated from redox reactions between heteroatoms, such as nitrogen and oxygen, and the electrolyte, can contribute about 5 to 10 % to the total capacitance [22]. Because the BET surface area is the main property effecting the capacitance, a linear relationship should be obtained. The results in Figure (4.67) do not show a linear relationship between capacitance and BET surface area, which indicates that other properties

also strongly effects the specific capacitance. The pore structure and pore size distribution are also important for the performance of electrical double-layer capacitors [30]. Figure (4.68) shows the specific capacitance of a single electrode versus the total pore volume.

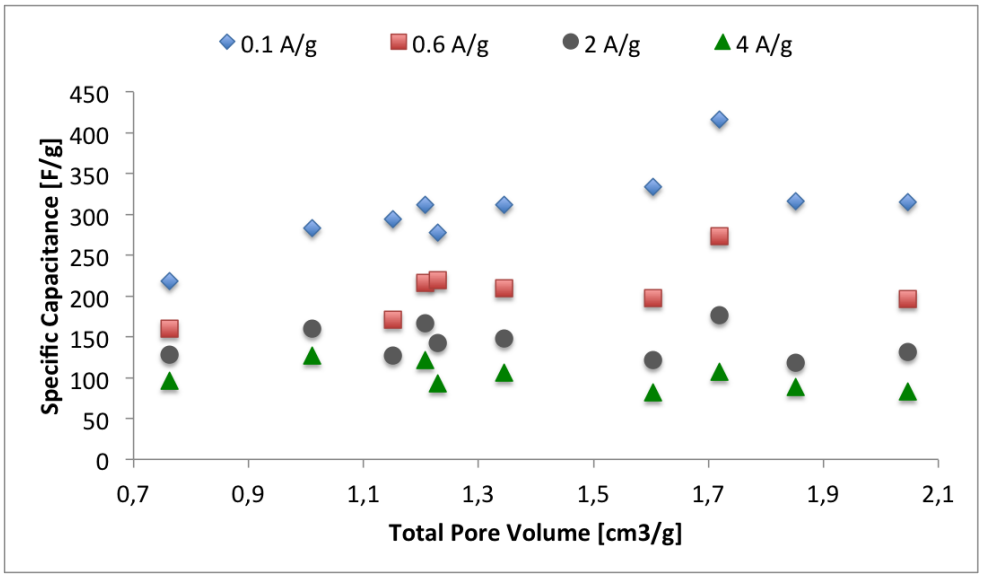

Figure 4.68: Specific capacitance of a single electrode versus total pore volume for electrode materials prepared from activated carbons derived from PANI, excluding the electrode material prepared from carbon spheres and sample P650a950-3h-80CO2-50H2O-1h-Ar.

These results shows that at low current densities of 0.1 and 0.6 A/g, the specific capacitance mainly increases with increasing pore volume. This indicates that also the total pore volume effects the performance of electrical double-layer capacitors, which is consistent with literature [30]. However, the specific capacitance at 0.1 A/g obtained with a total pore volume of about 1.85 and 2 cm^3g^{-1} is expected to be higher. From the obtained trend in specific capacitance with total pore volume, the specific capacitance at about 1.85 and 2 cm^3g^{-1} is expected to be in the 400 to 450 F/g region. The reason why the specific capacitance is lower than expected could be due to the fact that the yield is very low when producing activated carbon fibers with such high pore volumes. As previously discussed, the production of activated carbons with a pore volume of about 2 cm^3g^{-1} by the combined CO_2 and steam activation process, includes a burn-off of about 91 %. The small amount of activated carbon fibers obtained after the activation process, is more exposed to contaminations during preparation of electrode material. Hence, contaminations could be the cause of a lower specific capacitance than expected.

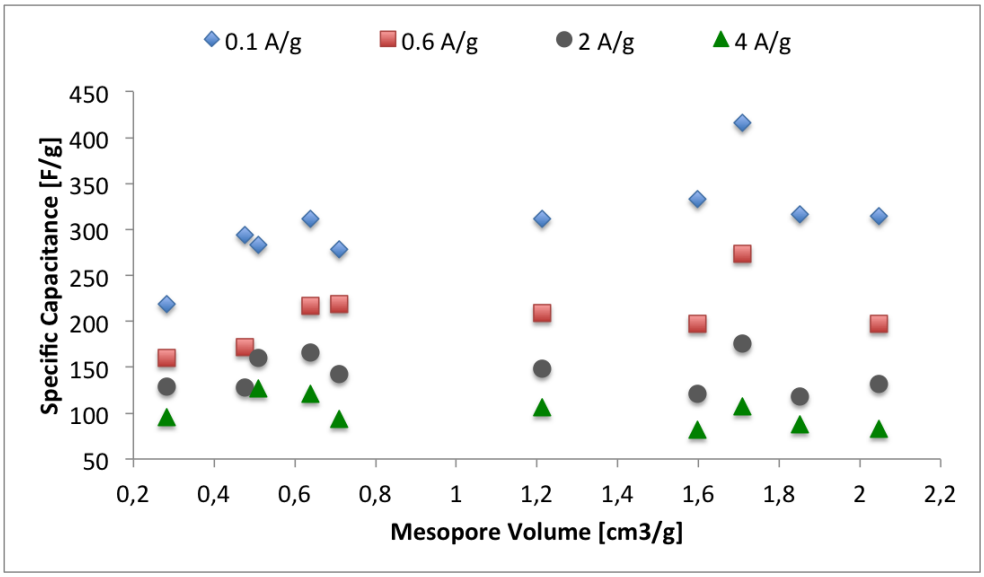

Figure 4.69: Specific capacitance of a single electrode versus mesopore volume for electrode materials prepared from activated carbons derived from PANI, excluding the electrode material prepared from carbon spheres and sample P650a950-3h-80CO2-50H2O-1h-Ar.

Figure (4.69) shows the specific capacitance of a single electrode versus the mesopore volume. At low current densities of 0.1 and 0.6 A/g, the specific capacitance show an increasing trend with mesopore volume between about 0.2 and 0.6 cm^3g^{-1}. However, the specific capacitance seems to not be very much effected by the mesopore volume at a mesopore volume ranging from about 0.6 to 2 cm^3g^{-1}. The presence of mesopores is important, since they provide less resistance during transferring of ions, compared to micropores [30]. Hence, these results suggest that some mesopores present in the electrode material are favorable to the specific capacitance.

Figure (4.70) shows the specific capacitance versus the nitrogen content and oxygen content of electrode materials derived from activated carbon fibers. These results suggest that both the nitrogen content and the oxigen content do not significantly effect the specific capacitance. This is reasonable, since the contribution of pseudocapacitance to the total capacitance is usually very small, compared to the contribution of the storage of electrical charges [22]. However, it is difficult to draw conclusions based on these results, since other properties such as the BET surface area and pore structure changes with both the nitrogen and oxygen content. Ideally, the effects of nitrogen and oxygen should be investigated at constant BET surface area, mesopore volume and micropore volume, like the results

obtained in the previous section. In the previous section, as can be seen from Table (D.1), the BET surface area and pore structure of the two electrode materials were similar. However, it was assumed that the oxygen and nitrogen content had decreased after the heat treatment, instead of being measured by EDX.

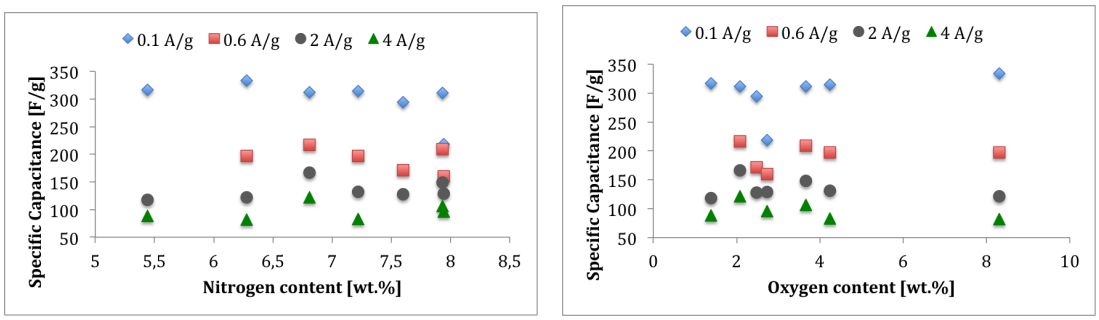

Figure 4.70: Specific capacitance of a single electrode versus the nitrogen and oxygen content of electrode materials prepared from activated carbons derived from PANI.

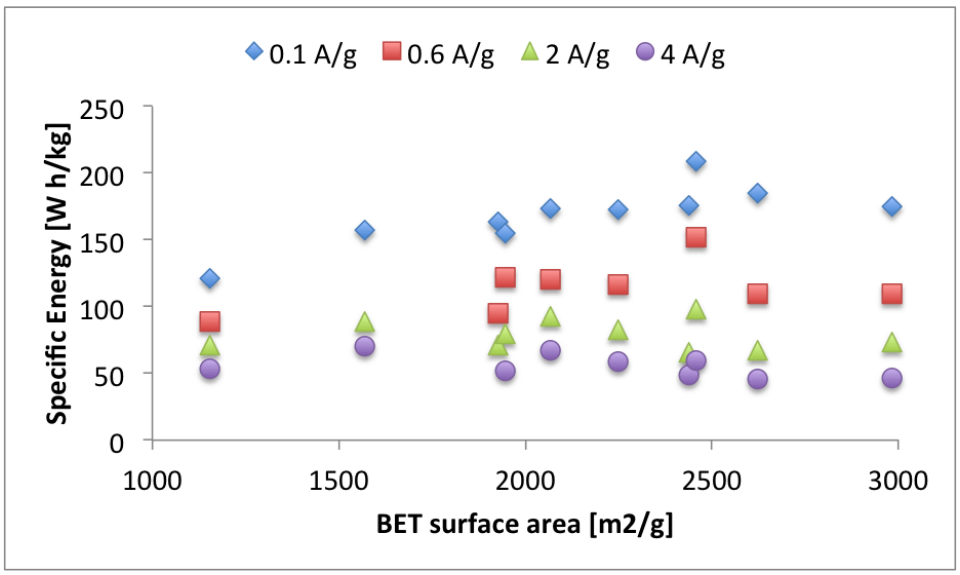

Figure 4.71: Specific energy versus BET surface area for electrode materials prepared from activated carbons derived from PANI, excluding the electrode material prepared from carbon spheres and sample P650a950-3h-80CO2-50H2O-1h-Ar.

Figure (4.71) shows the specific energy versus the BET surface area of activated carbons derived from PANI. The trend in specific energy with the BET

surface area at various current densities, is very similar to the trend in specific capacitance with the BET surface area. This is because the specific energy is closely related to the specific capacitance through equation (3.2). Therefore, like the specific capacitance, the specific energy decreases with increasing current density. At a current density of 0.1 A/g, the highest obtained specific energy was 208.8 W h/kg with a BET surface area of 2458,4 m^2g^{-1}. In general, the specific energy of supercapacitors using ionic liquid as electrolyte is larger, compared to the specific energy of supercapacitors using aqueous electrolyte. This is because ionic liquids have a very high operating voltage window of 4 to 4.5 V [22]. The specific energy is proportional to the square of the operating voltage window, which means that the specific energy can be enhanced by increasing the specific capacitance of the ionic liquid [26]. In this work, a high operating voltage window of 4 V was used, which resulted in very good specific energies ranging from about 120 to 208 W h/kg at a current density of 0.1 A/g.

However, the drawback of using ionic liquids as electrolyte in the supercapacitor device, is that a fast reduction in the specific capacitance and energy occurs when increasing the current density. This is because the ion sizes in ionic liquids are large, which results in a high ion transportation resistance during charging and discharging. The charge and discharge rate increases with increasing current density. The ion transportation resistance increases with increasing charge and discharge rate, which results in a significant drop in the specific capacitance [26]. Hence, it is reasonable to assume that the large ion sizes in the electrolyte used in this work ($EMIMBF_4$), is a major factor to the poor rate capabilities obtained, as can be seen in the previous subsections.

A specific energy of 208.8 W h/kg was obtained at a specific power of 107,1 W/kg. This is a much higher specific energy than the specific energy of 160 W h/kg at a specific power of 100 W/kg for activated carbon fibers derived from PANI through chemical activation with KOH [26]. Compared to batteries, supercapacitors have a higher specific power, but their specific energy is a bit lower [21]. This is consistent with literature, in which the theoretical specific energy of nickel–cadmium batteries is 220 W h/kg [29]. Also, it is reported that a high specific capacitance at 60°C was obtained with the use of activated carbon fibers derived from PANI through KOH activation. With the use of a large voltage window, a specific energy of 204 W h/kg was reported [29]. This large specific capacitance and energy reported are reasonable because an increase in operation temperature results in a decrease in viscosity of the electrolyte. Hence, the electrolyte moves easier in the pore structure of the electrode material, because the ion transportation resistance is lower. Considering the reported specific energies in the literature, the

very high specific energy of 208.8 W h/kg obtained in this work is very fascinating.

Figure (4.72) shows the rate capabilities versus the nitrogen content, oxygen content, total pore volume and mesopore volume of electrode materials prepared from activated carbon fibers. It is not easy to see a relationship between rate capability and the content of heteroatoms, such as nitrogen and oxygen. Oxygen and nitrogen groups generate pseudocapacitance, which is usually introduced through addition of metal oxides and conducting polymers in order to enhance the specific capacitance [26]. In general, pseudocapacitive materials, such as nitrogen and oxygen groups, are not known to have negative effects on the rate capability, whereas the main drawbacks include shorter cycling life and a reduction in operating voltage window [26]. As previously discussed, the highest rate capability was obtained for activated carbon spheres having a capacitance retention of 53.3 % at a current density of 3.68 A/g. This is a poor rate capability compared to activated carbon fibers derived from PANI through chemical activation with KOH, which showed an excellent rate capability with a capacitance retention of 72 % at a current density of 5 A/g. This excellent rate capability was most likely due to the retention of macroporosity [26]. Considering that the macroporosity of carbon spheres was maintained during the activation step, suggests that there are other reasons for the poor rate performance. One assumption is that the presence of nitrogen groups decreases the stability through strong adsorption of ions, which could result in blocking of pores. This leads to an increased ion transportation resistance during charging and discharging, which again increases with increasing charge and discharge rate [26].

It may look like the rate capability mostly decreases with increasing total pore volume and mesopore volume. This is unexpected, since other carbon materials that contain only micropores and mesopores show high ion-transport resistance, which results in low rate capability [26]. Moreover, mesopores are shown to be favorable for fast transportation of ions, because of the larger pore diameter compared to micropores. This fast transportation of ions leads to a good rate capability [29]. The poor rate capability obtained in this work is inconsistent with literature, considering that all of the active electrode materials prepared during this work is mostly mesoporous.

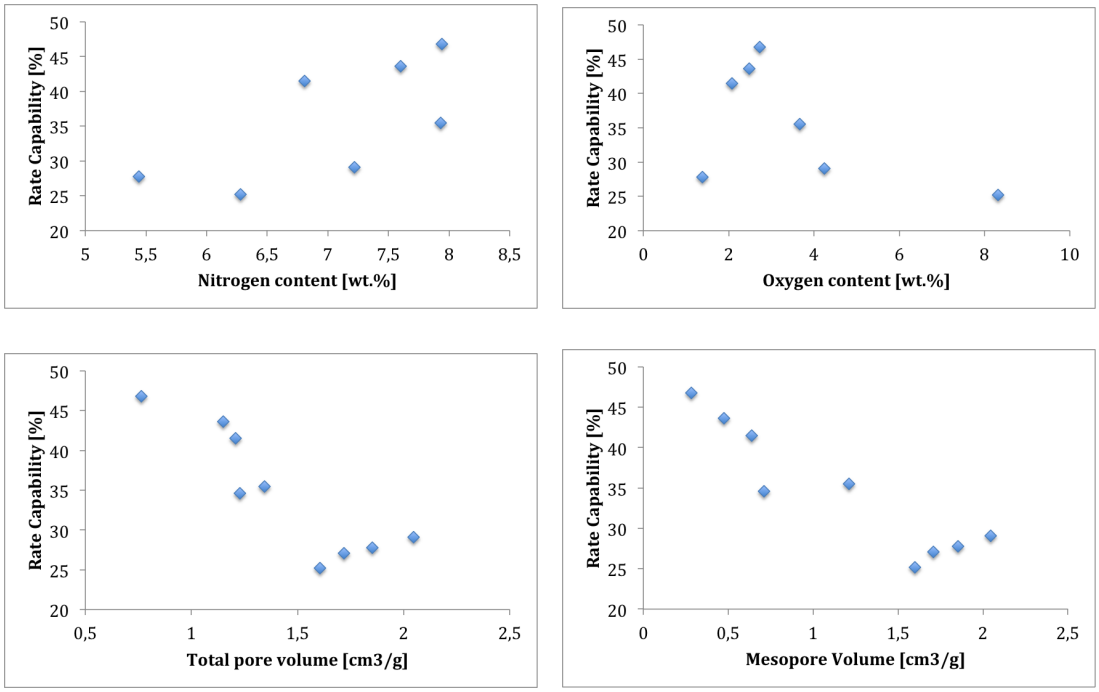

Figure 4.72: Rate capability at a current density of 3.68 A/g versus the nitrogen and oxygen content, total pore volume and mesopore volume of electrode materials prepared from activated carbons derived from PANI.

4.6.6 Cycling stability

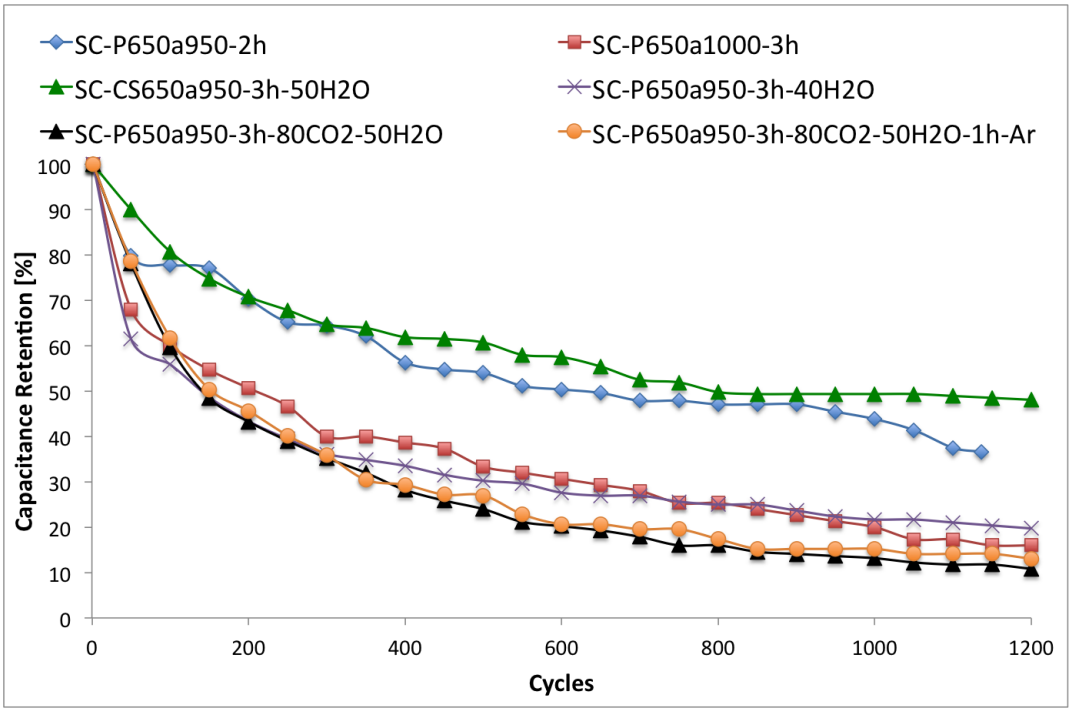

Figure 4.73: Cycling stability of various electrode materials at a current density of 1 A/g for 1200 cycles of charge/discharge.

Figure (4.73) shows the cycling stability of supercapacitors based on various electrode materials. It can be seen that all of the supercapacitors represented in Figure (4.73) show a poor cycling stability, with a large initial decrease in specific capacitance with increasing number of cycles. These results are unexpected, as electrical double-layer capacitors normally exhibit very high cycling stability with the potential of maintaining stability up to 10^6 cycles of charge and discharge [31]. It is reported that supercapacitors based on activated carbon fibers derived from PANI through KOH activation, showed a very good stability, where 87 % of the initial specific capacitance was retained after 5000 cycles [26].

The highest cycling stability in this work is achieved by using activated carbon spheres as electrode material, which results in a 48 % retention of the initial capacitance after 1200 cycles. The reason why activated carbon spheres provides the highest cycling stability could be due to the fact that the spherical morpholgy, and hence the macropore volume, is retained after the activation process. The results show that the second highest cycling stability is obtained by using activated

carbon fibers obtained with the two hour CO_2 activation process. This results in 37 % retention of the initial specific capacitance. As previously discussed, Figure (4.6) shows that the nanofiber structure is maintained after two hours of CO_2 activation at 950°C, which preserves the macroporosity of the carbon fibers. Figure (4.10) shows that the nanofiber structure is partially destroyd during the CO_2 activation process carried out with an activation temperature and an activation time of 1000°C and three hours, respectively. This results in a decrease in macroporosity. As seen from Figure (4.73), activated carbons prepared under these conditions results in a lower cycling stability of only 16 % retention of the initial capacitance after 1200 cycles. Thus, these results indicates that macroporosity is an important factor to obtain good cycling stability.

It can also be seen that the cycling stability of the carbon fibers prepared with the combined CO_2 and steam activation process with water a temperature of 50°C, (sample P650a950-3h-80CO2-50H2O and P650a950-3h-80CO2-50H2O-1h-Ar) show a similar decrease in capacitance with increasing cycles. This is reasonable because these two samples have the same degree of activation and a very similar pore structure, as seen from Figure (D.1) in appendix D. The sample subjected to the one hour heat treatment at 950°C in an inert atmosphere shows a slightly higher cycling stability of 13 % retention of the initial capacitance, compared to the sample not exposed to the heat treatment, where a 11 % retention of the initial capacitance is obtained. The better cycling stability of sample P650a950-3h-80CO2-50H2O-1h-Ar is reasonable, since the MS results shown in Figure (4.44) indicates that oxygen is released as CO and CO_2 during the heat treatment, which results in a decrease in oxygen content. It can be assumed that a decrease in oxygen content results in a decrease in pseudocapacitance, which increases the cycling stability. It has been shown that pseudocapacitance has a negative effect on the cycling stability, in which the cycling life is shortened [29].

The very low cycling stability and the sharp initial decrease in capacitance during the first hundred cycles, could indicate that the pore structure within the electrode materials gets destroyd during charging and discharging. As the pore structure gets destroyd, the ion transportation resistance increases, which results in a lower capacitance, because ions are transported less efficient to the electrical double-layer. The destruction of pores could also reduce the specific surface area, which results in a reduction of the electrical double-layer, which leads to less storage capacity of electrical charges. SEM or transmission electron microscopy (TEM) could be used after the cycling stability analysis, in order to check if the pore structure is maintained. SEM was applied after the cycling stability analysis in this work, but the SEM images obtained was unclear, most likely due to

remaining electrolyte in the material. In the future, the electrode material should be washed prior to SEM analysis.

All of the activated carbon fibers obtained with the combined CO_2 and steam activation process, with the exception of activated carbon spheres, show the lowest cycling stability, togheter with the activated carbon fibers prepared with CO_2 activation at 1000°C. As steam is a stronger activation agent than CO_2 [4], the combined CO_2 and steam activation process and the CO_2 activation process at 1000°C produce carbons with a high degree of activation. A high degree of activation is usually accompanied by a reduction in carbon strength [21]. Since the carbon strength is heavily reduced during these activation conditions, the low cycling stability supports the assumption that the pore structure is destroyd during charging and discharging. It has been reported that the formation of stage structure caused by an intercalation reaction, introduces a volume change in the electrode material, which results in electrode collapse at short cycling times [30]. In this work, the rate capability was determined before the cycling stability, which means that high current densities (short cycling times) were used prior to the cycling stability analysis. The high current densities could have caused the collapse in pore structure, which resulted in low cycling stability. Hence, in the future work, cycling stability tests should also be performed prior to the rate capability tests.

5 Conclusion

The first part of this paper involves the study of the preparation of activated carbon fibers through the CO_2 activation process. The effects of carbonization temperature, activation time, activation temperature and partial pressure of CO_2 on the resulting activated carbon fibers were investigated. It was found that a temperature of 650°C was the optimum carbonization temperature for producing activated carbon fibers with large BET surface area and pore volume. Also, it was found that the BET surface area, total pore volume and mesopore volume increases with increasing activation time at an activation temperature of 950°C. However, the micropore volume goes through a maximum at an activation time of 3 hours. The largest BET surface area obtained at an activation time was 2066.7 m^2g^{-1} with a burn-off equal to 80.6 wt.%. In addition, it was observed a decrease in both nitrogen content and oxygen content with increasing activation time, which is due to more oxygen and nitrogen being released through thermal breakage of chemical bonds as the time increases [7]. Also, SEM images supports that CO_2 activation is able to generate porosity without destroying the morphology of carbon fibers, however a small decrease in macropore volume could be observed at an activation time of 4 hours.

The results indicates an increase in reactivity of the endothermic oxidation reaction with increasing activation temperature, as more CO was formed at higher temperatures. The increase in reactivity results in a higher degree of activation, which provides larger BET surface areas and mesopore volume. The micropore volume goes through a maximum at 950°C, suggesting that the oxidation reaction becomes partially diffusionally controlled at temperatures higher than 950°C. It was also observed a decrease in both nitrogen content and oxygen content with increasing activation temperatures, as a result of thermal breakage of chemical bonds. The decrease in nitrogen content was also suggested by the formation of different nitrogen-containing gases during the activation process. SEM images showed that the fiberous structure was mostly maintained with increasing activation temperatures, where a small reduction of macroporosity could be observed at an activation temperature of 1000°C.

In the combined CO_2 and steam activation process, the carbon fibers were gradually destroyd with increasing amount of steam introduced in the activation process. This is reasonable since steam is more reactive than CO_2, hence the fiber structure becomes more fragile as more steam is reacting with the carbon. The oxygen content increases with increasing amount of steam in the activation process, while the nitrogen content remained constant, which suggests that the dop-

ing of oxygen from the reaction between steam and carbon increases with increasing amount of steam. This is reasonable since more H_2O molecules are present, which leads to more doping of oxygen to the carbon surface. The highest BET surface area was obtained with a water temperature of 40°C. Also, the introduction of steam resulted in a wider pore size distribution, which is in accordance with literature [3]. The introduction of steam in the combined CO_2 and steam activation process resulted in higher BET surface areas and pore volumes compared to that obtained with pure CO_2 activation at equal reaction conditions. Activated carbon spheres obtained by the combined CO_2 and steam activation process resulted in the largest BET surface are in this work. Also, SEM images showed that the spherical morphology was completey retained during the activation process.

All of the supercapacitors prepared in this work showed poor rate capabilities, compared to that reported in the literature. This could be due to the fact that the macroporous structure is reduced after activation for most of the electrode materials [26]. However, the activated carbon sphere showed a complete retention of macroporosity during the activation step, which suggest that other factors could be the reason for the poor rate performance. The high nitrogen content in the electrode materials could reduce the rate capability, by causing ions to strongly adsorb, which results in pore blockage. Also, the cycling stability of the supercapacitors was very low, which could be due to destruction of pores during charge and discharge. This increases the ion transportation resistance, which results in lower capacitance.

The CV curves showed that pseudocapacitance was present in all of the supercapacitors prepared in this work. The CV curves was not rectangular in shape, which is characteristic for pure electrical double-layer capacitors [21]. The pseudocapacitance contributed most likely to the high specific capacitance obtained at low current densities. Also, it was shown that an increasing trend in specific capacitance occured with both increasing BET surface area and total pore volume. The BET surface area is known to be the most important factor in regards to the specific capacitance [30]. This was not proved in this work, as a linear relationship between the specific capacitance and BET surface area should have been obtained.

6 Future work

Future work involves further optimization of the activation process, in order to achieve high BET surface area and pore volume accompanied with a lower burn-off. In addition to the characterization techniques applied in this work, transmission electron microscopy (TEM) could be used in order to examine mesopores generated during the activation process, as the limitations of SEM makes it difficult to examine mesopores in this paper. Also, XPS could be used in order to examine nitrogen and oxygen-containing groups present on the surface of activated carbons. XPS is beneficial for this purpose, because it is a surface sensitive technique, which allows examination of different nitrogen and oxygen groups present on the surface.

The future work will focus more towards the activation of carbon spheres instead of carbon fibers, since carbon spheres showed the best performance as electrode material in the supercapacitor cell. The supercapacitor constructed of activated carbon spheres as electrode material did not provide the highest specific capacitance, but it did show the best rate capability and cycling stability of all the supercapacitors prepared in this work.

The electrodes were manufactured by pressing the active electrode material into a nickel foam, which makes it impossible to measure the electrode volume. The electrode volume needs to be determined in order to calculate the volumetric capacitance, which is an important designation of supercapacitors. This can be achieved by making pellets consisting of the active electrode material. In addition, electrochemical measurements can also be carried out at elevated temperature, in order to enhance the performance of the supercapacitor cells. It has been reportet that the specific capacitance and specific energy is determined at a temperature of 60°C, which increases the performance. Another method to increase the performance is the addition of salts to the electrolyte, which increases the amount of ions present in the cell.

References

[1] Jerzy Choma et al., 2016, Developing microporosity in Kevlar-derived carbon fibers by CO_2 activation for CO_2 adsorption, Elsevier

[2] Silva et al., 2016, Mesoporous activated carbon from industrial laundry sewage sludge: Adsorption studies of reactive dye Remazol Brilliant Blue R, Elsevier

[3] Amphol Aworn, et al, 2008, Preparation and characteristics of agricultural waste activated carbon by physical activation having micro- and mesopores, Elsevier

[4] Omer Sahin, et al, 2013, Preparation and characterization of activated carbon from acorn shell by physical activation with H2O–CO2 in two-step pretreatment, Elsevier

[5] C.A. Crutchfield and W. Clarke, 2017, HIGH RESOLUTION ACCURATE MASS (HRAM) MASS SPECTROMETRY, Chapter 12, Elsevier

[6] Horacio G. Pontis, 2017, General Introduction to Mass Spectrometry and Nuclear Magnetic Resonance, Chapter 5, Methods for Analysis of Carbohydrate Metabolism in Photosynthetic Organisms, Pages 71–76, Academic press

[7] Vilas G. Pol, et al, 2014, Tunable, Functional Carbon Spheres Derived from Rapid Synthesis of Resorcinol-formaldehyde Resins, Applied materials and interfaces

[8] Abdullah A. Alazemi, et al, 2015, Ultrasmooth Submicrometer Carbon Spheres as Lubricant Additives for Friction and Wear Reduction, Applied materials and interfaces

[9] TKP 2 Lecture slides

[10] Mohamed L. Sekirifa, 2012, Preparation and characterization of an activated carbon from a date stones variety by physical activation with carbon dioxide, Elsevier

[11] M. Plaza-Recobert, 2017, Superactivated carbons by CO2 activation of loquat stones, Elsevier

[12] Suhas, et al, 2017, An innovative approach to develop microporous activated carbons in oxidising atmosphere, Journal of Cleaner Production, Elsevier

[13] Ugur Ozveren, Z. Sibel Ozdogan, 2013, Investigation of the slow pyrolysis kinetics of olive oil pomace using thermo-gravimetric analysis coupled with mass spectrometry, Elsevier

[14] Zhongyue Zhou, et al, 2016, A thermal decomposition study of pine wood under ambient pressure using thermogravimetry combined with synchrotron vacuum ultraviolet photoionization mass spectrometry, Elsevier

[15] Prakash Parthasarathy, et al, 2013, Study on kinetic parameters of different biomass samples using thermo-gravimetric analysis, Elsevier

[16] Daniel Skodvin, 2016, Synthesis and Applications of Carbon Spheres, Specialization project, Catalysis Group, Department of Chemical Engineering, NTNU

[17] Izzati Izni Yusoff, 2016, Investigation of the formation characteristics of polyaniline and its application in forming free-standing pressure filtration membranes, CrossMark

[18] Jiaxing Huang and Richard B. Kaner, 2004, Nanofiber Formation in the Chemical Polymerization of Aniline: A Mechanistic Study, Angewandte chemie

[19] Ahmed M. ElKhatat and Shaheen A. Al-Muhtaseb, 2011, Advances in Tailoring Resorcinol-Formaldehyde Organic and Carbon Gels, Advanced materials

[20] Abdelhakim Elmouwahidi, et al, 2017, Activated carbons from KOH and H3PO4-activation of olive residues and its application as supercapacitor electrodes, Elsevier

[21] A.G. Pandolfo and A.F. Hollenkamp, 2006, Carbon properties and their role in supercapacitors, Elsevier

[22] Balasubramanian Viswanathan, 2016, Chapter 13 – Supercapacitors, Energy Sources, Elsevier

[23] Carbon Materials for Electrochemical Capacitors, chapter 11, 2014, Elsevier

[24] Elzbieta Frackowiak, et al, 2000, Carbon materials for the electrochemical storage of energy in capacitors, Carbon

[25] Michio Inagaki, et al, 2010, Carbon materials for electrochemical capacitors, Elsevier

[26] Xuehang Wang and De Chen, 2016, Boosted Supercapacitive Energy with High Rate Capability of aCarbon Framework with Hierarchical Pore Structure in an Ionic Liquid, CHEMSUSCHEM

[27] Jon Alvarez, et al, 2016, Preparation of adsorbents from sewage sludge pyrolytic char by carbon dioxide activation, Elsevier

[28] I. Chorkendorff, W. Niemantsverdriet: "Concepts of Modern Catalysis and Kinetics", Second Edition, 2007, WILEY-VCH

[29] Xuehang Wang and De Chen, 2015, Geometrically confined favourable ion packing for high gravimetric capacitance in carbon–ionic liquid supercapacitors, Energy Environmental Science

[30] Yasushi Soneda, 2013, Carbons for Supercapacitors, Chapter 2.12, Handbook of Advanced Ceramics

[31] Fan Huang, 2011, Doctoral theses, 3D Carbon/polyaniline Nanostructures for Energy Storage, NTNU

[32] Chafia Bouchelta, et al, 2007, Preparation and characterization of activated carbon from date stones by physical activation with steam, Elsevier

[33] R. Bruce Prime "Thermal Analysis of Polymers: Fundamentals and Applications" Chapter 3: THERMOGRAVIMETRIC ANALYSIS (TGA), 2009, John Wiley Sons, Inc.

[34] Jian Liu, et al, 2011, Extension of The Stöber Method to the Preparation of Monodisperse Resorcinol-Formaldehyde Resin Polymer and Carbon Spheres, Angewandte Chemie

[35] Hao Tian, et al, 2016, Revisiting the Stöber method: Design of nitrogen-doped porous carbon spheres from molecular precursors of different chemical structures, Elsevier

[36] Guang-Ping Hao, et al, 2010, Rapid Synthesis of Nitrogen-Doped Porous Carbon Monolith for CO_2 Capture, Advanced materials

[37] Marta Sevilla et al., 2011, N-Doped Polypyrrole-Based Porous Carbons for CO_2 capture, Materials Views, Advanced functional materials

[38] Jerzy Choma et al., 2016, Developing microporosity in Kevlar-derived carbon fibers by CO_2 activation for CO_2 adsorption, Elsevier

[39] S. Aravinth et al., 2012, Synthesis and characterization of hexagonal nano tungsten carbide powder using multi walled carbon nanotubes, Elsevier

[40] Yujiao Kan et al., 2016, Comparison of activated carbons from epoxy resin of waste printed circuit boards with KOH activation by conventional and microwave heating methods, Elsevier

[41] Wei Ge et al., 2016, Master thesis, Chemical engineering, NTNU

[42] Jitong Wang et al., 2016, Organic Amine-Mediated Synthesis of Polymer and Carbon Microspheres: Mechanism Insight and Energy-Related Applications, APPLIED MATERIALS AND INTERFACES

[43] Chengdu Liang et al., 2008, Mesoporous Carbon Materials: Synthesis and Modification, Angewandte Chemie

[44] http://www.hidenisochema.com/glossary/65-barrett$_j oyner_h alenda_(bjh)_a nalysis$/

A Chemical activation with CO_2

Properties	P650	P650a950-1h	P650a950-2h	P650a950-3h	P650a950-4h
S_{BET} [m^2/g]	298.3	687.8	1154.9	1927.7	2066.7
V_T [cm^3/g]	0.202	0.482	0.763	1.151	1.208
V_{micro} [cm^3/g]	0.109	0.295	0.481	0.675	0.570
V_{meso} [cm^3/g]	0.093	0.187	0.282	0.476	0.638
V_{meso}/V_T [%]	46.0	38.8	37.0	41.4	52.8
V_{micro}/V_T [%]	54.0	61.2	63.0	58.6	47.2
Burn-off [wt.%]	-	39.8	55.9	67.5	80.6

Table A.1: Physical properties of activated carbon fibers derived from polyaniline. The carbonization temperature and the activation temperature were 650 and 950°C, respectively. The duration of activation was varied from 1 to 4 hours.

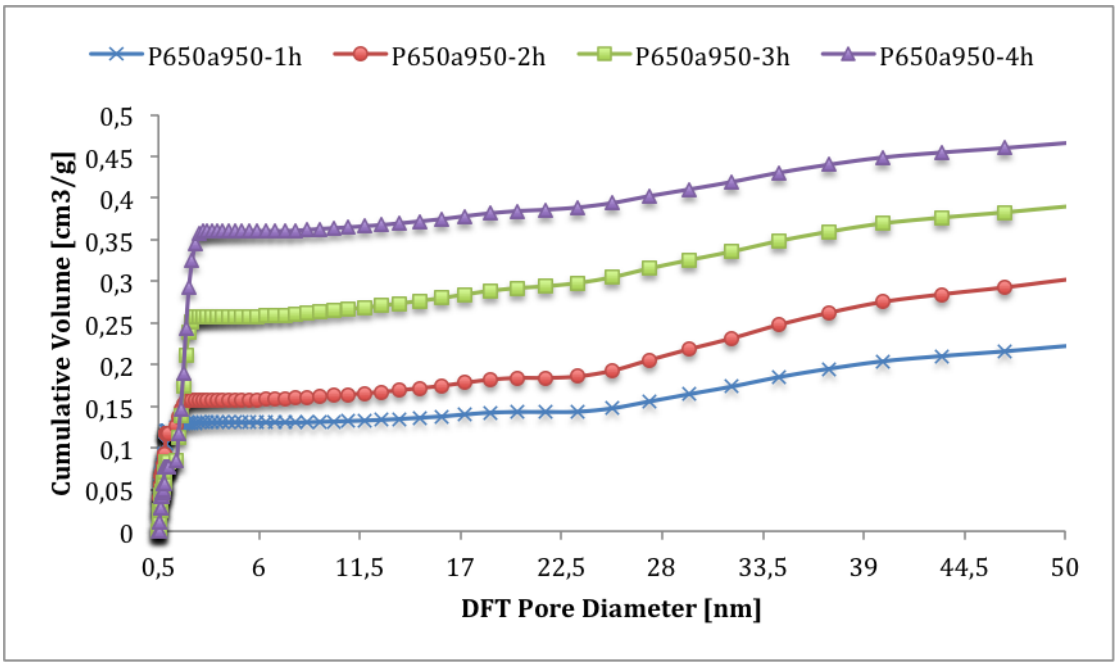

Figure A.1: Cumulative pore volume, obtained from CO_2 and N_2 adsorption/desorption, of activated carbon fibers derived from polyaniline through a carbonization temperature and an activation temperature of 650 and 950°C, respectively. Duration of activation was varied from 1 to 4 hours.

Properties	P650a750	P650a850	P650a900	P650a950	P650a1000
S_{BET} [m^2/g]	86.8	395.7	679.7	1927.7	2439.2
V_T [cm^3/g]	0.104	0.286	0.520	1.151	1.852
V_{micro} [cm^3/g]	0.016	0.157	0.284	0.675	0
V_{meso} [cm^3/g]	0.088	0.129	0.236	0.476	1.852
V_{meso}/V_T [%]	84.6	45.1	45.4	41.4	100
V_{micro}/V_T [%]	15.4	54.9	54.6	58.6	0
Burn-off [wt.%]	6.1	17.8	38.2	67.5	98.0

Table A.2: Physical properties of activated carbon fibers derived from polyaniline through a carbonization temperature of 650°C and an activation time of 3 hours. The activation temperature was varied from 750 to 1000°C.

Properties	a950-2h-80CO_2	a950-2h-100CO_2	a950-3h-80CO_2	a950-3h-100CO_2
S_{BET} [m^2/g]	1154.9	1476.1	1927.7	1570.4
V_T [cm^3/g]	0.763	0.909	1.151	1.011
V_{micro} [cm^3/g]	0.481	0.537	0.675	0.501
V_{meso} [cm^3/g]	0.282	0.372	0.476	0.510
V_{meso}/V_T [%]	37.0	40.9	41.4	50.4
V_{micro}/V_T [%]	63.0	59.1	58.6	49.6
Burn-off [wt.%]	55.9	60.7	67.5	68.8

Table A.3: Physical properties of activated carbon derived from polyaniline through a carbonization temperature and an activation temperature of 650 and 950°C, respectively. The gaseous environment was a mixture of CO_2 and argon with a total flow rate of 100 ml/min, where the partial pressure of CO_2 was 0.8 or 1.0.

B Chemical activation with CO_2 and H_2O

Properties	a950-25H_2O	a950-40H_2O	a950-50H_2O	a950-70H_2O	a950-90H_2O
S_{BET} [m^2/g]	2247.8	2981.6	2622.6	1196.1	1148.2
V_T [cm^3/g]	1.344	2.047	1.604	0.758	0.782
V_{micro} [cm^3/g]	0.132	0.000	0.006	0.052	0.000
V_{meso} [cm^3/g]	1.212	2.047	1.598	0.706	0.782
V_{meso}/V_T [%]	90.2	100.0	99.6	93.1	100.0
V_{micro}/V_T [%]	9.8	0.0	0.4	6.9	0.0
Burn-off [wt.%]	85.9	91.4	90.3	81.9	91.0

Table B.1: Physical properties of activated carbon derived from PANI through a carbonization temperature and an activation temperature of 650 and 950°C, respectively. The water temperature was varied from 25 to 90°C and the duration of activation was 3 hours.

Properties	a950-1h-40H_2O	a950-2h-40H_2O	a950-3h-40H_2O
S_{BET} [m^2/g]	1592.9	1823.9	2981.6
V_T [cm^3/g]	1.092	1.167	2.047
V_{micro} [cm^3/g]	0.485	0.419	0.000
V_{meso} [cm^3/g]	0.607	0.748	2.047
V_{meso}/V_T [%]	55.6	64.1	100.0
V_{micro}/V_T [%]	44.4	35.9	0.0
Burn-off [wt.%]	70.1	75.4	91.4

Table B.2: Physical properties of activated carbon fibers derived from PANI through a carbonization temperature and an activation temperature of 650 and 950°C, respectively. The water temperature was 40°C and the activation time was varied from 1 to 3 hours.

Properties	a850-50H_2O	a900-50H_2O	a950-50H_2O
S_{BET} [m^2/g]	848.0	1547.1	2622.6
V_T [cm^3/g]	0.570	1.019	1.604
V_{micro} [cm^3/g]	0.364	0.520	0.006
V_{meso} [cm^3/g]	0.206	0.499	1.598
V_{meso}/V_T [%]	36.1	49.0	99.6
V_{micro}/V_T [%]	63.9	51.0	0.4
Burn-off [wt.%]	46.5	70.1	90.3

Table B.3: Physical properties of activated carbon fibers derived from PANI through a carbonization temperature and an activation time of 650°C and 3 hours, respectively. The water temperature was 50°C and the activation temperature was varied from 850 to 950°C.

Properties	a950-60CO_2-50H_2O	a950-80CO_2-50H_2O	a950-100CO_2-50H_2O
S_{BET} [m^2/g]	2273.6	2458.4	2622.6
V_T [cm^3/g]	1.523	1.719	1.604
V_{micro} [cm^3/g]	0.227	0.011	0.006
V_{meso} [cm^3/g]	1.296	1.708	1.598
V_{meso}/V_T [%]	85.1	99.4	99.6
V_{micro}/V_T [%]	14.9	0.6	0.4
Burn-off [wt.%]	84.7	90.7	90.3

Table B.4: Physical properties of activated carbon derived from polyaniline through a carbonization temperature and an activation temperature of 650 and 950°C, respectively. The gaseous environment was a mixture of CO_2, argon and steam with a total flow rate of 100 ml/min, where the partial pressure of CO_2 was varied from 0.6 to 1.0.

C Carbon spheres

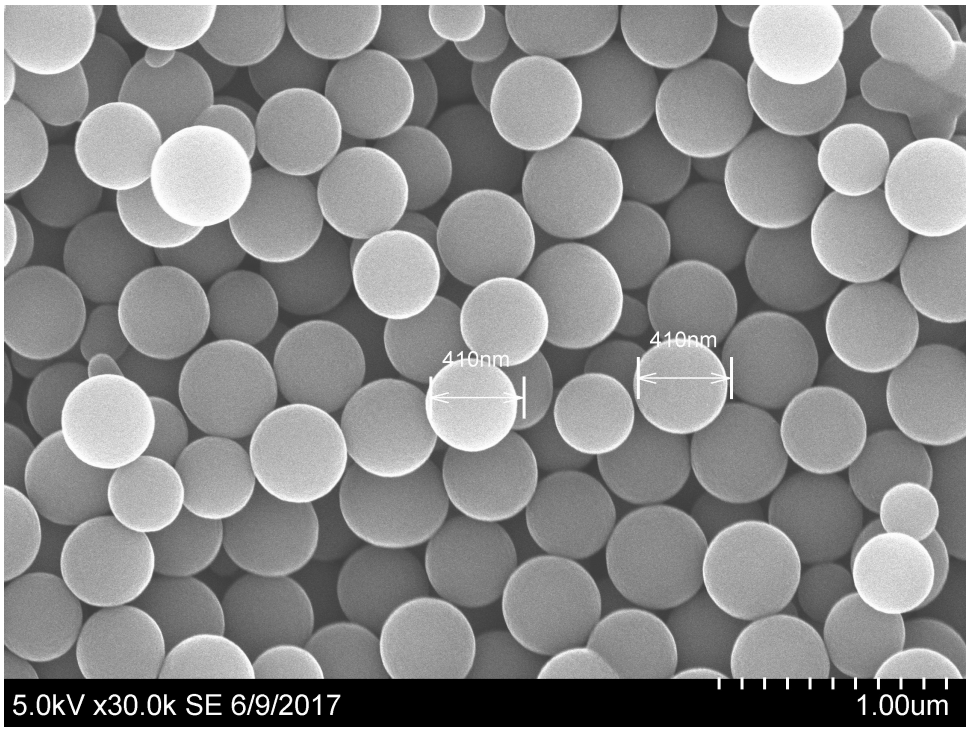

Figure C.1: Carbon spheres derived from RF polymer spheres through a carbonization temperature of 650°C. The heating rate was set to be 1.5°C min^{-1} and the duration was 2 hours. The cooling rate was set to be 10°C min^{-1}.

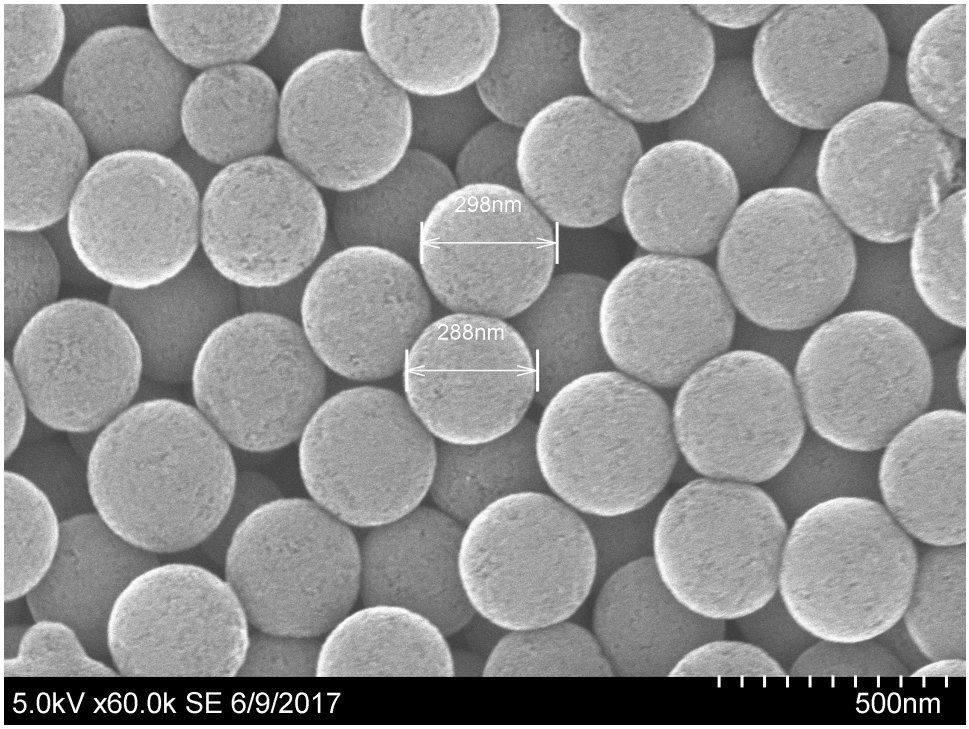

Figure C.2: Activated carbon spheres derived from RF polymer spheres through a carbonization temperature and an activation temperature of 650 and 950°C, respectively. The duration of the carbonization and activation process was 2 and 3 hours, respectively. The carbon spheres were subjected to the combined CO_2 and steam activation process, where the water temperature was set to be 50°C.

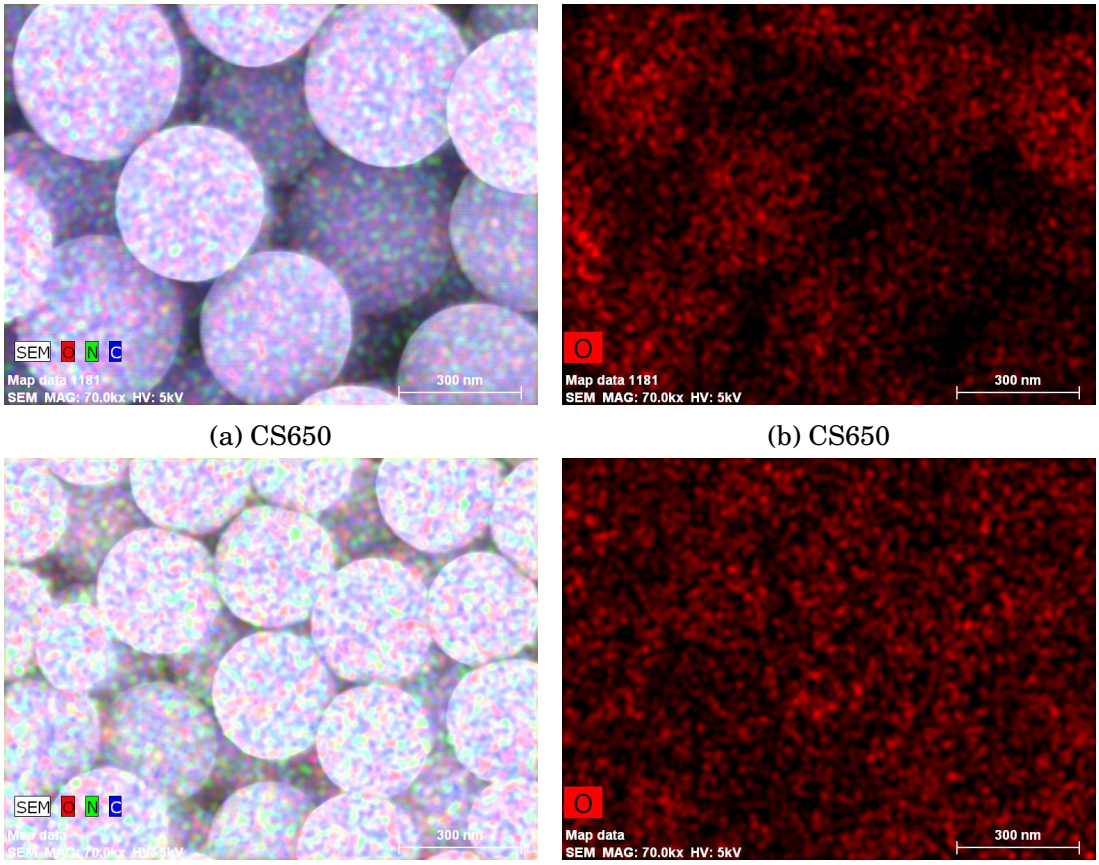

(a) CS650

(b) CS650

(c) CS650a950-3h-50H_2O

(d) CS650a950-3h-50H_2O

Figure C.3: EDX mapping of carbon spheres and activated carbon spheres. Carbonization and activation temperature were 650 and 950°C, respectively. The duration of the carbonization and activation process were 2 and 3 hours, respectively. The carbon spheres were subjected to the combined CO_2 and steam activation process, where the water temperaure was 50°C.

D Surface oxygen groups

Properties	P650a950-80CO2-50H_2O	P650a950-80CO2-50H_2O-1h-Ar
S_{BET} [m^2/g]	2458.4	2496.2
V_T [cm^3/g]	1.719	1.708
V_{micro} [cm^3/g]	0.011	0.051
V_{meso} [cm^3/g]	1.708	1.657
V_{meso}/V_T [%]	99.4	97.0
V_{micro}/V_T [%]	0.6	3.0

Table D.1: Physical properties of activated carbon fibers derived from PANI through a carbonization temperature and an activation temperature of 650 and 950°C, respectively. The water temperature was 50°C and the activation time was 3 hours. Sample P650a950-80CO2-50H_2O-1h-Ar was subjected to one hour of heat treatment at 950°C in an argon atmosphere.